WASHINGTON UNIVERSITY
SEVER INSTITUTE OF TECHNOLOGY
DEPARTMENT OF CHEMICAL ENGINEERING

CATALYTIC WET OXIDATION OVER PILLARED CLAY CATALYST IN PACKED-BED REACTORS: EXPERIMENTS AND MODELING

by

Jing Guo

Prepared under the direction of

Prof. M. H. Al-Dahhan

A dissertation presented to the Sever Institute of

Washington University in partial fulfillment

of the requirements for the degree of

DOCTOR OF SCIENCE

May, 2005

Saint Louis, Missouri, USA

WASHINGTON UNIVERSITY
SEVER INSTITUTE OF TECHNOLOGY
DEPARTMENT OF CHEMICAL ENGINEERING

CATALYTIC WET OXIDATION OVER PILLARED CLAY CATALYST IN PACKED-BED REACTORS: EXPERIMENTS AND MODELING

by

Jing Guo

Prepared under the direction of

Prof. M. H. Al-Dahhan

May, 2005

Saint Louis, Missouri, USA

Abstract

As an important approach for the wastewater treatment, catalytic wet oxidation (CWO) in packed-bed reactors has drawn significant attention in the chemical and petrochemical industries. A packed-bed reactor, especially in the upflow mode of operation, has been shown to be more suitable for the CWO process than other reactor types. CWO of phenol in aqueous phase is studied in this work over a newly developed Al-Fe pillared clay catalyst. This catalyst has shown potential for wastewater treatment, as it reduces the reaction temperature and pressure and provides better resistant to deactivation. For reactor design and scale-up, the interactions between the involved reaction kinetics, hydrodynamics, interphase and intraparticle transport in the catalytic packed bed at different reaction conditions needs to be addressed. The goal is to get

complete mineralization of phenol at mild conditions and to identify the corresponding operating conditions.

In the experiment part, pillared clay catalyst performance for wastewater treatment (phenol removal) was investigated in both batch and packed-bed reactors. Batch experiments, using a basket reactor, were performed to identify the suitable operating conditions, and to derive the apparent reaction kinetics for phenol removal. Appropriate kinetic models were derived and used to predict packed bed performance. The performance of the pillared clay catalyst for phenol oxidation in a packed bed process was investigated with co-current downflow and upflow. Under rather mild conditions, the Al-Fe pillared clay catalyst can achieve total elimination of phenol and significant mineralization (80-100%) of total organic carbon (TOC). The catalyst deactivation is investigated via three different detection methods: particle pore BET analysis, scanning electron microscopy (SEM), and inductively coupled plasma (ICP).

In the modeling part, a suitable reactor scale model is evaluated and extended to predict the performance of packed-bed reactors under employed conditions. The effects of key parameters, such as extent of liquid-solid contacting, gas/liquid limitation, and mass transfer resistance, have been investigated. The model is modified to account for the volatilization of the solvent. Such a modeling strategy is aimed to provide a tool for further evaluation of the new catalyst design and various operating conditions.

Contents

Page

Tables

Figures

Figure Page

Acknowledgments

I wish to express my deep gratitude to my advisor, Professor M. H. Al-Dahhan, for the opportunity to undertake this work under his supervision. His encouragement of independent thought, advice, and patience was indeed invaluable in making this work feasible. I would also like to thank Professor M. P. Dudukovic and Professor P. A. Ramachandran for their advices and suggestions in all aspects of the project, which help me overcome many technical obstacles. I would like to acknowledge other members of my committee, Dr. Pratim Biswas from Department of Environment Engineering and Dr. Ramesh K. Agarwal from Department of Mechanical Engineering for taking interest in my work, examining my thesis, and providing useful comments and suggestions.

I thank Professor N. Papayannakos of National Technical University of Athens (NTUA), Greece, for the kind supply of the mixed (Al-Fe) pillared clay catalyst. I wish to acknowledge the financial support of the industrial participants of the CREL consortium, which made the research possible. It has been my pleasure to work at CREL, which has provided me great opportunities to experience the developments of various multiphase chemical reactors and to learn extensively from a diversity of experts inside and outside CREL. My special appreciation is to Dr. Jiang Yi and Dr. Khadilkar Mohan who have been working on the fields of flow distribution and reaction in the packed bed. Their supports and help were precious throughout my simulation and experimental work on several projects. My colleagues at CREL and in the Chemical Engineering Department have made significant contributions in making my work and life at Washington University a pleasant experience. Numerous discussions with them were particularly important for this work I had at CREL. My sincere gratitude goes to Dr. P. Spicka, Dr. M. Rafique, Dr. A. Rommohan, Dr. P. Chen, Dr. J Xue, S. Roy, H. Luo, S. Bhusarapu, E. Palmisano, P. Steve, R. Magan, V. Gupta, and many others. I also wish to thank the entire

Chemical Engineering Department, particularly the secretaries for their precious help and consistent assistance.

I am also glad that I was able to enjoy the three-month internship at Corning Incorporated in summer 2004. Special acknowledgements go to Dr. Dipak Chowdhury, Mr. Leslie Button, Dr. Hasan Saleheen, and Dr. Yi Jiang of Corning Incorporated for this great opportunity and for their professional guidance, which allowed me to adapt myself to company life and gain practical experiences in the field of catalytic converters .

Finally, my heartfelt gratitude goes to my parents and my wife, Weiling Li, for their support, patience, and sustained belief in my abilities, which help me attain a fruitful student life in Washington University.

Jing Guo
Washington University, St. Louis
May 2005

Nomenclature

[A] phenol concentration, mol C/m^3 solution

[B] concentration of dissolved intermediate organic lump, mol C/m^3 solution

[C] carbon concentration of end product lump mol C/m^3 solution

[H_2O_2] concentration of H_2O_2, mol/m^3 solution

[O_2] oxygen concentration in liquid phase, mol /m^3 solution

AARE average absolute relative error, AARE=$\sum_{i=1}^{N} \left| \left(y_{Sim,i} - y_{Exp,i} \right) / y_{Exp,i} \right| / N$

a catalyst specific surface area per unit reactor bed,m^2/m^3

a_c $= 6(1-\varepsilon_B)/d_p$ catalyst specific surface area per unit reactor bed volume, m^2/m^3

a_{GL} gas-liquid interphase area per unit reactor bed volume, m^2/m^3

C_{cat} catalyst concentration, kg catalyst/m^3 solution

$C_{e,k}$ hypothetical liquid concentration in equilibrium with bulk gas concentration for species k, mol/m^3

$C_{k,G}$ concentration of species k in gas, mol/m^3

$C_{k,GS}$ concentration of species k on the dry side of catalyst, mol/m^3

$C_{k,L}$ concentration of species k in liquid, mol/m^3

$c_{k,,L}$ dimensionless concentration of species i in liquid

$C_{k,LS}$ concentration of liquid species k on the wetted catalyst surface, mol/m^3

D_e effective diffusivity of the reactant, m^2/s

$D_{e,k}$ effective volumetric diffusion coefficient for species k, m^2/s

D_{EL} axial dispersion coefficient of the liquid phase, m^2/s

d_p particle diameter, m

$d_{p,v}$ $=6V_p/S_x$, pellet equivalent diameter based on the catalyst volume

H_k = $C_{k,G}$ / $C_{k,L}$ at G-L interface, Henry's law constant of solubility for species k, m^3 liquid/ m^3 gas

k number of species

k' lumped rate constant

K, K' adsorption equilibrium constants, m^3/mol

k_1 heterogeneous reaction rate constant, mol C(m^3 solution)$^{n-1}$/kg^n/min for LHHW model

k_{GS} gas-solid mass transfer coefficient. m/s

k_H heterogeneous reaction rate constant, (m^3/kg catalyst)^p/min

k_h homogeneous reaction rate constant, m^3/mol/min

$(K_L a)_{GL}$ overall volumetric mass transfer coefficient from gas to flowing liquid, 1/s

$(k_L a)_{GL}$ Liquid side mass transfer coefficient for gas to flowing liquid, 1/s

k_{LS} liquid-solid mass transfer coefficient. m/s

L reactor length, m

p potential order for the catalyst loading influence in heterogeneous model

P reactor pressure, MPa or atm

Pe Péclet number, $Pe = \frac{u_{SL} L}{D_{EL}}$

q potential order for the oxygen concentration influence in power-law model

r number of reaction

Re = $d_{p,v}u/\nu$, Reynolds number based on pellet equivalent diameter $d_{p,v}$

r_H reaction rate due to heterogeneous contribution, mol C(m^3 solution)$^{p-1}$/kg^p/min

r_h reaction rate due to homogeneous contribution, mol C/m^3 solution /min

r_i reaction rate based on the species i , mol/m^3/s or mol/kg/min

R_r overall reaction rate, mol/ m^3/s, positive for product

S_p external surface area of a catalyst pellet, m^2

SQR residual sum of squares, $SQR = \sum_{i=1}^{n} \left[([A]_{Sim,i} - [A]_{Exp,i}) / [A]_{Exp,i} \right]^2$

t reaction time, min

T temperature, K or ^oC

TOC total organic carbon, mol C/m^3 solution

u_G gas superficial velocity, m/s

u_{SL} liquid superficial velocity, m/s

V volume of the aqueous solution, ml

V_p volume of a catalyst pellet, m^3

X conversion of biphenyl, %

Z bed axial position, m

Greek Letters

η reaction effectiveness factor

ξ dimensionless position

φ inlet concentration

ϕ catalyst diameter

β_1, β_2 dimensionless parameter

ε_B bed porosity

η_{CE} catalyst wetting efficiency

$\alpha_{G,L}$ dimensionless parameter

ν_k stoichiometric coefficient for species k

ε_l liquid holdup

$\alpha_{L,S}$ dimensionless parameter

ρ_B density of catalyst bed, kg/ m^3

ρ_S density of catalyst pellet, kg/ m^3

Sub/superscripts

* free site, adsorbed

0 input

A gas reactant, H_2 or O_2

B phenol

C oxidation intermediate product

D	oxidation end-product lump
e	equilibrium
Exp	experimental data
G	gas phase
H	heterogeneous reaction
h	homogeneous reaction
L	liquid phase
S	solid phase
Sim	simulation data

Chapter 1 Introduction to Catalytic Wet Oxidation

Industrial processes and agricultural activities generate a large quantity and a large variety of wastewater streams containing organic pollutants. Such wastewater has become a major social and economic problem, as health-quality standards and environmental regulations have gradually become more restrictive (Yurii and Moshe, 1998). Discharge of such wastewater without treatment into a natural water body is often environmentally unacceptable. Among all the organic materials that we are concerned with, phenol is proved important by its ever-increasing presence due to its increased production that reached 1900 million kilograms in 1995 for the USA alone (Fortuny, 1998). Phenol and phenolic substances are used widely as raw materials for organic compounds, such as dyes, pharmaceuticals, plasticizers, antioxidants, etc. Phenol is also considered to be an intermediate product in the oxidation pathway of higher-molecular-weight aromatic hydrocarbons (Aurora et al., 2001). Phenol, in addition to having strong disagreeable odor and taste in water even at very small concentrations, is extremely toxic to the aquatic life and resistant to biodegradation. In the past 2 decades, wastewater containing phenol has received increased attention because of its toxicity and prevalence (Moore and Ramamoorthy, 1984). Therefore, phenol is usually taken as a model compound for advanced wastewater treatment studies.

At present, the various treatment methods available are: chemical, physical (adsorption, reverse osmosis, etc.), biological, wet air oxidation (WAO), incineration, etc. In selecting a wastewater treatment process among these methods, one should take into account the toxicities and concentrations of the pollutants in the waste stream.

Chemical oxidation, using O_3, ClO_2, Cl_2, and H_2O_2 as oxidants, is a popular method.

However, it is prohibitively expensive if large volumes are to be treated, particularly if the waste is predominantly organic in nature. In view of this, chemical treatment is usually used as the pretreatment step for color removal and removal of some toxic compounds so that other treatment methods, such as the biological treatment, can be used downstream (Yurii and Moshe, 1998). UV/O_3 oxidation allows the combination of photocatalysts and UV light to achieve higher reaction rates in aqueous streams. The waste stream passes through a reactor with ozone and organics reacting under the highly energetic UV light. This system is highly reactive, but the ozone and UV lighting requirements can be expensive as well as difficult to scale up to industrial sized reactors (Matthews, 1992).

As a physical treatment method, adsorptive process over activated carbon (and some synthetic resins) is used frequently to treat wastewater. High molecular weight organics (particularly those having lower solubility in water) are adsorbed preferentially on the carbon surface. Carbon treatment becomes attractive if the spent carbon can be regenerated by biotreatment, solvent extraction, WAO, etc. Reverse osmosis is a membrane process used for desalting of brackish water and removing dissolved solids from certain industrial wastewaters. A concentrated and much smaller waste stream is produced, presumably making disposal simpler. However, the technique is not frequently used primarily due to high membrane replacement costs.

Conventional biological methods are not effective for treatment of highly concentrated wastewater polluted with organics such as surfactants, phenols, chlorinated compounds, pesticides, aryl-and chlorinated alkylsulfonates, polyethylene, and aromatic hydrocarbons (Dojlido, 1993). For example, it is generally difficult to biotreat waste streams having phenols above 200 ppm (Pruden and Le, 1976). Pauli and Franke (1971) and Katzer et al. (1976) have put this limit at 50 and 70 ppm, respectively. In any case all the above limits are exceeded in most of the waste streams. In addition, biodegradation processes are inherently slow and do not allow for high degrees of removal (Aurora, 2001). The sludge formed during biological treatment has to be disposed of either by land filling or by burning with a corresponding expenditure of energy following elaborate thickening and

dewatering procedures. It requires a large area of land, which is costly and may not be always available. Evidently, the biological treatment of industrial wastewater is of limited use only, and specifically designed pre-treatment processes are frequently required to reduce the impact of the toxic organics on the classical activated sludge plants, otherwise biodegradation processes fail (Yurii and Moshe, 1998).

Noncatalytic wet oxidation has been applied for the treatment of wastewaters that are toxic or refractory for biological treatment. This process becomes energetically self-sustaining with no auxiliary fuel requirement when the feed chemical oxygen demand (COD) is higher than 30 g/L, while incineration requires more than 300 g COD/L to sustain self-combustion (Imamura, 1999). However, noncatalytic wet oxidation is carried out under severe reaction conditions that necessitate high operating and installation costs. The contaminated aqueous stream is oxidized by air or oxygen at subcritical conditions at temperature from 200 to 300^{o}C and pressure from 70-230 atm (Mishra et al., 1995); while supercritical oxidation process requires even severer conditions, typically around 500 ^{o}C and 270 atm (Ding et al., 1996). At these operating conditions, the reactor is pressurized to prevent the liquid from boiling and evaporation. Due to the required large investment in high-pressure equipment and the high cost of running the reaction at high pressures and temperatures, the subcritical or supercritical noncatalytic wet oxidation is rather expensive.

The severity of oxidation conditions can be reduced by use of a suitable (cheap, stable, and resistant to poisoning) catalyst system. Catalytic wet oxidation (CWO) destroys a variety of organics released in wastewater effluents, achieving a high conversion of the organic pollutants. Such recourse to solid catalysts offers a practical technological alternative to the conventional noncatalytic or homogeneously catalyzed routes. Not only can the treatment use milder conditions (temperature and pressure), but, in principle, the catalyst can also be easily recovered, regenerated, and reused. Another considerable advantage of catalytic methods is the possibility of treating only a single pollutant, or a group of similar pollutants, in complex mixtures of pollutants (as in selective catalytic reduction) (Imamura, 1999). A less conventional technique for purifying wastewaters,

CWO improves the oxidation of the refractory compounds by reducing the number of intermediates and lowering the concentration of organics to levels that enable biological methods to be used as a complementary application. Table 1-1 lists the typical examples of the noncatalytic and catalytic wet oxidation process reported in the literature.

Table 1-1. Miscellaneous applications of noncatalytic and catalytic wet oxidation

Reference	Substrate	Treatment conditions and observations
Pradt, 1972	Chemical plant effluent containing phenol (COD=76,300 and phenol =3292 mg/L)	COD of effluent =32,500mg/L, phenol =7mg/L
Wilhelmi and Ely, 1976	Chemical industry wastewater (COD=55000mg/L and BOD =23000 mg/L)	74.5% COD reduction, 93% BOD reduction
Canney and Schaeffer, 1983	Non-chlorinated pesticides (toxic concentration=6.7-13000 mg/L)	T=225-300 ^{o}C, 94-99.6% toxic components removed
	Phenolic waste (toxic components =204-11750 mg/L)	T=280-320 ^{o}C, 95.1-99.9% toxic removed, last traces removed by treatment with ozone
De Angelo, 1983	Spent caustic liquor (COD =20660, sulfides =4000-8000, TOC =2680 and total CN^- =201mg/L)	T=178-320 ^{o}C, P=14 MPa; residual level of sulfide 1 mg/L; overall COD reduction of 62-98%
Green et al., 1983	Coal gasifier unit wasterwater	T=200-225 ^{o}C, P_{O2} =3.55 MPa, supported CuO as catalyst; 64% COD and 58% TOC removal
Baillod et al., 1985	Caustic liquor from petrochem plant (COD=70 000mg/L)	T=232 ^{o}C, t=60 min, 73% COD reduction obtained
Dietrich et al., 1985	Chlorinated organics spiked wastewater	T=280 ^{o}C, t=60 min, 92.3-99.5 chloroform and chlorobenzene removed
Chowdhury and Copa, 1986	Spent caustic scrubbing liquor	T=320 ^{o}C, P=20.7MPa, t=64min, 96.2% COD and >99.9% toxic removal
	Coke plant effluent	T=279 ^{o}C, P=10.75 MPa, t=69min, Cu^{2+} catalyst; 91.3% COD and >99% toxic removal
	Herbicide wastewater	T=281 ^{o}C, P=10.75MPa, t=60min, Cu^{2+} catalyst; 90.5% COD and >99% toxic removal

Gao et al., 1988	Cotton slurry black liquor	T=240-250 ^{o}C, P=5.4-5.9MPa, t=40min; 42-48% COD and 95% color removal
Imamura and Ando, 1989	Aliphatic compound with TOC= 2 g/L	T=200 ^{o}C, P=1.0 MPa, MnO_2/CeO_2 as catalyst; t=60min, 50% TOC removal
Ito et al., 1989	Aminaacids, amines, aminoalhogos with TOC= 2 g/L	T=200 ^{o}C, P=1.0 MPa, Co_2O_3 as catalyst; t=30-60min, 99% TOC removal
Matsuno et al., 1989	Wastewater with 11.3 and 38 g/L COD and TOC from diisopropylbenzene	T=200 ^{o}C, P_{O2}= 0.6 MPa, t=4h, 69% COD reduction
Lin et al., 1992	Caprolactam Wastewater	T=260 ^{o}C, P=6.9MPa, t=60min; 89%COD removal
	Dyeing wastewater	T=240 ^{o}C, P=6.9MPa, t=60min; 95%COD removal
Hao et al., 1992	TNT red wastewater (1:100 dilution)	T=340 ^{o}C, P=14.8MPa, 99% org carbon and COD removal
Pintar and Levec, 1994	Aromatic 1,4-chlorophenol with TOC= 0.1-0.5 g/L	T=150-190 ^{o}C, P=3.0 MPa, CuO-ZnO-CoO as catalyst; t=30-200min, 90% TOC removal
Higashi et al., 1994	Aromatic 1,4-nitrophenol with TOC=2.0 g/L	T=250 ^{o}C, P=1.0 MPa, Pt/TiO_2 as catalyst; t=30min, 93% TOC removal

As an alternate method for purifying wastewaters, CWO involving solid catalysts has been successfully applied to wastewaters discharged from petroleum and petrochemical industries that are contaminated with toxic or refractory substances inappropriate for biological treatment (Keckler et al., 1993). Catalytic studies of the oxidation of phenol, which has been frequently used as a model substance, were performed with many industrial and specially designed catalytic systems (Table 1-2).

Table 1-2. Listing of studies on catalytic wet oxidation of phenol in aqueous solution

Reference	Catalyst	Reactor type [a]	Temp (^{o}C)	Press. (atm)	C_o (g/L)	Reaction time (min)	Conversion
Katzer et al., 1976	CuO/ $\tilde{\gamma}$-Al_2O_3	S	114-200	3.4-17	3.6-5.1	9	99
Imamura et al., 1985	Ru/CeO_2	S	200	10	2.0	60	94.8

Higashi et al., 1991	$Pt/\tilde{\gamma}$-Al_2O_3	S	200	10	1.0	175	58
Jie et al., 1991	MnO_2 (TGS-3)	S	50-60	1	.5-2.0	30	90
Kochetkova et al., 1993	CuO-CoO-TiO_2	S	140-200	1.8	4-5.5	30	85
Pintar and Levec, 1992	CuO-ZnO-Al_2O_3	S	105-132	5.6	–	–	–
Lin et al., 1996	$CuSO_4$, Co_2O_3, ZnO	B	150-250	50	24.5	–	–
Lin et al., 1996	$CuSO_4$, $Cu(NO_3)_2$	B	150-250	70	15-30	–	–
Maugans, 1997	Pt/TiO_2	B	150-200	34-82	1.15	–	–
Hamoudi et al., 1998	MnO_2/CeO_2	S	80-130	30	.13-10	–	100
Hamoudi et al., 1998	Pt/Al_2O_3	S	130-175	2.0-25	.13-10	–	100
Zhang et al., 1999	Pd-Pt/Al_2O_3	B	120-170	12	0.7	–	–
Harf et al., 1999	Fe^{2+}	B	140-220	8.4-18	2.0	–	–
Aurora et al., 2001	Cu-203T	B	127-180	3.2-16	4-1150		

[a] Reactor type: B, batch; S, slurry.

Among them, packed-bed reactor is a popular choice for potential industrial application. Different catalysts and suitable operating conditions in packed-bed operation have been reported, as grouped and listed in Table 1-3.

Table 1-3. Application of packed-bed reactors in catalytic wet oxidation

Reference	Catalyst	Temp (^oC)	Press. (atm)	C_o (g/L)	Reaction time (min)	Conversion
Imamura et al., 1988	MnO_2/CeO_2	220	10	2.0	20	92.7
Pintar and Levec, 1994	CuO-ZnO-CoO	50-210	3-8	0.1-0.5	1	100
Krajnc and Levec, 1994	CuO-ZnO/ cement	380-390	230	5.0	0.25	–
Fortuny et al., 1995	CuO/ $\tilde{\gamma}$-Al_2O_3	120-160	6-12	5.0	30	80

Ding et al., 1995	Cr2O3,V2O5 /Al_2O_3	390-410	241	.23-8.4	–	–
Ding et al., 1995	Cr_2O_3	390	241	0.5	–	–
Ding et al., 1995	V_2O_5	390	241	0.5	–	–
Tukac and Hanika, 1998	Active C / Ni, V, Fe	120-160	20-50	5.0	60	100
Zhang and Savage, 1998	MnO_2 / CuO / Al_2O	380-430	250	0.1	–	–
Fortuny et al., 1999	CuO/ $\tilde{\gamma}$-Al_2O_3	120-160	30-60	5.0	60	97
Stuber et al., 2001	Active C	140-160	27-38	2.5-5	120	100
Clayton et al., 2002	Pt/TiO_2	15-205	35-47	.2-1.2	400	60

1.1 Motivation

The development of better catalysts and processes involves different stages of research. These include exploratory screening of catalyst formulations, optimizing the process conditions over the most promising catalyst as identified from screening tests, and evaluating reaction kinetics for design of the commercial reactor (Satterfield, 1980). In some cases, experiments are also carried out to study the performance of an established catalyst for the processing of a selected feedstock.

The key issue in the effective catalytic oxidation of organics in wastewater is finding a suitable catalyst (Pintar and Levec, 1994). The adequate choice of catalyst, the design and scale-up of the process is an engineering feature of eminent importance. Water-insoluble (heterogeneous) catalysts have been preferred in catalytic wet air oxidation to minimize unwanted contamination of liquid effluents. Transition metal oxides, noble metals, and metallic salts are extensively used as active components in catalytic oxidation. Oxides of V, Cr, Mn, Fe, Co, Ni, and Cu are the most active single metal oxide catalysts for a variety of gaseous oxidation processes (Spivey, 1987). These metal oxides, as well as some noble metals, have been used previously as catalysts in CWO treatment operations.

Although a diversity of catalysts has been developed for the oxidation of various organic compounds in wastewater (Luck, 1996), the lack of catalysts that are active and durable under these process conditions has prevented CWO from being fully implemented for environmental remediation. In addition, catalyst deactivation may occur due to a diversity of factors, including reduction of the catalyst surface or poisoning of the catalytic agents by halogen-containing compounds formed during CWO (Yurii and Moshe, 1998). Deactivation by fouling due to surface deposition and strong adsorption of a polymeric carbon overlayer is another kind of surface deactivation (Hamoudi et al., 1998). Furthermore, the elution of the catalyst is connected with the exposure to hot acidic water, which promotes the solubility of some metal oxides. The dissolution of the metal in the hot acidic reaction medium prevents the use of catalysts which themselves are soluble in hot acidic water or can be transformed to a soluble state during reaction in the presence of oxygen. For example, supported copper oxide is the most active catalyst for phenol oxidation in the temperature range 160-250 ^{o}C (Yurii and Moshe, 1998). Despite the fact that such Cu-based catalyst is very active in batch processes, tests using continuous reactors reveal that there is a substantial loss of activity due to the dissolution of the catalytic species in the acidic reactive medium (Alejandre et al., 2001). The activity of the same type of catalyst after five to seven runs decreased by 40% and the copper ions concentration in the solution increased to 150 mg/L (Pintar and Levec, 1994). The activity loss can also occur on active carbon and graphite supports, which are resistant to leaching in acidic medium. However, they are slowly oxidized at temperatures higher than 150^{o}C and therefore cannot be used for continuous operation over a long period of time (Beziat et al., 1999).

Some newly developed catalysts (Ru/CeO_2, Pt/TiO_2, etc.) have partially overcome the problems of activity loss, but the presence of noble metals or low surface supports make them too expensive or of too low activity for them to be considered commercially (Clayton et al., 2002; Maugans, 1997). In addition, the use of noble metals for water-phase oxidation applications appears to be limited by their high sensitivity to poisoning. Trace contaminants formed during the oxidation of phosphorus- and sulfur-containing

compounds, such as chlorine, chloride (Baker et al., 1989; Frish et al., 1994), are generally poisonous for oxidation catalysts. There have been many studies to develop efficient catalysts that are resistant to poisoning, for example, alkali- and alkaline-earth-supported catalysts which are used for the destruction of halogenated organic chemicals (Berty, 1991).

The other challenge that a catalyst needs to overcome is to reduce the severity of the CWO conditions. The typical features of CWO operation are high temperature (200-325 ^{o}C) and high pressure (5-20 MPa, higher than the vapor pressure of water at these temperatures). Further improvement of catalyst performance, however, is needed for wider use of the wet oxidation process. If a catalyst can be developed that works effectively below 150 ^{o}C, catalytic wet oxidation would be a potential process for more general water treatment (Autenrieth et al., 1991). To reduce the severity of the operating conditions, several newly developed catalysts have been proposed, such as MnO_2/CeO_2 and Pt-promoted MnO_2/CeO_2 (Hamoudi et al., 1998). Although wet oxidation of phenol over composite oxide was remarkably fast at mild temperature (80-130 ^{o}C) and pressure (0.5-2.5 MPa, O_2) conditions, the catalyst underwent severe deactivation. This deactivation was found to be induced by the formation of carbonaceous deposits on the catalyst surface, which irreversibly adsorbed on its active sites (Hamoudi et al., 1999). The catalyst's poor selectivity to CO_2 was also demonstrated to result from deposition of carbon on the catalyst surface. Promotion of MnO_2/CeO_2 with platinum improved the CO_2 yield of phenol oxidation. However, platinum-promoted MnO_2/CeO_2 was more sensitive to deactivation and exhibited systematically lower degradation rates of phenol and total organic carbon (Hamoudi et al., 1998).

Pillared clay represents a new class of microporous materials that have potential for use as catalysts. A great deal of progress has been made in understanding these materials, particularly their catalytic behavior. The impetus behind the original work was to create three-dimensional porous structures from two-dimensional clay minerals. It was expected that pores larger than those available in zeolites would be obtained (Moser, 1996). Recently, by using powdered catalyst and hydrogen peroxide as the oxidant, clay-based

catalysts pillared by mixed Al-Fe complexes have shown encouraging results for oxidizing organic compounds in aqueous media in a slurry laboratory-scale reactor. Under mild experimental conditions (atmospheric pressure, $T < 70^{o}C$) and in low excess (20 %, mole) of hydrogen peroxide, 80% of the initial amount of phenol and significant total organic carbon (TOC) were converted mainly to CO_2 within 4 h. The Al-Fe pillared clay catalyst can be used several times without significant catalyst leaching and deactivation (Barrault et al., 2000). About 60% of the iron is bonded to the aluminum pillars. The remaining iron is likely engaged in small oxide clusters dispersed in the solid, inside or outside the porosity. The low observed leaching means that whatever their location, the iron species are highly stabilized by the clay matrix (Barrault et al., 2000). Therefore, the Al-Fe pillared clay is going to be employed in this work in order to further explore its potential.

The pathway to develop an optimum catalyst design starts with screening of prepared catalysts by evaluation of catalytic properties. If the desired results are not achieved, then samples with modified properties are prepared and the screening procedure is repeated until a promising catalyst is found. After the catalyst is selected, the reactor and process design for the catalytic reaction should also be addressed. In selecting an appropriate reactor, the catalysts need to be tested in their commercially applied size and shape reactors (Bej et al., 2001).

The choice of a proper experimental apparatus is of utmost importance in order to obtain reliable data at a minimum cost. The CWO is usually carried out in packed-bed reactors, bubble columns, mechanically agitated reactors, etc. The reactions proceed differently depending whether they are carried out in a slurry reactor or a packed-bed reactor. For instance, formation of phenolic polymers was observed in CWO of phenol using a copper oxide catalyst in slurry reactors (Sadana and Katzer, 1974), whereas no polymers were found when a packed-bed reactor was used (Fortuny et al., 1995). The tentative explanation is based on assumed simultaneous presence of two different reactions for phenol removal: the classical oxidation and the condensation reactions that form polymers. From a chemical point of view, the very high liquid to solid ratio in the

slurry reactor could enhance the formation of heavy polymers through oxidative coupling. These polymers could irreversibly adsorb on the catalyst surface and progressively block the active sites, thereby lowering the rate of phenol removal and preventing further oxidation of intermediate molecules (Pintar and Levec, 1994). Consequently, reactors with high liquid-to-catalyst volumetric ratio (such as a slurry system) should not treat wastewaters containing pollutants that tend to polymerize (e.g., aromatic compounds) (Pintar and Levec, 1997).

On the other hand, the oxidation of phenol towards intermediates (aromatic compounds, carboxylic acids) and end product (carbon dioxide) was experimentally found to be strongly enhanced in the packed bed system (Fortuny et al., 1995). The same conclusion was also drawn via the simulation by Larachi et al., (2001). After analyzing the CWO performance of different reactor configurations, such as packed-beds, three-phase fluidized beds, and slurry bubble columns, the simulation results showed that packed-bed reactors should outperform fluidized beds and slurry bubble columns.

For the reaction type: A (g) + ν_B B (l) $\rightarrow$ Products, where the gaseous species, A, reacts with the aqueous species, B. As pointed by Khadilkar et al. (1996), most gas-liquid reaction systems promoted by a solid catalyst can be classified as being liquid reactant or gas reactant limited, which can be delineated by the ratio of the diffusion fluxes of the two reactants scaled by the ratio of stoichiometric coefficients ($\gamma=(D_{eB}C_{Bi}/\nu_B(D_{eA}C_A^*)$. It is indicative of the relative availability of the species at the reaction site. The reaction can be considered gas reactant limited for $\gamma>>1$ or liquid reactant limited for $\gamma<1$. For liquid-limited reactions upflow reactor should be preferred as it provides for complete catalyst wetting and for the fastest transport of the liquid reactant to the catalyst. For gas-limited reactions, downflow reactor, especially at partially wetted conditions, is to be preferred as it facilitates the transport of the gaseous reactant to the catalyst from the dry portion of the catalyst.

Packed-beds possess high catalyst to volume ratio, but they require a stable and non-deactivating catalyst that is active at low temperatures, such as the Al-Fe pillared clay catalyst. The newly developed extrudates of Al-Fe pillared clay catalyst, suitable for

packed-bed operations, have been manufactured for further investigation utilizing different oxidants (e.g., peroxide only and air only). The catalyst particles, in cylindrical form (2 × 8 mm, approximately), were manufactured and supplied by Professor N. Papayannakos' Process Analysis and Plant Design Group, at the National Technical University of Athens (NTUA), Athens, Greece. The intrinsic kinetics has been studied using hydrogen peroxide as oxidant and reported by Barrault et al., (2000), which showed that the Al-Fe pillared clay catalyst was stable and active at mild conditions. Hence, before the performance of this catalyst can be evaluated in packed-bed reactors for the purpose of process development and optimization, the apparent kinetics and the catalyst performance need to be studied in a basket stirred tank reactor using air and/or hydrogen peroxide as the oxidant. The apparent kinetics expression needs to be developed for reactor scale modeling, and a comparison between CWO using air and/or peroxide needs to be analyzed. The fate of both phenol and intermediates will be followed. This requires reliable kinetic data, which are usually obtained in slurry reactor or basket stirred tank reactor (BSTR). The latter could give the apparent kinetics, which is of interest for evaluating the technology of phenol catalytic oxidation using extrudate catalysts. It should be noted that in such an approach intrinsic kinetics are not necessarily obtained, as extrudates and not fine particles are used, because the diffusion resistance within the catalyst particles may mask the intrinsic reaction kinetics. Quantifying the intraparticle diffusion is important to optimize the design of the porous particle in the packed bed. This can be accomplished by testing the reaction rates based on different catalyst pellet sizes.

Based on the basket reactor studies, and the knowledge of whether the reaction is gas or liquid reactant limited, the performance of the pillared clay catalyst for the continuous operation will be tested experimentally in a packed-bed reactor with co-current downflow and upflow. Clearly for a lab scale close to isothermal reactor a 1D model is sufficient. Scale up will be done at equal LHSV and the effect of velocities on apparent rate at equal LHSV will be examined.

In summary, the processes of CWO fall into the category of gas-liquid-solid reactions, which are still not at a mature stage of technological development. Due to the complex geometry of the tortuous pore space and the complicated fluid-fluid and fluid-particles interaction, the complexity of multiphase flow interaction, plus the difficulty in handling the complex kinetics remains unresolved. There is an urgent need of new knowledge and information on packed-bed reactors for the CWO process, which will be investigated in this work.

1.2 Objectives

The overall objective is to study the performance of Al-Fe pillared clay catalyst for CWO of phenol in aqueous solution in packed-bed reactors, and identify conditions needed for complete mineralization. The following issues are to be addressed:

(1) The catalyst characterization and apparent kinetics for such oxidation reactions via different oxidants in a basket semibatch reactor;

(2) The performance of the bench-scale packed bed (upflow and/or downflow) using the proposed pillared clay catalyst for phenol oxidation in aqueous solution and optimize operating conditions;

(3) Application of a suitable two-phase packed-bed model for process evaluation and design.

In order to address these issues, the work consists of the following goals:

1) In a stirred basket reactor, evaluate the pillared clay extrudate type catalyst and its apparent kinetic rates for phenol oxidation via air by using the analysis procedures shown in Figure 1-1. Develop suitable apparent kinetic models. These investigations should lead to the selection of the most efficient and economical oxidation conditions (i.e., temperature, pressure) for application in packed-beds. In addition, test different particle sizes to estimate the diffusion effect.

2) Evaluate the activity of the pillared clay type catalyst for CWO treatment using trickle-bed (downflow) and packed-bed bubble column (upflow) reactors. Experimentally

investigate the effect of different operating conditions and operating modes (downflow / upflow) on the performance of the pillared clay catalysts for the treatment of phenol in water.

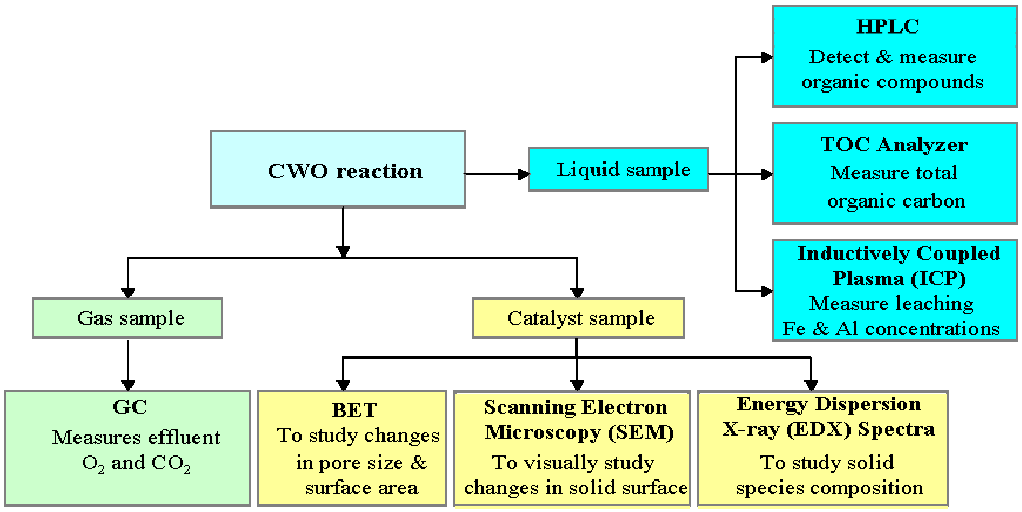

Figure 1-1. Flow scheme of the analysis procedure for liquid, gas, and catalyst samples.

3) Characterize the pore structure (size, surface area) for fresh and used catalyst pellets. Study the catalyst stability.

4) Apply a suitable model with adequate features to simulate the process of CWO in packed-bed reactors and validate the simulation results against the experimental data. Such model involved parameters for taking care of incomplete wetting of catalyst, external mass transfer resistance, and nonideal flow pattern of liquid.

1.3 Thesis Structure

The thesis contents are structured in the following manner.

Chapter 1 represents a general introduction in which the background, motivation and overall objectives of this study are given.

Chapter 2 describes the implementation of the stirred-tank experiments to evaluate the catalyst, investigate the apparent kinetics and estimate the intrapaticle diffusion effect. The variables studied include reaction temperature, air pressure, solution pH, initial phenol concentration, catalyst loading concentration, and catalyst dimension.

Chapter 3 provides the experimentation details on the catalyst activity and performance of packed-bed reactor with two modes of operation, downflow and upflow. The investigated operating parameters are liquid hourly space velocity (LHSV), gas flowrate, feed concentration, and reactor temperature and pressure. The interaction between the reactor hydrodynamics, mass transfer, and reaction kinetics is discussed.

Chapter 4 highlights the experimental study on catalyst stability and catalyst characterization related to pore size distribution, specific surface area, surface topology, and active site composition.

Chapter 5 discusses the selected model scheme and its simulation results. The simulation results provide valuable insights on the effect of operating conditions on the reactor performance, which are useful in interpreting the experimental data, designing further experiments and optimizing the process conditions for industrial scale operations.

Chapter 6 summarizes the thesis accomplishments and broaches the issues that deserve future research efforts.

To comply with the thesis format requirement, each chapter is written as an integrated manuscript which consists of (i) introduction of the topics, (ii) results and discussion, and (iii) summary.

Chapter 2

Kinetics Investigation

2.1 Introduction

The development of efficient and inexpensive processes for wastewater treatment under intermediate conditions is of considerable interest for industrial activities. One feasible alternative is catalytic wet oxidation (CWO), which uses air (oxygen), ozone, or hydrogen peroxide as the oxidative agent. Although a packed-bed reactor has been shown to be more suitable for the CWO process than a slurry bubble column (Larachi, et al., 2001), further understanding is needed before the performance of pillared clay catalyst can be evaluated in packed-bed reactors.

The kinetic studies can be carried out under different sets of experimental conditions depending on whether the kinetic data is generated in the presence or absence of internal or external mass transfer limitations. Accordingly, experiments can be conducted in two levels: (i) Experiments that are carried out using a fine size of catalyst particles and under appropriate conditions to eliminate both internal and external mass transfer limitations. This gives the intrinsic kinetics of the catalyst. (ii) Experiments that are conducted using commercial size catalyst but eliminating only the external mass transfer resistances. This provides the apparent kinetic model. Although apparent kinetic models are not usually favored for scientific or academic studies, it has frequently been used by the industrial researchers for the scale-up of commercial reactors (Bos et al., 1997). This is because it helps predict the performance of the catalyst in the form in which it is manufactured and eliminates lots of modeling studies for incorporating the diffusional effects. However,

such kinetics cannot be extrapolated to a different catalyst shape. Thus, it is advisable to conduct such kinetic studies when the shape of the catalyst has been decided for other process application. The apparent kinetics needs to be studied in a stirred basket reactor.

Although we attempted the use of hydrogen peroxide as an alternative oxidant, as described in the next section, the cost and corrosion issues prevent us from its further application. Therefore, air oxidation of aqueous phenol becomes our focus. To study the efficiency of air oxidation, the temperature, oxygen partial pressure, phenol concentration, and catalyst concentration were varied over a wide experimental range. Global kinetic models are proposed to represent the experimental observations of phenol removal, and their fit to those experimental data is compared.

2.2 Hydrogen Peroxide (H_2O_2) Oxidation

Employing hydrogen peroxide as the oxidant, the CWO of phenol was carried out in a semibatch basket reactor over extrudates of Al-Fe pillared clay catalyst. The details of the peroxide oxidation can be found in (Guo and Al-Dahhan, 2003 a). For the sake of conciseness, only the summary is given in this section. Operational parameters were studied under the following rather mild conditions, as listed in Table 2-1. Under these conditions, the Al-Fe pillared clay catalyst achieves a total elimination of phenol and significant mineralization (80-100%) of total organic carbon (TOC).

Table 2-1. Operating conditions for peroxide oxidation

Property	Range
Temperature, ^oC	25 -90 ^oC
Total pressure, MPa	0.1
Catalyst particle size, mm	$\phi 2 \times 8$
Catalyst loading, g/L	0-10
Input H_2O_2 concentration, mol/L	0.15-0.6
Phenol feed concentration, mg/L	100-2000
Initial solution pH	3.9-4.0

Temperature increase favors phenol and TOC removal rates for the studied conditions in the range of 25-90 ^{o}C. The temperature effect on the phenol removal rate from 70 to 90 ^{o}C is not as significant as the effect of increasing the temperature from 50 to 70 ^{o}C, because of the higher decomposition rate of H_2O_2 at higher temperature. A higher initial rate of phenol removal results from a higher H_2O_2 concentration, which also allows faster degradation of intermediate products. The homogeneous reaction in the absence of catalyst is pronounced. Still, the presence of the catalyst significantly enhances the oxidation rate of phenol. This catalyst can be used several times without any change in its catalytic properties. In addition, the cumulative elution of Al-Fe iron in three experiments (4 hours each) was found to be less than 0.2% of the total iron content in this catalyst.

The apparent kinetics of the peroxide oxidation was treated using a homogeneous-heterogeneous model, which reflected the homogeneous noncatalytic reaction oxidation based on a set of second-order reactions and the heterogeneous catalytic reaction pathway in the framework of a LHHW scheme.

2.3 Air Oxidation

Because of the noticeable corrosion and undesirable H_2O_2 decomposition, we restrained our efforts on H_2O_2 oxidation and focused on oxidation process by air only. The details of experimental setup and observations are given in the following subsections.

2.3.1 Experimental Setup

The experiment setup was designed to withstand the conditions of high temperature (up to 500 ^{o}C) and high pressure (up to 6 MPa). In a stainless steel basket stirred tank reactor (BSTR), the liquid phase was in batch operation, while the purified air of zero grade was continuously fed into the reactor. The experimental scheme is depicted in Figure 2-1. The pressure gauge, gas inlet, and cooling water feed line were mounted on the top of the reaction vessel. The electric heating jacket and PID temperature controller

held the temperature of the liquid phase constant within ± 0.5 ^{o}C. Because of the small amount of catalyst available, reactors using batch autoclave are typically used for this stage of initial catalyst screening. The reactor was charged with a known concentration of phenol solution and pure nitrogen at a total pressure of 1.0 MPa before the reactor was heated to the reaction temperature. Once the temperature became steady, a sample was withdrawn before sparging air to a predetermined pressure level. From then on, the reactor pressure and airflow rate were maintained constant.

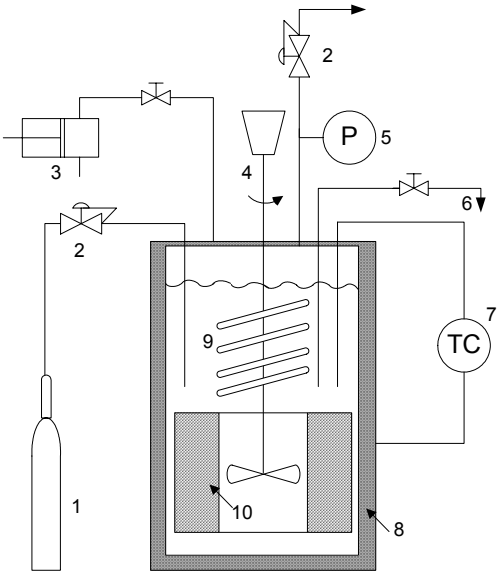

Figure 2-1. Diagram of the experimental setup.

1. Air cylinder; 2. Pressure controller; 3. Positive displacement pump; 4. Magnetic drive; 5. Pressure gauge; 6. Liquid sampling; 7. Temperature controller; 8. Heating jacket; 9. Cooling coil; 10. Catalyst basket.

The range of catalyst loadings (0-10 g/L) and the initial phenol concentrations (500-2000 ppm) were the same as in the work of peroxide oxidation, whereas the ranges of experiment temperatures (90-150 ^{o}C) and total pressures (P = 0.8, 1.5, 2.5 MPa) were different. The investigate conditions for kinetics study over extrudates of Al-Fe pillared clay catalyst are listed in Table 2-2.

Table 2-2. Operating conditions for air oxidation

Property	Range
Temperature, ^{o}C	90-150
Total pressure, MPa	0.8- 2.5
Catalyst particle size, mm	$\phi 2 \times 8$
Catalyst loading, g/L	0-10
Phenol feed concentration, mg/L	500-2000
Initial solution pH	3.9-4.0

The concentration of organics, the total organic carbon (TOC), and the pH value of liquid samples were the key variables measured at preset time intervals. The phenol conversion and product distribution were analyzed by high-performance liquid chromatography (HPLC) with a system consisting of a Waters 510 HPLC pump, a Micromeritics 725 autoinjector, and an LDC/Milton Roy SpectroMonitor 3000 as detector. UV detection was employed at λ = 211 nm. The column contained Waters Spherisorb 5-μm ODS2 (4.6 × 250 mm) as the stationary phase and a mixture of 35/65 (methanol/water, v/v, HPLC grade) as the mobile phase. The flow rate of the mobile phase was set to be 1 ml/min. Total organic carbon (TOC) was detected by a Shimadzu TOC-500 analyzer. Total carbon (TC) was measured first, followed by inorganic carbon (IC) measurement. TOC was determined by subtracting IC from TC. The evolution of the pH value of the liquid sample was tracked by a model IQ240 pH meter from Scientific Instruments Inc.

The reactor was equipped with a six-blade turbine-type impeller mixer, with the rotation speed being increased until the external mass-transfer resistance was minimized. The very high diffusivity of oxygen in the gas phase and its low solubility in water mean the insignificance of gas-side mass-transfer resistance. The external mass transfer resistance from liquid phase to the catalyst surface depends on the level of turbulence in

the liquid phase. The impeller speed was kept at 800 rpm in order to ensure that the reaction was kinetically controlled under the employed experimental conditions.

2.3.2 Liquid Sample Composition

By using the HPLC setup, the retention time of a single compound was identified by injecting pure samples of the expected partial oxidation products. Then, by using aqueous samples of known composition, calibration curves were developed for each detected intermediate product. Phenol (Ph, >99.5% purity) was purchased from Sigma-Aldrich Corporation. Analytical-grade hydroquinone, benzoquinone, oxalic acid, acetic acid, and catechol used to identify the reaction intermediate were also supplied by Sigma-Aldrich Corporation.

A series of adsorption peaks were observed in liquid chromatograms of the sample withdrawn at different retention times. The main detected intermediates in the product effluent were acetic acid, catechol, and hydroquinone. Oxalic acid and benzoquinone were also identified in measurable quantities. However, malonic and formic acids were detected only as traces, below 10 ppm. No other compounds were detected in measurable amounts. No condensation products were found in the exiting solution or deposited on the catalysts.

Figure 2-2 shows the history of product distribution sampled at different reaction times. Quinone-like products such as hydroquinone, benzoquinone, and catechol were identified in the first stages of the phenol oxidation pathway. These byproducts need to be removed because they are as toxic as phenol. Benzoquinone itself could lead to the observed color change of the reacting solution, whereas fresh phenol solution is colorless. With increasing reaction time, the color of the solution gradually changed from light to dark brown, and then back to light brown. The dark brown color is due to the formation of benzoquinone during phenol oxidation. With further oxidation, benzoquinone is mineralized or degraded to low-molecular-weight organic acids, leading to a colorless solution. On the other hand, the acetic acid and oxalic acid still remained, which dropped the pH from its initial value to the range of 2.8-3.0. This behavior is due to the resistance

of low-molecular-weight carboxylic acids, acetic acid in particular, to catalytic wet oxidation. This phenomenon confirms the general statement that the first step of phenol oxidation corresponds to the formation of intermediate ring compounds, while the subsequent period represents the formation of ring cleavage intermediates, mainly carboxylic acids (Devlin and Harris, 1984).

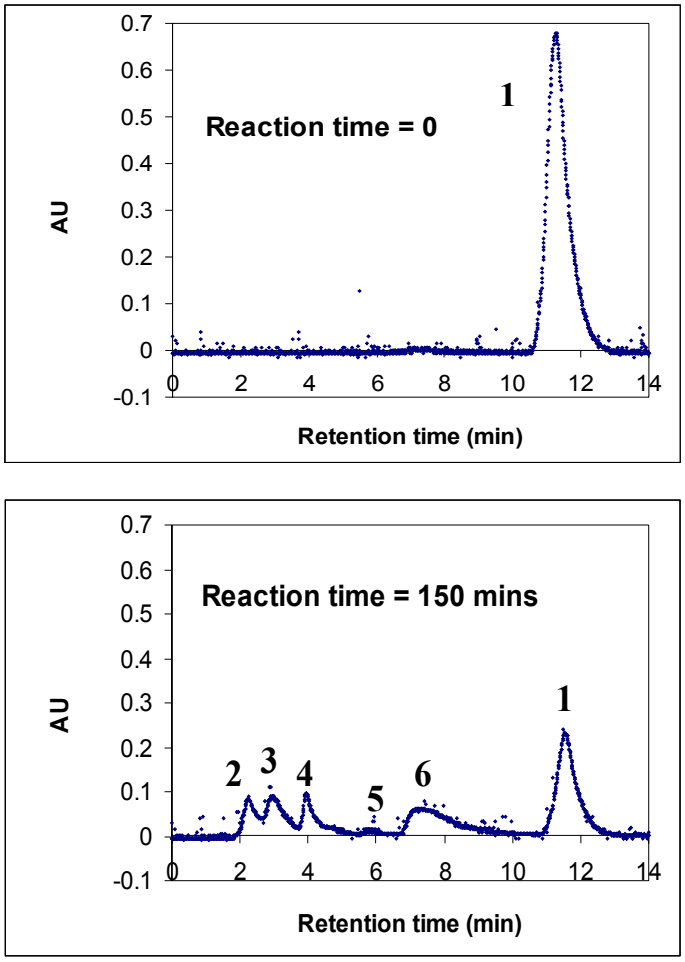

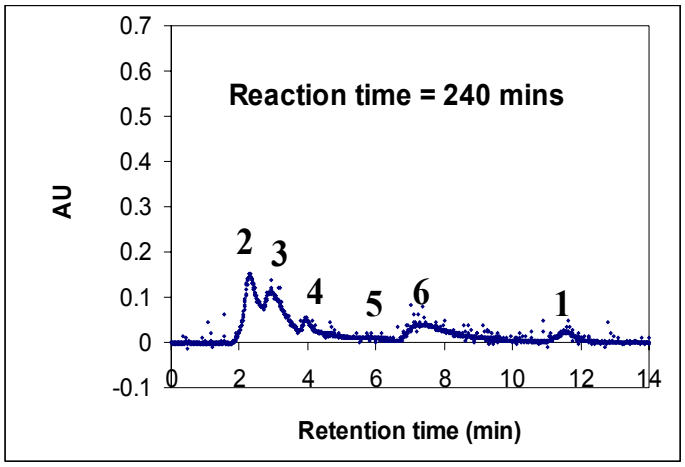

Figure 2-2. Typical liquid chromatograms of organics in liquid sample.

1. Phenol; 2. Acetic acid; 3. Oxalic acid; 4. Hydroquinone; 5. Benzonquinone; 6. Pyrocatechol.

2.3.3 Effect of Initial Solution pH

A fresh solution of phenol, a relatively weak acid with initial pH value between 5.7-5.9, was used in the current experiments, unless it underwent pH adjustment. When H_2O_2 was used to oxidize the aqueous phenol, pH values between 3 and 4 led to the least decomposition of H_2O_2 and higher amounts of available hydroxyl radicals in the solution (Bishop et al., 1968). Without pH adjustment, phenol conversion curves show a sigmoidal profile, which is typical of radical reactions. Two different regions exist, with the initial part of the curve standing for the induction period and the part after the inflection point representing the steady state. The initial rate of oxidation is markedly affected by pH, since the oxidation rate with pH adjustment to 4.0 can be three times greater than without pH adjustment. The steady-state activity, however, is a much weaker function of the pH, since the phenol conversion curves fall almost into the same line when the steady state is reached. In the present work with air as the oxidant, the pH effect was also tested by adding sulfuric acid into the solution to adjust the initial pH value to 3.9-4.0. As shown in Figure 2-3, none of the curves show an induction reaction region, which is different from the observation for the oxidation using H_2O_2. However, a similar gap exists between the

solution with and without pH adjustment. For temperature at either 110 ^{o}C or 130 ^{o}C, it is evident that a solution with the pH adjustment led to a phenol removal rate two times greater than without pH adjustment. This observation confirms the well-known fact in phenol chemistry that the optimum pH for the maximum reaction rate is about 4.0 (Sadana and Katzer, 1974). Consequently, all of the following experiments were based on an initial solution pH of 3.9-4.0.

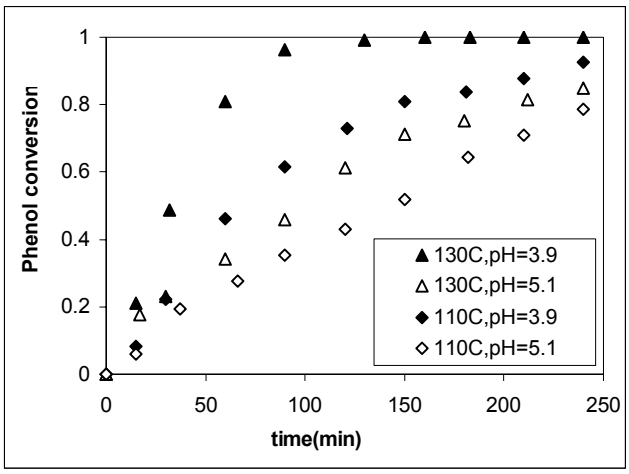

Figure 2-3. Effect of initial solution pH on the catalytic phenol conversion (500 ppm phenol, 6.6 g/L catalyst, 1.5 MPa).

2.3.4 Effect of Temperature

The performance of pillared clay catalyst at different temperatures in the range of 90-150 ^{o}C is shown with respect to time, in Figure 2-4a as phenol conversion and in Figure 2-4b as intermediate carbon concentration. It is seen that temperature strongly affects the evolution of phenol and intermediate carbon. Higher phenol removal rates were observed at higher temperatures. A 20 ^{o}C increase of temperature can lead to a doubled phenol removal rate when the reaction time is 1 h. This strong effect of temperature on phenol removal rate was not observed when H_2O_2 acted as the oxidant, where the reaction rate increased by only 50% with an increase of 20 ^{o}C at 1 h of reaction time. However, at the same temperature, H_2O_2 can lead to a higher reaction rate than air only. Continuously

added H_2O_2 could eliminate 500 ppm of aqueous phenol within 175 min at 90 ^oC. In contrast, at 90 ^oC, it was found in the present work that air removed 500 ppm of phenol completely within 300 min.

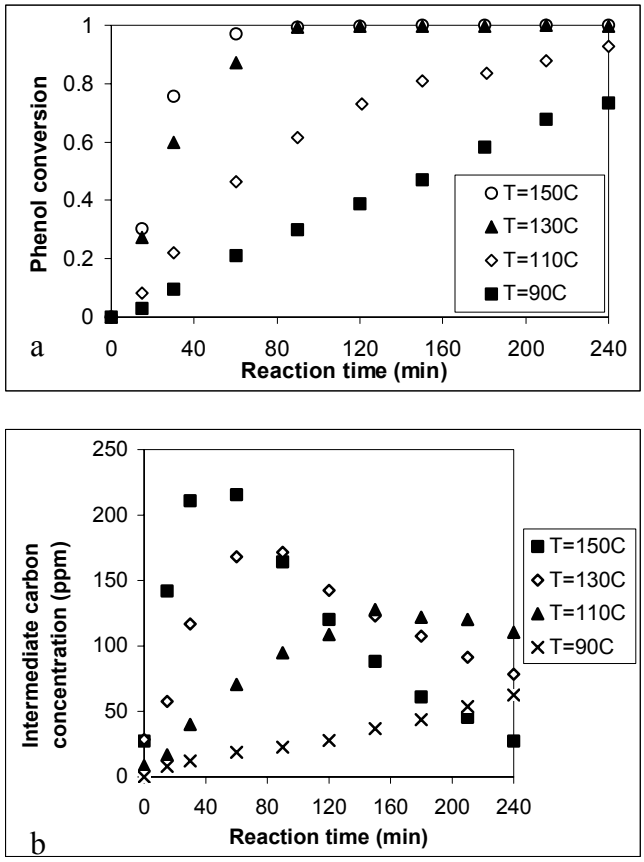

Figure 2-4. Effect of temperature on (a) phenol conversion and (b) Intermediate carbon concentration (500 ppm phenol, 6.6 g/L catalyst, 1.5 MPa).

The faster reaction rate for H_2O_2 is due to the fact that H_2O_2 is a stronger oxidant, and for air only, mass transfer of oxygen from the gas phase to the liquid phase is required. Nevertheless, several concerns exist if H_2O_2 is taken as the oxidant. The destruction rate of H_2O_2 to O_2 and H_2O increases with temperature. In addition, reactor corrosion and reagent cost also make H_2O_2 an unsatisfactory oxidant in wastewater treatment. Therefore, as a relatively cheap and well-established process, WAO should be given first

priority when one wants to choose a feasible method for wastewater treatment. It was found in the present work that air could completely remove phenol within 100 min at 130 ^{o}C. Compared with the typical industrial CWO operation temperature (200-325 ^{o}C), the lower temperature required by pillared clay catalyst might highlight its savings potential in the sense of energy and reactor construction cost.

Intermediate carbon concentration was derived to evaluate the degree of intermediate carbon mineralization in the liquid phase during the course of oxidation. Clearly, the removal of phenol occurs much faster than the degradation of intermediate carbon. The concentration profiles in Figure 2-4b display the maximum, after which the concentrations of intermediate carbon decreased. Eventually, plateaus are expected to be reached, because the short-chain organic acids formed from the phenol oxidation are stable and refractory to further oxidation into CO_2 and H_2O in CWO. Higher temperature resulted in a lower level of plateau, indicating the formation of less recalcitrant intermediates, such as carboxyl acids.

2.3.5 Effect of Initial Phenol Concentration

If we know how the global reaction rate responds to changes in the concentrations of the components in the reactant stream, we can draw the functional form of the kinetic rate law. Therefore, the effect of the initial concentration of phenol was investigated in the range of 500-1500 ppm at 130 ^{o}C and 2.5 MPa. Under otherwise identical conditions, the phenol conversion with time at three initial phenol concentrations demonstrates that a lower conversion results from higher initial phenol concentration, as shown in Figure 2-5. When the same range of aqueous phenol was oxidized by H_2O_2 at 70 ^{o}C and atmosphere pressure, a similar effect of initial phenol concentration on the reaction rate was observed. In the present work, when the solution was more concentrated, e.g., 1500 ppm, the pillared clay catalyst remained active and completely removed phenol within 4 h of reaction time. However, Larachi et al. (1999) found that deactivation was observed for MnO_2/CeO_2 catalyst at phenol concentrations in the range of 1,000-10,000 ppm, since each phenol oxidation reaction stopped after 1 h of reaction. The explanation was given

as a laydown of foulant or carbonaceous deposits which irreversibly adsorbs on the catalyst's active sites until their total blockage (Hamoudi et al., 1999). It is known that, during the CWO of phenol, polymeric compounds can be formed and promoted by acidic sites on the catalyst, which can adsorb at the surface of the catalyst and decrease its activity (Pintar and Levec, 1992). In comparison, pillared clay catalyst shows more resistance to polymeric fouling, although further detailed investigation into higher concentrations of phenol solution and longer reaction times is necessary.

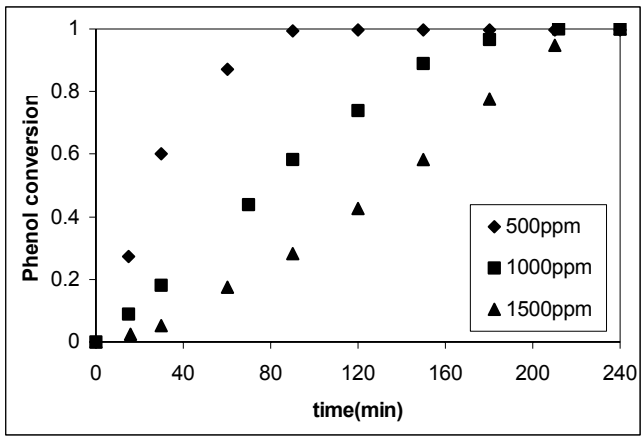

Figure 2-5. Effect of initial phenol concentration on phenol reduction by catalytic oxidation (130 ^{o}C, 2.5 MPa, 6.6 g/L catalyst).

2.3.6 Effect of Air Pressure

Compared with atmospheric pressure employed for H_2O_2 oxidation, for air oxidation, high pressure was maintained in the reactor to increase the dissolved oxygen concentration in the liquid phase. At elevated temperature and in the presence of water and catalyst, oxygen is capable of different oxidation reactions. It can substitute an oxygen atom into an aromatic ring to form a dihydric phenol or quinone. Oxygen is also capable of attacking carbon to carbon double bonds to form carbonyl compounds, and in oxidizing alcohols and carbonyl groups to form carboxylic acids (Devlin and Harris, 1984). Because the concentrations of these substances in the aqueous phase were very low, the oxygen concentration in the liquid phase was considered equal to the solubility

in water. In pure water the solubility of oxygen has been shown to follow Henry's law at high temperature and pressure (Crammer, 1980). The practical Henry's law constant was estimated from the data published by Crammer (1980). By assuming that the vapor phase behaves as an ideal solution, the fugacity of the pure gas ϕ_g, expressed as the deviation from ideal gas behavior, is evaluated at the temperature and total pressure of the vapor phase (Walas, 1985). Taking into account the vapor pressure of water, partial pressure of O_2 was calculated from the total pressure. The applied air pressure exceeded the vapor pressure of the liquid phase at a given temperature, so that the wet air oxidation was kept in the liquid phase. Corresponding to the temperature range of 90-150 ^oC, the value of equilibrium vapor pressure is from 0.1 to 0.45 MPa (Lin et al., 1996).

Figure 2-6 shows the effect of air pressure in the range of 0.8-2.5 MPa on phenol removal at 130 ^oC, where the equilibrium vapor pressure is 0.25 MPa. A drastic change of phenol conversion was noticed when the air pressure was changed from 0.8 to 1.5 MPa. However, only marginal enhancement of phenol oxidation rate resulted from air pressure higher than 1.5 MPa, which has also been reported for high concentration wastewater treatment at 200 ^oC over catalyst $CuSO_4/Co_2O_3/ZnO$ (Lin et al., 1996).

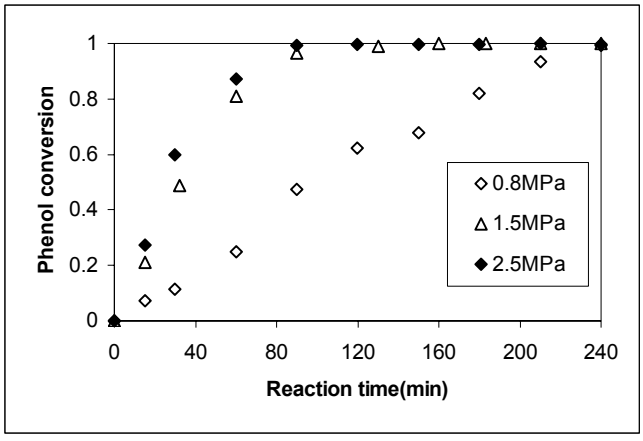

Figure 2-6. Effect of air pressure on phenol conversion during CWO (130 ^oC, 500 ppm phenol, 6.6 g/L catalyst).

2.3.7 Effect of Catalyst Loading

Phenol oxidation conversion was investigated at 110 ^{o}C and 1.5 MPa air pressure over different catalyst loadings. Uncatalyzed homogeneous oxidation led to phenol conversion of 6% at 1 h to 15 % at 4 h. Therefore, not considering homogeneous reaction would not cause considerable error in the global kinetics derivation. In fact, most CWO studies have utilized pure O_2 or air as oxidant and found no significant effect of the homogeneous reaction exists (Hamoudi et al., 1999). As shown in Figure 2-7, the heterogeneous reaction with the presence of catalyst significantly enhances the oxidation rate of phenol. A similar observation was also reported for heterogeneous oxidation of phenol when H_2O_2 acted as the oxidant. However, the homogeneous reaction due to the oxidation of H_2O_2 is pronounced, which is different from the observation of the present work. Even though the solution is acidic and at high temperature, the deactivation of pillared clay catalyst due to fouling and leaching of active substance was insignificant.

If the reaction took place only on the surface of the catalyst via either a radical or nonradical mechanism, the observed rate per unit weight of catalyst would normally be independent of the catalyst concentration. In other word, the observed rate would be always proportional to the weight of catalyst, regardless of the catalyst concentration. However, the observed catalytic reaction rate per unit weight of catalyst shown in Figure 2-7 turns out to be a function of the catalyst concentration. Such behavior indicates that the reactions involve a free-radical mechanism, which includes the initiation of a chain on the catalyst surface and the propagation of the reaction chain in the liquid bulk solution.

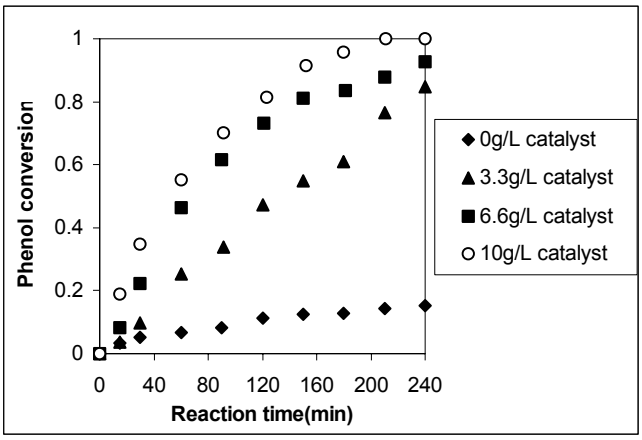

Figure 2-7. Effect of catalyst loading on phenol oxidation (110 ^{o}C, 500 ppm phenol, 1.5 MPa).

2.3.8 Apparent Reaction Kinetics

Conversion of phenol to daughter organics or inorganic carbon is the main objective of current research for wastewater treatment. Hence, an apparent rate law for phenol removal is important for evaluating the technology of phenol catalytic oxidation using extrudate catalysts. It should be stressed that such kinetic approach does not correspond to actual intrinsic kinetics as the extrudates and not fine particles have been used. The effect of diffusion limitation within the catalyst particles may mask the intrinsic reaction kinetics. However, the apparent kinetics studied can be used in scaling up and process development studies.

For the catalytic oxidation of aqueous phenol or similar organic pollutants, the apparent kinetic models proposed in the literature are in terms of either the power law (Sadana and Katzer, 1974) or more complex equations based on adsorption-desorption mechanisms, i.e., Langmuir-Hinshelwood-Hougen-Watson (LHHW) models (Pintar and Levec, 1994). Both have provided reasonable simulations of the observed degradation kinetics for the majority of water pollutant compounds explored to date. When H_2O_2 acted as the oxidant, we suggested a comprehensive network model to account for the significant reaction in both the homogeneous liquid bulk phase and on the heterogeneous catalytic surface. The reaction kinetics were taken as first-order for both the organic

reactant and H_2O_2 for the homogeneous oxidation, while a LHHW model was proposed for the heterogeneous oxidation. In contrast, the present work neglects the homogenous reaction and focuses only on the heterogeneous reaction.

To account for the effect of catalyst loading on the CWO reaction rate, different correlations have been proposed in the literature. When only one catalyst concentration is used to obtain the kinetic model, the reaction rate is assumed to be directly proportional to the catalyst concentration. (Pintar and Levec, 1994; Shende and Levec, 1999; Hamoudi et al., 2001). However, when this variable is modified over an interval, it is observed that the reaction rate does not increase linearly with the catalyst concentration. This fact is accounted for in the kinetic model by expressing the catalyst concentration in terms of an empirical correlation (Aurora, et al., 2001) Thus, the actual phenol disappearance rate could be expressed as equation (2-1).

$$-\frac{d[A]}{dt} = r_H C_{cat}^n \qquad (2\text{-}1)$$

where the initial conditions are: $[A] = [A]_0$.

A unique kinetic model should be constructed which reasonably matches the physical mechanism and fits quite adequately the experimental observations. The irreversible oxidation reaction consists of the following steps occurring in series: the dissolution of oxygen from the bulk gas phase to the bulk liquid phase, the competitive or parallel adsorptions of the dissolved oxygen and phenol on the catalyst active sites, the surface reactions due to the enhanced compounds' reactivity on the catalyst active centers. Based on the reaction mechanism where the steps of adsorption and desorption are assumed to be instantaneous compared to surface reaction, the kinetic equations proposed for the heterogeneous contribution, r_H, are listed in Table 2-3. These models include most of the kinetic expressions found in the literature for CWO of aqueous organic pollutants (Aurora, et al., 2001; Hamoudi et al., 2001, Shende and Levec, 1999; Pintar and Levec, 1994). The simplest form of surface reaction rate could be correlated by the power law kinetic model M1. The LHHW rate laws are commonly used to correlate heterogeneous catalytic kinetics. Based on the LHHW rate laws, model M2 consists of reversible

adsorption of phenol and oxygen molecules on the same catalyst site on the catalyst surface and of a rate-determining irreversible surface reaction step between the adsorbed phenol and adsorbed O_2. Model M3 is similar to M2 in terms of its single site mechanism, except that oxygen molecules undergo the dissociation and the surface reaction occurs between adsorbed oxygen atoms and the adsorbed phenol. On the other hand, if the dissociated oxygen and phenol adsorb on distinctly different active sites on the catalyst surface, then the surface reaction rate is depicted as model M4. The dual site adsorption mechanism in model M4 was also employed in our previous work for peroxide oxidation. In all rate expressions, k_1 is the rate constant for the surface reaction step, and K_A and K_{O2} are the adsorption equilibrium constants for phenol and oxygen on the catalyst surface, respectively. These parameters were identified based on the heterogeneous experimental data. As discussed earlier, the heterogeneous experimental data were measured at four different temperatures, three different phenol initial concentrations, three different O_2 partial pressures, and three different catalyst loading concentrations.

Table 2-3. Kinetic models proposed for air CWO heterogeneous reaction

Kinetic model	Equation	Mechanism
M1	$r_H = k_1[A]^p[O_2]^q$	Empirical approach
M2	$r_H = \frac{k_1 K_A K_{O_2}[A][O_2]}{(1 + K_A[A] + K_{O_2}[O_2])^2}$	Single site, $O_2 + * \Leftrightarrow O_2^*$
M3	$r_H = \frac{k_1 K_A K_{O_2}^{0.5}[A][O_2]^{0.5}}{(1 + K_A[A] + K_{O_2}^{0.5}[O_2]^{0.5})^2}$	Single site, $O_2 + 2* \Leftrightarrow 2O^*$
M4	$r_H = \frac{k_1 K_A K_{O_2}^{0.5}[A][O_2]^{0.5}}{(1 + K_A[A])(1 + K_{O_2}^{0.5}[O_2]^{0.5})}$	Dual site, $O_2 + 2* \Leftrightarrow 2O^*$

With all models, rate coefficients and adsorption parameters independent of all reactant concentration could be obtained. The parameters determination scheme is shown

in Figure 2-8 for fitting the experimental data with the proposed models M1-M4. Basically the determination scheme was an algorithm coupling the 4th order Runga-Kutta numerical method (Press et al., 1992) with the nonlinear Simplex-Marquardt algorithm (Duggleby, 1984) to minimize the objective function (equation 2-2). The kinetic parameters were varied by a least-squares optimization scheme so that the minimum of residual sum of squares (SQR) could be identified eventually for models M1-M4, respectively.

$$SQR = \sum_{i=1}^{n} \left(\frac{[A]_{Sim} - [A]_{Exp}}{[A]_{Exp}} \right)^2 \qquad (2\text{-}2)$$

where the subscripts *Exp* and *Sim* represent the experimental and simulated values, respectively.

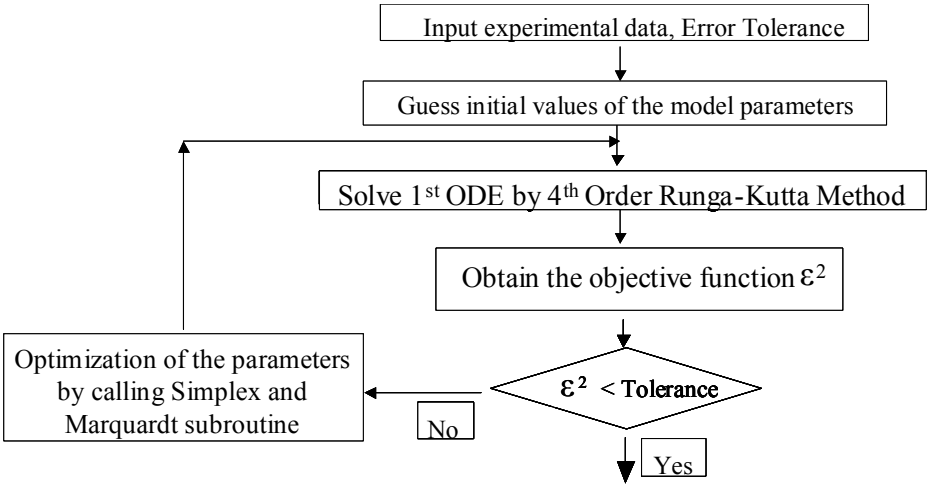

Figure 2-8. Schematic diagram for model parameter identification.

The initial guesses for the current model parameters were taken from the literature on phenol oxidation and varied widely. Convergence is achieved when the model's predicted values of phenol concentrations adequately match the corresponding experimental data. The four models shown in Table 2-3 have been tested for r_H with the kinetic parameter values given in Table 2-4, where n is the exponent term for catalyst loading in the overall reaction rate equation (2-1). All of the models could achieve convergence and yield statistically reliable parameters, whereas the power law model M1 yields the maximum

SQR (4.57). The other LHHW models result in residuals with only slight differences and a minimum of 1.29.

The quality of the models can be checked by comparing them with experimental data. Figure 2-9 exhibits parity plots that compare the experimental observations with those calculated from the four models proposed above. The kinetic models M2, M3, and M4 adequately fit the experimental data. No trend can be noticed and most of the relative residuals are bounded within ± 15 %, with the average absolute relative errors (AARE) equal to 9.7, 8.9, and 10.3 %, respectively. On the other hand, model M1, a power-law rate equation with fixed reaction orders, underpredicts the phenol concentrations of high values, with the AARE equal to 15.7%.

Table 2-4. Rate parameters for air CWO heterogeneous reaction

Model r_H	Parameters	SQR	AAAR
M1	$k_1 = 0.10\text{E}5\, e^{-53306/RT}$ p=0.96, q=0.65, n=0.90	4.57	0.157
M3	$k_1 = 0.15\text{E}5\, e^{-32183/RT}$ $K_A = 0.18\text{E}5 e^{-41782/RT}$ $K_{O_2} = 0.22\text{E}5 e^{-38130/RT}$ n=0.87	1.29	0.089
M2	$k_1 = 0.11\text{E}5\, e^{-30789/RT}$ $K_A = 0.81\text{E}4 e^{-39904/RT}$ $K_{O_2} = 0.77\text{E}4 e^{-34649/RT}$ n=0.85	1.38	0.097
M4	$k_1 = 0.31\text{E}5\, e^{-34290/RT}$ $K_A = 0.98\text{E}4 e^{-39060/RT}$ $K_{O_2} = 0.97\text{E}4 e^{-46061/RT}$ n=0.82	1.74	0.103

SQR - Equation 2. $\text{AAAR}=\sum_{i=1}^{N}\left|\left(y_{Sim,i}-y_{Exp,i}\right)/y_{Exp,i}\right|/N$.

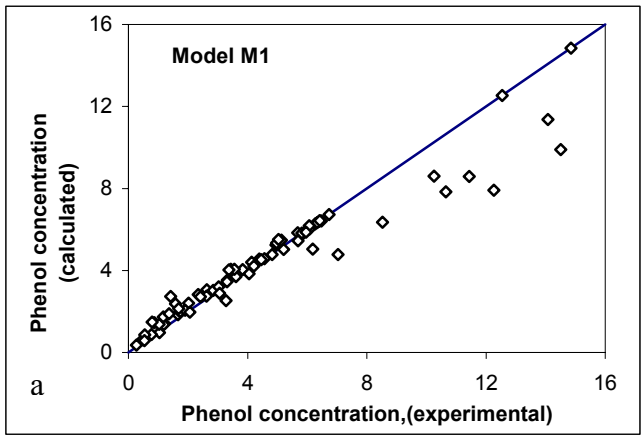
Model M1
Phenol concentration (calculated)
Phenol concentration,(experimental)
0
4
8
12
16
a

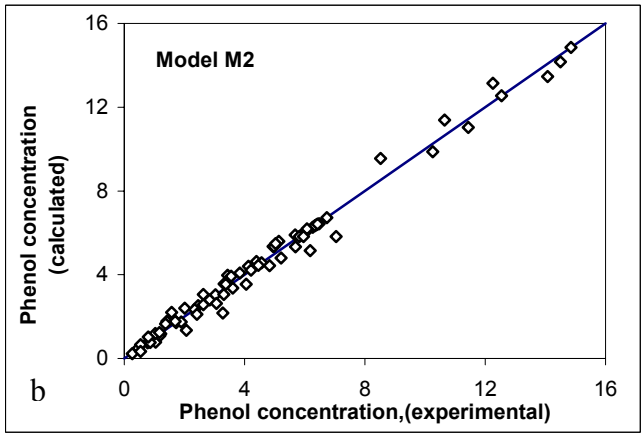
Model M2
Phenol concentration (calculated)
Phenol concentration,(experimental)
0
4
8
12
16
b

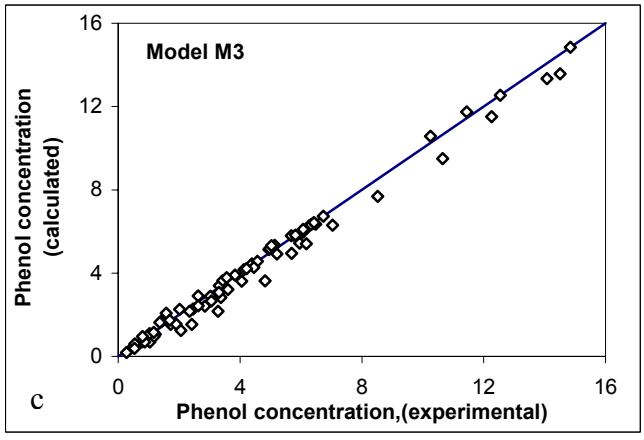
Model M3
Phenol concentration (calculated)
Phenol concentration,(experimental)
0
4
8
12
16
c

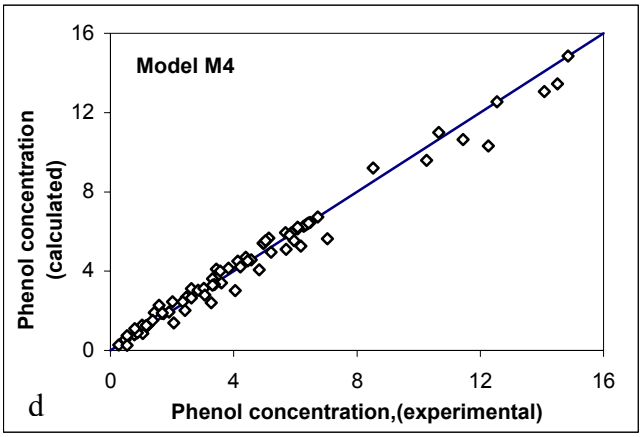

Figure 2-9. Parity plot for phenol concentration, (mol/m^3): (a) employing model M1; (b) employing model M2; (c) employing model M3; (d) employing model M4.

The reproductions of some representative experimental data by the models M3 and M4 are shown in Figure 2-10a and 2-10b, respectively, where the effects of different temperatures on catalytic phenol removal rate are tested. At the selected temperatures, both models provide satisfactory agreements between the simulation results and the experimental measurements. Nonetheless, it has to be noted that the physical meaning of the mathematical models cannot be overinterpreted, because different models can be employed to describe the same experimental observations. Model M3 is slightly better in terms of the statistical standard. However, model M4, representing a dual site mechanism, is widely taken in the literature to describe the reaction, regardless of catalyst type (Levec and Smith, 1976; Pintar and Levec, 1994).

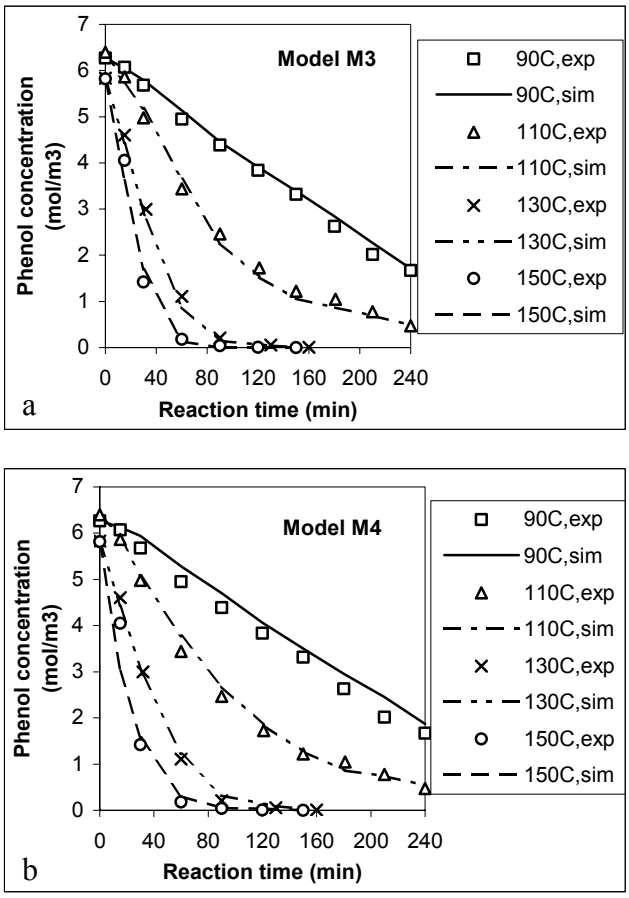

Figure 2-10. Measured and predicted time profiles of phenol removal at different temperature: (a) employing model M3; (b) employing model M4 (6.6 g/L catalyst, 500 ppm phenol, 1.5 MPa).

As mentioned earlier, a similar mechanism was also reported for H_2O_2 oxidation in the previous work. Therefore, model M4 was selected for further consideration in the present work. It should be mentioned that, in model M4, the product of the oxygen adsorption constant, K_{O_2}, and the oxygen concentration, C_{O_2}, was found to be insignificant compared to other terms in the denominator. Hence, this term was neglected without noticeable loss in precision, and model M4 was further simplified to the final form.

$$r_H = \frac{k_1 K_A K_{O_2}^{0.5} [A] C_{O_2}^{0.5}}{1 + K_A [A]} \qquad (2\text{-}3)$$

The resulting SQR and AARE for equation (2-3) are 1.76 and 10.8%, respectively. A kinetic expression similar to equation (2-3) has been derived in several literature studies, such as the CWO of aqueous phenol over CuO/ZnO/CoO catalyst, (Pintar and Levec, 1994) and the CWO of acetic acid over iron oxide and zinc aluminate spinel promoted by Cu, Mn and La (Levec and Smith, 1976). Considering the general applications of equation (2-3) to the oxidation of organics, one can speculate that the mechanism of phenol oxidation can be described well by the simplified form of model 4 (equation 2-3). Therefore, equation (2-3) has been chosen as the final expression for the kinetics of CWO of phenol based on phenol disappearance. The overall expression is

$$-\frac{d[A]}{dt} = \frac{k_1 K_A K_{O_2}^{0.5} [A] C_{O_2}^{0.5}}{1 + K_A [A]} C_{cat}^{0.82} \qquad (2\text{-}4)$$

The expressions for k_1, K_A, and K_{O2} are given in Table 2-4.

Having discriminated the rate expression that falls in line with the experimental results, we now attempt to explain the reaction mechanism in detail. As discussed above, the catalyst plays the key role in the activation of both reactants in the liquid-phase oxidation of aqueous phenol. Phenol undergoes the hemolytic one-electron transfer initiation process where free radicals appear. In other words, phenol adsorbs on metal ion sites at their higher oxidation states and is transformed to phenoxy radicals via the surface redox cycle and hydroxyl hydrogen abstraction (Sadana and Katzer, 1974) The rate-limiting surface reaction step is directly proportional to the fractional coverage of active sites by reactant species, with both coverage being related to the Langmuir adsorption concept. The adsorption steps between phenol and oxygen depend on the dual site mechanism.

2.4 Summary

The catalytic wet oxidation of aqueous phenol was tested by either H_2O_2 or air. For the former case, all experiments were carried out at atmospheric pressure. While for the latter, high pressure was maintained in the reactor to increase the dissolved oxygen

concentration in the liquid phase. Because of the noticeable corrosion and undesirable H_2O_2 decomposition, we restricted our efforts on H_2O_2 oxidation and focused on oxidation process by air only. A drastic change of phenol conversion was noticed when the air pressure was changed from 0.8 to 1.5 MPa. However, only marginal enhancement of phenol oxidation rate resulted from air pressure higher than 1.5 MPa, which means that the liquid reactant became limiting once the gas diffusion flux increased to a certain extent. Confirmation of the liquid reactant limited reaction for the air pressure higher than 1.5 MPa also came from the value of parameter γ, which was calculated to be less than one ($\gamma<1$), and revealed that the relative availability of the gas reactants was higher than the liquid reactant. The heterogeneous reaction with the presence of catalyst significantly enhances the oxidation rate of phenol.

A group of kinetic models considering both the power-law and Langmuir-Hinshelwood approaches was evaluated to describe the catalytic kinetics of the phenol disappearance. The nonlinear dependence of the phenol removal rate on the catalyst concentration was taken into account via the empirical power-law function of this variable. Finally, a kinetic model was derived on the basis of equilibrium adsorption of phenol and dissociated oxygen on two distinct types of active. The model is able to predict well the experimental results over the entire range of the variables studied. Because packed-bed reactions have been employed frequently in treating a diversity of industrial aqueous waste organics, the kinetic model provided in this work will assist in the future process evaluation and design of packed-beds for CWO technology.

Chapter 3
Packed-Bed Experiments

3.1 Introduction

Catalytic wet oxidation (CWO) of liquid-phase phenol has been widely performed with many reactor systems (Table 1-2). The severity of oxidation conditions can be reduced by use of a suitable (cheap, stable, and resistant to poisoning) catalyst system. Among the promising materials, Al-Fe pillared clay catalyst has shown encouraging results for oxidizing organic compounds in a basket stirred tank reactor in extrudate form and in a slurry reactor in powder form. This novel catalyst allows for mild conditions and can be used for a rather long time without significant catalyst leaching and deactivation. Therefore, Al-Fe pillared clay catalyst selected through previous screening tests is formed into a cylindrical shape and undergoes further experimentation for process development and optimization.

Packed-bed reactors with downflow of gas and liquid phases are widely encountered in industrial practice (Table 1-3), while different modes of operation, such as gas-liquid upflow, are also becoming important. The principal question is whether a downflow or an upflow mode of operation optimizes the conversion and selectivity. Considering the complicated fluid-fluid and fluid-particle interaction, and the complex geometry of the tortuous pore space, the selection of operation mode is dependent on the characteristics of a specific reaction system. Therefore, in this work, based on the previous basket reactor studies, the performance of the pillared clay catalyst for the continuous CWO of phenol will be tested experimentally in a packed-bed reactor with co-current downflow and

upflow. In addition, operating parameters needed for complete mineralization will be identified.

3.2 Experimental Setups and Procedures

The configuration of the reactor system, which is shown in Figure 3-1, allowed for the isothermal and isobaric conditions. The reactor was made of ϕ2.1×60 cm stainless steel tubing. The packing material was supported by a stainless steel screen placed near the bottom of the reactor tube. The Fe-Al pillared clay catalyst was packed to a height of 30 cm, with glass beads (ϕ 3mm) packed on the top and bottom sections, and each section had a 15cm long inert zone. Upon entering the reactor inlet, the liquid and gas reactants were mixed and heated in the inert packing to a preset temperature. Then the heterogeneous reactions took place after the air and liquid contacted the catalyst. The temperature in the reactor was monitored by three thermocouples inserted into the packed bed through side openings evenly spaced along the reactor length. The temperature at each section was controlled using LABVIEW software via a National Instruments SCXI-1325 data acquisition board, which regulated the voltage supplied to the heating tapes wrapped around the reactor sections. Since the phenol feed concentration was low, no temperature rise due to reaction was considered. The temperature value was held constant to within $\pm$ 1 K, which confirms that the reactor was operated isothermally.

The liquid reactant, an aqueous solution of phenol, was loaded in the feed tank and fed to the system at high pressure through a Waters 510 HPLC pump capable of volumetric flow rates up to 10ml/min with high precision and continuous flow. In order to saturate the gas and prevent solvent evaporation effects, before air entered the reactor it was bubbled through two cylinders containing water. The pressure and flow rate of the gas system was controlled with a high-pressure regulator and the backpressure regulators on the exit of the system.

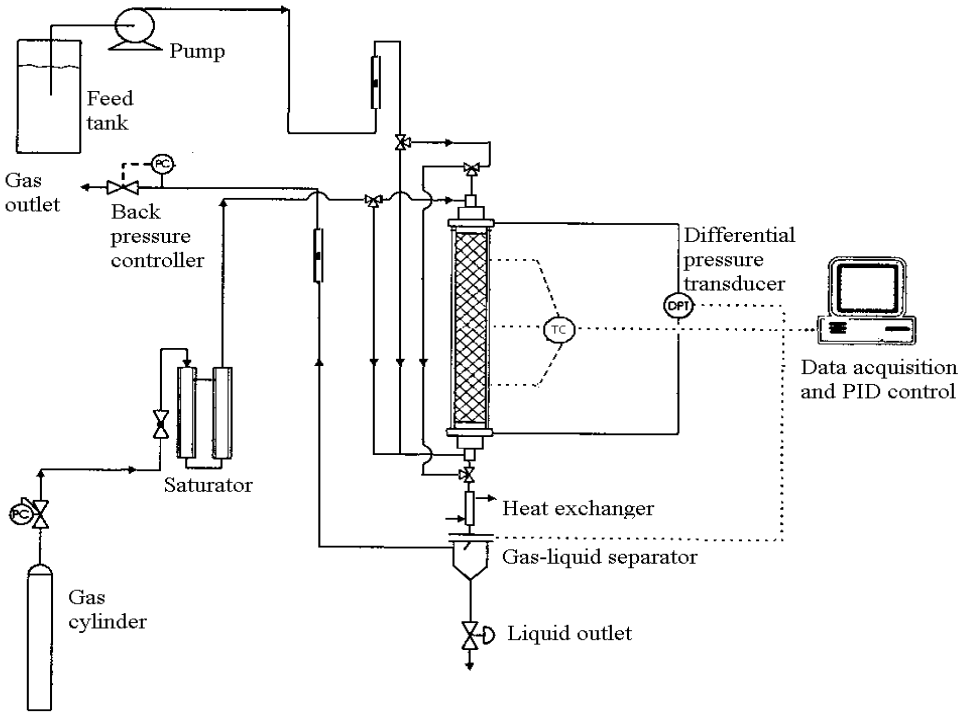

Figure 3-1. Experimental setup of a catalytic packed-bed reactor suitable for gas-liquid cocurrent downflow and upflow.

Liquid and gas were fed to the reactor through stainless steel lines equipped with three-way valves to allow for both down-flow and up-flow configurations by merely switching the valve positions. Switching between the two modes of operation without discharge enables performance comparisons at identical catalyst activities. The gas and liquid distributions are critical in downflow operation, while gas distribution is important in upflow operation. The experimental facility was operated with uniform gas-liquid distributors and control valves for both downflow and upflow operation modes. Distributors were placed at the top and the bottom of the reactor column. If the reactor was in trickle flow configuration, the liquid was channeled into several tubes and flowed out a perforated disk to distribute the liquid evenly over the whole catalyst bed, and the gas entered the space surrounding the tubes. The up-flow connection was designed in the form of a U-shaped stainless steel box. Seven holes on top of the box distributed the gas

uniformly, while the liquid line is concentric to the gas delivery line and feeds the liquid all around the gas distributor box. The distributors were tested using a clear acrylic reactor to ensure that no channeling effect occurred during operation.

After the mixture exited the reactor and was cooled in a heat exchanger, the reactor effluent was then separated into the gas and liquid phase in a high-pressure separator. The bottom of the separator had a liquid exit controlled either by a micrometric valve or by the liquid level control device. The micrometric valve allowed for sampling of the liquid collected in the separator. The amount of liquid in the separator was adjusted by a level sensor. The liquid control device monitored vibrations in a paddle that extended down into the separator. As the liquid level changed, the frequency of the vibrations of the paddle changed. This change was transformed into a signal that turned on/off the liquid exit valve to maintain the preset liquid level. Abrupt changes in volume of the liquid contained in the separator could cause changes in pressure. The gas stream from the separator was discharged through a back-pressure controller which maintained constant pressure in the reactor. To prewet the packing, before the experiments were started, the reactor was flooded with liquid phase for 10 hours, followed by draining.

Liquid and gas samples will undergo the analysis procedures listed in Figure 1-1. The concentration evolution of phenol and intermediates will be traced by the high-performance liquid chromatography (HPLC). The extent of the phenol mineralization will be measured by total organic carbon (TOC) analyzer. Gas chromatography (GC) will be used to track the species concentration in the gas phase.

To understand the reaction progress of aqueous phenol in the liquid phase, one has to learn the corresponding liquid phase residence time distribution for each experimental measurement of the reactant conversion at the packed-bed reactor outlet. The experiments has been carried out to investigate the residence time distribution, liquid holdup, and pressure drop over porous Al-Fe pillared clay catalyst particles, which was operated in the packed-bed reactor under the similar operating conditions used for the reaction of CWO of aqueous phenol solution. Details can be found in (Guo and Al-Dahhan, 2004 b).

3.3 Comparison of Trickle-Bed and Upflow Reactor Performance

Knowledge of flow regime is indispensable in the analysis of downflow and upflow packed bed performance. In a trickle-bed reactor, at low gas and liquid flow rates, the flow regime is characterized by a continuous gas phase and some discontinuous liquid films driven by gravity force. While in an upflow packed-bed reactor, the buoyancy force leads to a bubble flow regime with a continuous liquid phase which contains small spherical bubbles. In this regime, the solid particles are fully wetted by the continuous liquid phase.

The differences in downflow and upflow modes give rise to varied liquid holdup, external catalyst wetting, axial dispersion, wall effects, and maldistribution, which in turn affect the chemical reaction process. The importance of the degree of catalyst wetting and liquid back mixing in the up-flow or down-flow mode is dependent on the size of catalyst, the length of the catalyst bed, and the level of space velocity used. Actually, it has been suggested that the phenol liquid-solid mass transfer coefficient values do not differ much for the two modes of operation, if everything else is kept identical (Iliuta and Larachi, 2001). Moreover, the relative difference between the overall effectiveness factor for a partially wetted catalyst pellet and a fully wetted catalyst particle has been found not to exceed 8% (Iliuta and Larachi, 2001). To correctly understand the underlying aspects that are responsible for the reactor performance, it is necessary to study the operating parameters individually.

Prior to the experimentation in a packed-bed reactor, a stirred basket reactor test at different temperatures in the range of 90-170 ^{o}C had revealed that phenol conversion becomes significant (> 20%) after 0.5 h and complete mineralization takes place after 4 h, as seen in Figure 2-4. Therefore, in order to get the desired high phenol conversion in the packed bed, the LHSV was chosen to let the liquid residence time range between 0.2-5 h, as listed in Table 3-1. The diameter of a small scale (bench scale) trickle bed reactor is much smaller than those of a commercial reactor. Hence, the ratio of the reactor diameter

to catalyst particle diameter is very low. The ratio of the catalyst bed height to the particle diameter is also low in these reactors. Due to the smaller volume of catalyst used, the liquid flow rate is also lower. Because of the low values of these factors, a number of problems such as incomplete wetting of catalyst in downflow operation mode and back mixing of liquid in downflow and upflow operation modes are present in these small-scale reactors (Bej et al., 2001).

Table 3-1. Selection of design and operating conditions

Property	Range
Temperature, ^{o}C	110 -210 ^{o}C
Equilibrium vapor pressure, MPa	0.14- 0.79
Total pressure, MPa	1.5 - 3.2
Reactor diameter, cm	2.5
Bed height, cm	60
Bed porosity	~ 0.4, ~0.6,
Catalyst particle size, mm	$\phi 2 \times 8$
LHSV, h^{-1}	0.2-5
Superficial gas velocity, cm/s	0.13-2.45
Superficial gas mass flux, kg/m^2/s	0.03-0.13
Phenol feed concentration, mg/L	500-2000

The operation regime was kept away from spray flow to assure the liquid film dominated the mass transfer resistance (Levenspiel, 1996). Therefore, for the downflow operation, according to the map of hydrodynamic flow regimes proposed by Fukushima and Kusaka (1977, a), gas velocity should be low ($Re_G < 350$). For the upflow operation, the hydrodynamic flow regimes proposed by Fukushima and Kusaka (1979) increased the limit ($Re_G < 800$) to avoid spray flow. In addition, the flow map reported by Turpin and Huntington (1967) gave an upper limit for the gas mass velocity (< 0.2 kg/m^2/s) for the upflow. Therefore, to satisfy the above conditions, the selected gas mass velocity is also listed in Table 3-1. For the selected liquid and gas mass flux, the resulting ratio of the

G/L molar flow rate falls into the range from 3000 to 10000, so that an excess of oxygen is supplied to the liquid bulk.

Before conducting experiments over catalysts, the reactor was filled up with inert glass beads. A group of experiments were performed at the mild conditions: 170 ^{o}C, 3.2 MPa, and different LHSV. Analysis of liquid-phase samples of the reactor's exit stream revealed that uncatalyzed homogeneous oxidation led to phenol conversions of less than 1% at LHSV of 1.2 h^{-1} to 10% at LHSV of 0.2 h^{-1}. On the basis of these results, it was evident that not considering homogeneous reaction would not cause significant error. In addition, the applied air pressure exceeded the vapor pressure of the liquid phase over the entire range of used temperatures to prevent evaporation inside the bed. Corresponding to the temperature range of 110-170 ^{o}C, the equilibrium vapor pressure is from 0.14 to 0.79 MPa (Lin et al., 1996), while the reactor pressure range is 1.5-3.2 MPa.

3.3.1 Limited Reactants

The reaction rate over externally incompletely wetted packing can be smaller or greater than the rate observed over completely wetted packing. This difference depends on whether the limiting reactant is present only in the liquid phase or in both gas and liquid phase. As pointed by Khadilkar et al. (1996), for the reaction A (g) + ν_B B (l) → Products, most gas-liquid reaction systems promoted by a solid catalyst can be classified as being liquid reactant or gas reactant limited, by the ratio of the diffusion fluxes of the two reactants scaled by the ratio of stoichiometric coefficients, ($\gamma=(D_{eB}C_B/\nu_B(D_{eA}C_A*)$. The reaction can be considered gas reactant limited for $\gamma>>1$ or liquid reactant limited for $\gamma<1$.

The transport of molecules from the gas phase to the active surface of the catalyst faces includes resistances from bulk gas to gas-liquid interface, from gas-liquid interface to bulk liquid, from bulk liquid to external catalyst surface, and finally diffusional resistances within the pores of the catalyst pellet. The contacting efficiency of the liquid around the catalyst particle also plays an important role on the overall rate of reaction. The limiting reactant in a gas-limited reaction can enter the porous particles through both

the actively and inactively wetted surfaces, but it enters at different rates. Accordingly, for a gas limited reaction, a trickle-bed reactor is expected to perform better than an upflow reactor, due to its partially wetted catalyst over which gas reactant has an easy access to the particles. In an up-flow reactor, the only access of the gaseous reactant to the catalyst is through the liquid film engulfing the catalyst. For a liquid-limited reaction, the liquid reactant can enter the catalyst particle only through its actively wetted surface, leaving the inactively wetted areas unutilized. Since upflow has higher external wetting efficiency (100%) than downflow, it will facilitate the transport of the liquid reactant to the catalyst and enhance the reaction rate. Liquid reactant limited conditions, therefore, result in a better performance for up-flow, where particles are completely surrounded by liquid, than for down-flow, where particles may be only partially externally wetted.

In this work, oxygen is not very soluble in water, and phenol is also present in low concentration. Based on the employed operating conditions, the resulting ratio of the diffusion fluxes of the two reactants are listed in Table 3-2, where only the highest and lowest temperatures and pressures are chosen to estimate the range of γ values. Because all the values of γ are less than unity ($\gamma<1$), the studied CWO reactions are liquid reactant limited. Hence, it is expected that the upflow will allow the catalyst to achieve better reactant conversion. However, such a theoretical expectation still needs experimental verification.

Table 3-2. Identification of the limiting reactant for the packed bed experiments

Temperature (°C)	Total pressure (MPa)	O_2 Solubility (mol/m^3)	Diffusion Coefficient[a] [cm^2/s]		γ^b	γ^c
			O_2	Phenol		
110	1.5	2.125	1.100E-04	4.816E-05	1.57E-01	6.26E-01
110	3.2	4.875	1.100E-04	4.816E-05	6.83E-02	2.73E-01
170	1.5	1.419	1.997E-04	8.743E-05	2.34E-01	9.38E-01
170	3.2	4.943	1.997E-04	8.743E-05	6.73E-02	2.69E-01

a: Diffusion coefficient calculated from Wilke-Chang method (Wilke and Chang, 1955)

b: Phenol concentration: 500 ppm. c: Phenol concentration: 2000 ppm.

3.3.2 Effect of Liquid Velocity

One comparison of the two reactors is achieved by studying the conversion at identical liquid hourly space velocity (LHSV, defined as superficial liquid velocity/reactor length) and identical reactant feed concentration. LHSV is the proper scale-up variable when the beds for downflow and upflow are identically packed and the reaction rate is based per unit volume of the catalyst. For gas-limited reactions, scale-up at constant LHSV can lead to very poor performance as the catalyst effectiveness factor drops with increased contacting efficiency due to a reduction in the gas reactant supply. Hence, for gas-limited reactions, constant LHSV and constant reactor height are required in order to maintain the same performance upon scale-up. However, since the CWO reaction covered in this work is liquid limited, scale-up at constant LHSV is forgiving since it results in improved wetting efficiency and better catalyst utilization (Dudukovic et al., 1999).

In laboratory scale packed beds, because low liquid velocity is frequently used in order to match the LHSV of the commercial unit, most of the downflow cases can be classified in the trickle flow regime. Similar liquid and gas flowrates were also applied to the upflow operation, using the same bed voidage. The effect of LHSV on phenol removal rate is presented in Figure 3-2.

For both operation modes, phenol conversion decreases with the increased liquid mass velocity, at a pressure of 3.2 MPa and a temperature of 170°C. The effect of liquid

superficial velocity on the axial phenol conversion profile is obvious. A lower feed flow rate is preferred because the longer residence time will allow for complete phenol removal. A similar trend of results can be obtained in the cocurrent upflow packed-bed reactor where gas flows through the liquid in bubble flow. The use of higher liquid hourly space velocity (LHSV) provides beneficial effect in both upflow and downflow modes of operation by enhancing the mass transfer coefficient. Higher LHSV improves catalyst wetting in downflow mode whereas it reduces axial dispersion of liquid in both up-flow and downflow modes of operation. However, it actually lowers the liquid reactant residence time, which corresponds to the decreased exit conversion.

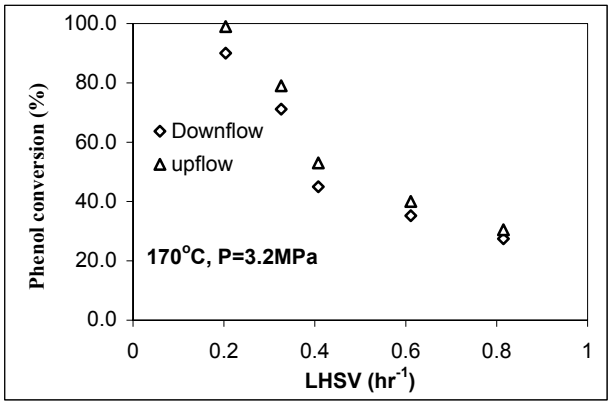

Figure 3-2. Trickle-bed (Pe_L=21~33) and upflow (Pe_L=3~4) performance at different LHSV (Pressure= 3.2 MPa, [phenol]=500 ppm, and u_G=0.28 cm/s).

It is evident that phenol conversion values were higher in the upflow system than in the downflow system. The differences between these two modes became more noticeable at lower LHSV, where the axial dispersion of liquid may be present and can reduce the overall rate of reaction. Liquid axial dispersion was calculated based on the correlations proposed by Cassanello et al., (1992). As shown by the reactor scale liquid Péclet number, for the same set of operating conditions, liquid backmixing is more prominent in the upflow configuration than in the downflow configuration, which is not beneficial for phenol conversion. However, in the downflow reactor, incomplete catalyst utilization

may occur. One cause is reactor scale liquid maldistribution that may leave certain portions of the bed poorly irrigated. The other cause is particle scale incomplete external wetting: at sufficiently low liquid mass velocity, the liquid flow available is insufficient to cover all the catalyst particles with a continuous liquid film at all times. In a time-averaged sense, the external surface of the particle is then only partially covered by the flowing liquid. In a liquid limited reaction, the conversion will be governed by the degree of catalyst wetting. Since downflow operation results in regions of poorly wetted catalyst, upflow has higher wetting (100%) than downflow and it will outperform downflow. As the liquid flowrate increases (i.e., space time is decreased), the wetting efficiency of the trickle-bed reactor is greatly enhanced, and its performance approaches that of upflow reactor, as shown in Figure 3-2. Therefore, catalyst wetting efficiency is one essential factor affecting a laboratory reactor's performance.

3.3.3 Effect of Gas Velocity

Figure 3-3 shows that the phenol conversion at a given LHSV was enhanced by increasing the gas velocity for both modes of operation at high reactor pressure. The conversion was found to increase almost linearly with an increase in the air velocity. The strong dependence was due to a linear increase in the gas-liquid and liquid-solid mass transfer coefficients with the gas velocity (Stuber et al., 1996). However, the effect of gas velocity on reactor performance diminished when gas velocities became moderate.

Both Figure 3-2 and Figure 3-3 reveal that the reactor performance was distinct for different flow direction when the fluid (liquid or gas) flowrate was low, while this distinction vanished at elevated flowrates. At low gas velocities, gravity (or buoyancy) force plays an important role. The flow regime was bubble flow in upflow and trickle flow in downflow, which created distinct hydrodynamics and reaction processes. However, when the flowrates of liquid and gas increased, the flow approached pulsing flow in both directions. The hydrodynamic characteristics were mainly governed by inertial force, and the flow direction does not play a role any more.

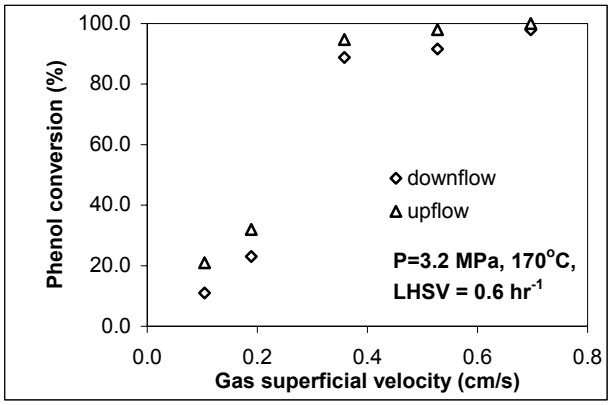

Figure 3-3. Effect of gas velocity on phenol conversion at downflow (Pe_L=31) and upflow (Pe_L=4) reactor.

At high pressure and low feed concentration of phenol, the reaction is liquid limited. In this case upflow performed better than downflow, although the former leads to higher liquid axial dispersion (lower Péclet number), as shown in Figure 3-3. In downflow operation, the catalyst articles are not fully wetted at the liquid flow rates used, which facilitates the access of the gas reactant to the pores of the catalyst from the externally dry parts. However, the availability of gaseous reactant was not a dominant factor in this case. The access of the reactant to the catalyst site was limited by the surrounding liquid film only.

At a given pressure and liquid mass flow rate, the liquid holdup decreased when the gas mass flow rate was increased. An abrupt decrease was observed at low gas flow rates, followed by a slight decrease at higher gas flow rates. Such trends have been confirmed regardless of the flow direction and the pressure (Larachi et al., 1991). In addition, the dimensionless pressure gradient ($\Delta P / \rho_L g Z$) increases significantly and so does the shear stress on the gas-liquid interface (Al-Dahhan and Dudukovic, 1995). Therefore, liquid film thickness at a constant liquid flow rate decreases, which leads to a better spreading of the liquid film over the external packing area and across the reactor diameter. Accordingly, the catalyst wetting efficiency and gas-liquid interfacial area improved considerably, which is supported by the finding of Larachi et al., (1992). Since

the trickle-bed pellets get progressively entirely wetted by increasing the gas superficial velocity, the difference in the performances by the two modes of reactor operation narrows, and the downflow performance approaches that of upflow.

3.3.4 Effect of Reactor Pressure

Figure 3-4a and 3-4b shows that the effects of increasing gas pressure on phenol disappearance rate. A significant improvement in phenol conversion occurred when pressure changed from 1.5 to 2.2 MPa as compared to the change in conversion when pressure changed from 2.2 to 3.2 MPa. This finding implies that the effect of pressure diminishes when pressure becomes high, because the reaction becomes liquid reactant limited at low feed concentrations of phenol (500 ppm) and high pressure (> 1.5 MPa). Further increase in the reactor pressure, and hence liquid phase oxygen concentration, will have a minimal effect since oxygen is not the limiting reactant anymore.

Elevated levels of pressure and temperature improve the solubility of oxygen (Himmelblau, 1960). This in turn increases the mass transfer driving force for gas to the inactively wetted catalyst surface in the downflow mode, and facilitates the rate of mass transport to the wetted catalyst surface in both modes. Below a critical value of superficial gas velocity ($\approx$1 cm/s), the elevated pressure causes a decrease in liquid holdup and an increase in catalyst wetting efficiency, but in a less pronounced manner since the pressure gradient is more sensitive to velocity changes than to gas density (Al-Dahhan and Dudukovic, 1995). In addition, neither of the two mass-transfer parameters, the interfacial areas and the liquid-side volumetric mass-transfer coefficients, depends on pressure (gas density) (Al-Dahhan et al., 1997). However, for gas velocities larger than 1-2 cm/s, pressure intensifies the gas shear over the trickling liquid films. The reactor flow regime shifts from a state predominantly controlled by gravity (trickle flow with low gas flow rate) to a state controlled by gas-liquid shear stress (Wammes et al., 1990). The gas-liquid interfacial area also increases at elevated pressure. Due to shear intensification, the liquid trickle films are invaded by tiny bubbles whose size results from a balance between viscosity and surface tension forces. It is the formation of such small bubbles that

enhances the interfacial area and the volumetric mass-transfer coefficient (Al-Dahhan et al., 1997). Hence, due to the enhanced gas-liquid interaction and interphase mass transfer, an increased gas pressure is favorable for the performance of both upflow and downflow reactors.

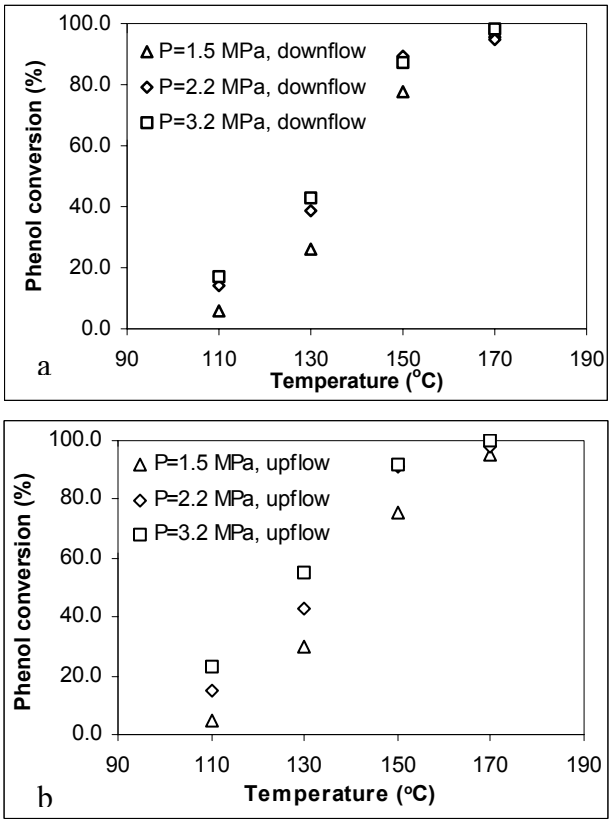

Figure 3-4. Effect of air pressure on phenol conversion at downflow (Pe_L=24) and upflow (Pe_L=3) reactor (LHSV = 0.3 hr^{-1}, [phenol]=500 ppm, u_G=0.53 cm/s).

At higher pressure, since the γ-ratio will diminish faster than the increase in wetting efficiency in downflow, it is expected that an upflow operation will remain more favorable for conducting CWO than downflow operation. From the aforementioned experimental observations, it is stressed that the experimental performance of these reactors becomes similar at high liquid mass velocities, high pressure, or high gas

velocity when the catalyst in the trickle-bed reactor becomes completely wetted, as usually encountered in the upflow reactor.

3.3.5 Effect of Reactor Temperature

The increased phenol removal rate at higher temperature is also shown in Figure 3-4a and 3-4b. The doubled gas pressure enhanced the phenol conversion only to within 20%, while a temperature increment of 80^{o}C resulted in an evident enhancement (up to 90%) of the phenol conversion. Therefore, having more pronounced effect, temperature is a key factor controlling the reaction rate in the catalytic oxidation. To confirm the distinct effect of temperature and seek an optimum range of operating conditions, more tests were performed by choosing various liquid and gas velocities.

Figure 3-5 illustrates temperature's impact at a low gas velocity of 0.13 cm/s. The effect of the temperature became weaker, and the conversion can reach only 70-80% at 210 ^{o}C. This is in contrast to Figure 3-4, where complete phenol conversion can be obtained around 190 ^{o}C at a gas velocity of 0.53 cm/s. Hence, when low gas velocity was employed, the oxidation reaction was limited by external mass transfer of the gas reactant, which is in agreement with the observed effect of the gas velocity on phenol conversion. Usually, temperature above 210^{o}C is not desirable in the wet oxidation process because high temperature requires a high reactor pressure to minimize the vaporization of liquid phase. To reduce the reaction's severity, i.e., temperature, moderate gas velocity (>0.5 cm/s) is necessary.

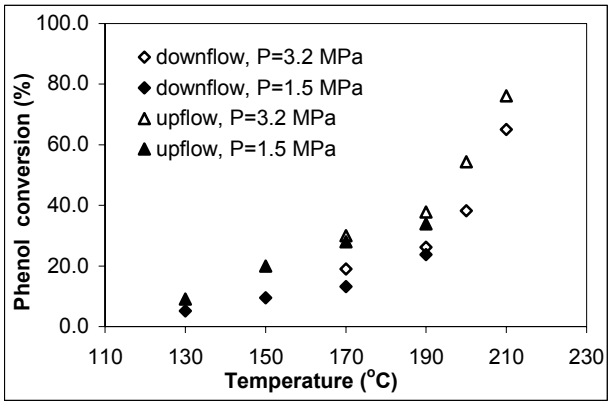

Figure 3-5. Trickle-bed (Pe_L=24) and upflow (Pe_L=3) performance at different reaction temperatures (LHSV = 0.3 hr^{-1}, u_G=0.13 cm/s, [phenol]=500 ppm).

The effect of temperature on phenol conversion in the range of 110 to 170 ^oC for LHSV between 0.3 and 1.2 hr^{-1} is depicted in Figures 3-6a and 3-6b, for downflow and upflow operation mode, respectively. The experimental data confirms that the reaction rates can be satisfying at a moderate gas velocity of 0.53 cm/s and low liquid velocity. When the reactant stays in the reactor for a rather long time, the temperature effect is dominant over the mass transfer effect, and the system is under chemical kinetic control. In particular, a temperature change from 150 to 170 ^oC led to an obvious acceleration of the reaction rate. High temperature is especially beneficial for the upflow mode, where flow maldistribution can be minimized.

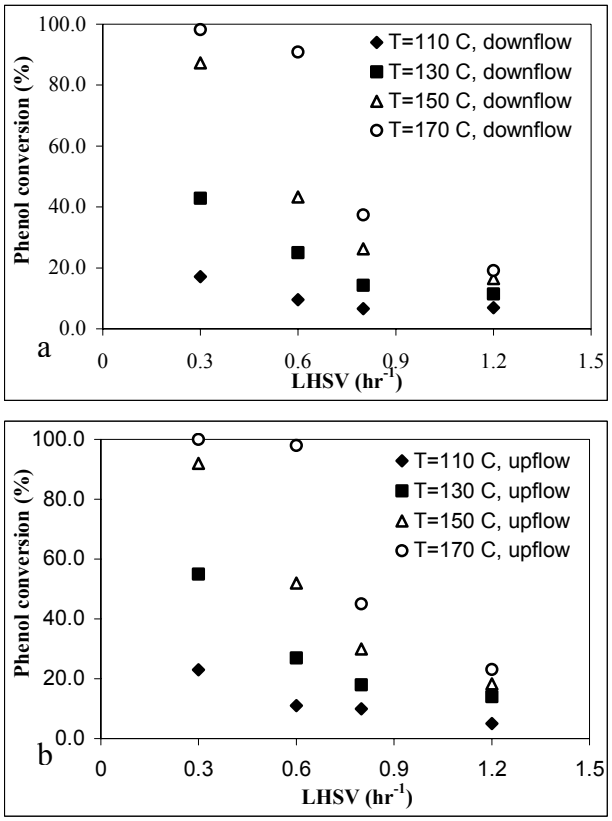

Figure 3-6. Phenol conversions at different LHSV and reaction temperatures for dowflow (Pe_L=24~39) and upflow (Pe_L=3~5) packed-bed reactors (Pressure=3.2 MPa, u_G=0.53 cm/s, [phenol]=500 ppm).

3.3.6 Effect of Feed Concentration

Since the catalyst was found active in the previous studies with moderate phenol loading (500 ppm), the CWO process was further tested with phenol solution in rather high concentrations (1000 and 2000 ppm), simulating industrial applications. The results, presented in Figures 3-7a and 3-7b, show that the difference among phenol reductions in the employed three concentrations was not significant. In fact, even for the solution with phenol loading of 2000 ppm, the final conversion still reached above 90% at 170^{o}C. A similar observation was reported by Stuber et al., (2001), where almost complete phenol elimination was achieved over active carbon catalyst for an initial phenol concentration

of 2500 ppm. The reaction kinetics expression for catalytic air oxidation of phenol is reported in equation (2-3) in Chapter 2, as shown below:

$$r_H = \frac{k_1 K_{PHOH} K_{O_2}^{0.5} C_{PHOH} C_{o_2}^{0.5}}{1 + K_{PHOH} C_{PHOH}}$$

When phenol concentration C_{PHOH} is low, the product of the phenol adsorption constant, K_{PHOH} and the phenol concentration C_{PHOH} will be fairly small compared to 1 in the denominator. In this case, it is reasonable to state that the oxidation rate is approximately first-order with respect to phenol. On the other hand, when phenol concentration C_{PHOH} increases so that the value of $K_{PHOH} C_{PHOH}$ becomes dominant in the denominator, the reaction of phenol oxidation will approach a zero-order reaction with respect to phenol.

The shift in reaction kinetics due to feed concentration change was confirmed by experimental data at high pressure (3.2 MPa) for both downflow and upflow operation modes, as shown in Figures 3-7a and 3-7b. Conversion was independent of feed concentration at low phenol loading, which is the indicative of a first-order reaction due to the phenol transport limit. As the phenol concentration became high, the first-order dependence vanished and zero-order dependence was noticed. An inverse proportionality of conversion with liquid reactant feed concentration (typical of zero-order behavior) was observed, especially at low temperature where the value of phenol adsorption constant K_{PHOH} was small.

Comparisons can be made between phenol overall conversions in the trickle bed and the upflow reactor for different inlet concentrations. Under the same test conditions, liquid back-mixing was more significant in the upflow reactor than in the trickle bed, but the former outperforms the latter regardless of the feed phenol concentration. Similar phenomena were reported for other liquid-limited reactions, such as ethanol oxidation (Goto and Mabuci, 1984).

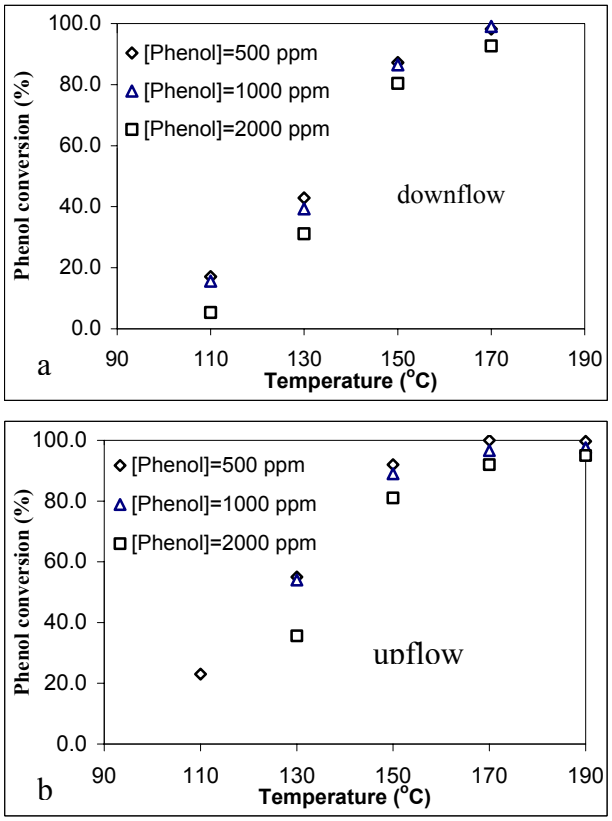

Figure 3-7. Phenol conversion at different phenol inlet concentrations for dowflow (Pe_L=24) and upflow (Pe_L=3) (Pressure = 3.2 MPa, LHSV = 0.3 hr^{-1}, u_G=0.53 cm/s).

3.3.7 Catalytic Wet Oxidation of TOC

In the previous work conducted in a stirred tank reactor, the main detected intermediates in the product effluent were acetic acid, catechol, and hydroquinone. Oxalic acid and benzoquinone were also identified in measurable quantities. However, once the catalytic oxidation process occurred in the packed-bed reactor, the main detected intermediates were acetic acid and oxalic acid, while catechol and hydroquinone in low amounts were identified as the remaining intermediates. In addition, the pH value of the aqueous solution at the reactor exit decreased considerably, thus suggesting that low-molecular-weight carboxylic acids were produced to an appreciable extent.

Figure 3-8 plots TOC conversion against temperature at different LHSV and constant air pressure. It is evident that a gap exists between the TOC conversion values obtained in

varied LHSV. This gap is narrow at low temperatures, where the reaction rate is rather low. However, the difference due to the varied LHSV becomes significant when the temperature increases. For low LHSV of 0.3 hr^{-1}, a temperature increase from 130 to 150 ^{o}C enhanced TOC conversion from 20 to 77%, while TOC removal was barely increased for the high LHSV of 0.6 hr^{-1}. The low flow rates allow the reactants a long time to contact the catalyst surface, where the reaction rate takes place. However, such a trend did not continue from 150 to 170 ^{o}C. Although this further temperature increment of 20 ^{o}C resulted in expedited reaction rates and noticeable TOC conversion for LHSV of 0.6 hr^{-1}, TOC removal was scarcely affected by increasing the temperature for LHSV of 0.3 hr^{-1}. For low LHSV and the resulting long reaction periods, TOC reduction reached a final stage that always involved a certain amount of organics refractory to the catalytic oxidation. The complete TOC mineralization would require that the operating temperatures be increased quite considerably.

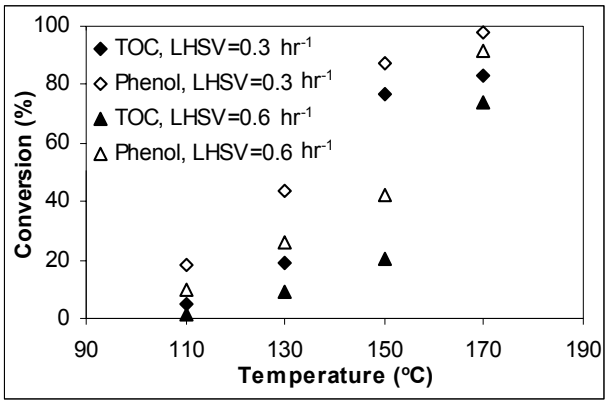

Figure 3-8. TOC and phenol conversions obtained in a trickle-bed reactor as a function of temperature (LHSV = 0.3 hr^{-1} and 0.6 hr^{-1}, Pressure = 3.2 MPa, u_G=0.53 cm/s).

There is a substantial difference between TOC and phenol conversion at low temperature (less than 150 ^{o}C), which is indicative of the large amount of partially oxidized products present in the liquid effluent. At 170 ^{o}C, it is clear that TOC conversion rate is very close to the phenol conversion rate, which means that during the

reaction small amounts of intermediates accumulated in the liquid phase. For the low liquid flowrate, HPLC analysis revealed that the quinone-like products accounted for about 10% of the intermediates detected in the liquid phase. When the flow rate was increased, the liquid residence time decreased, and the percentage of the quinone-like products increased up to 20% of the intermediates detected. As demonstrated by the existence of a maximum at the different residence times tested, these quinone-like intermediates are identified as first stages in the phenol oxidation mechanism and tend to degrade into low-molecular-weight acids. Unlike the quinone-like intermediates, the acetic acid and oxalic acid concentration did not show any maximum, thus indicating that they were refractory compounds in the complex phenol oxidation network.

The experiments conducted at different reaction temperatures with different flow directions also revealed their effects on the TOC reduction, as presented in Figure 3-9. In general, TOC and phenol conversion values were higher in upflow than downflow, while the corresponding gap that resulted from the different flow directions is quite narrow. Even though the effects of external mass transfer and diffusion are different in upflow and downflow, they were not the dominant factors. The major dependence of conversion values on temperature demonstrates that the process is controlled by reaction kinetics.

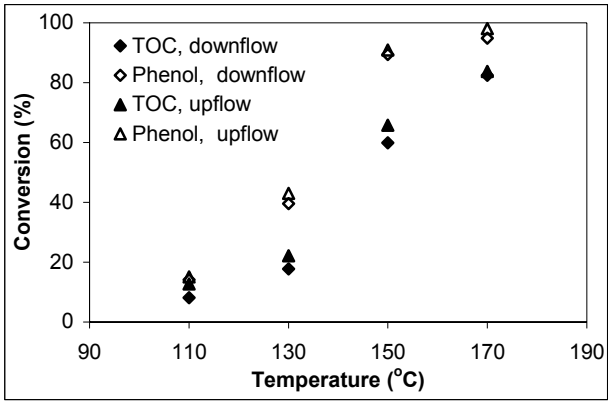

Figure 3-9. Effect of flow directions on TOC and phenol conversion, downflow (Pe_L=24) and upflow (Pe_L=3) (LHSV = 0.3 hr^{-1}, Pressure = 2.2 MPa, u_G=0.53 cm/s).

Both Figures 3-8 and 3-9 show that the TOC conversion increased as the operating conditions became more severe, which favors the oxidation of the intermediates, removing them from the exit solution. The small difference between phenol and TOC conversions suggests that the removal rate of phenol and nearly all intermediates are likely to be controlled by the same surface reaction steps. These reaction steps were not limited by benzene ring cleavage, which falls in line with the observations by Pintar and Levec (1994), who reported that the disappearance rates of 1,4-benzenediole and 1,4-benzoquinone are one order of magnitude greater than that of phenol. In addition, the accumulation of short chain carboxylic acids during the oxidation of phenol seems inevitable at low temperatures, since little TOC removal has been observed under these conditions. It is well known that compounds such as acetic acid, oxalic acid, and other lower carboxylic acids are very resistant to total oxidation even under severe conditions, and their mineralization to carbon dioxide is usually the rate-limiting step in a wet oxidation process (Imamura, 1999).

The results presented in Figure 3-10 show that the TOC degradation rate for the selected 1000 ppm phenol inlet concentration was higher than the one for 2000 ppm phenol input, and yet the difference is not significant for all the temperatures tested. For both the selected feed concentrations, the high temperature (170 ^{o}C) allowed for conversions above 90% for phenol and TOC, respectively, proving that this catalyst is still active at industrial high concentration levels. A similar phenomenon was observed by Silva et al., (2003), who studied CWO of formaldehyde on Mn/Ce catalyst and reported that high TOC reduction (>90%) can be achieved for different formaldehyde concentrations (800 and 1500 ppm).

It is worthwhile to emphasize that using Fe-Al pillared clay catalysts in the CWO process for a rather high pollutant loading enables a significant TOC reduction. The treated effluent is suitable for further microorganism digestion, so a post-biological treatment can be used as a complement to the CWO reaction process. If intensified energy input is possible (i.e., high temperature and high air flowrate), the Fe-Al pillared

clay catalyst can assist the CWO process to achieve the required TOC removal for the direct discharge of wastewaters containing phenol into the environment.

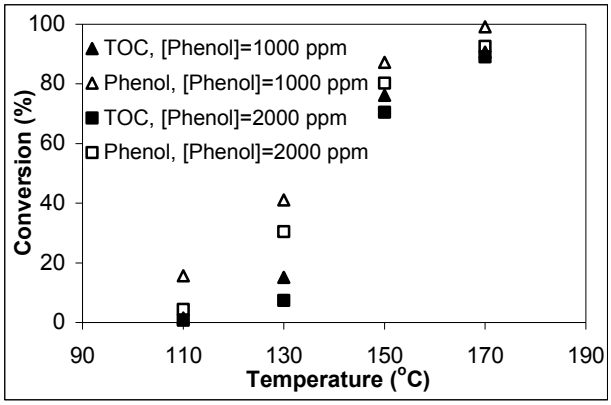

Figure 3-10. TOC conversion for different phenol inlet concentrations in a trickle-bed reactor (LHSV = 0.3 hr^{-1}, Pressure = 3.2 MPa, u_G=0.53 cm/s).

3.3.8 Catalyst Stability

In the reaction process, there is competition between the classical oxidation reaction and the condensation reaction that forms polymers. The polymers, if formed, could irreversibly adsorb on the catalyst surface and progressively block the active site, thereby lowering the rate of phenol removal. However, in the period of 200 h during which data were collected at various operating conditions, the physical blockage of active sites exhibited no considerable influence on the catalytic activity for phenol removal. Moreover, energy dispersion spectroscopy (EDS) analysis performed at the end of each test identified no carbon polymers deposited on the catalysts. The packed bed preventing condensation products from being formed is in a good agreement with the observations of Pintar et al., (1997), who studied catalytic wet air oxidation of phenol on a catalyst composed of copper, zinc, and cobalt oxides.

In addition, liquid samples were collected every 4h at the reactor exit and analyzed by the inductively coupled plasma (ICP). The analysis revealed no significant dissolution of the active ion (<0.4 ppm Aluminum and <0.2 ppm Iron). The pH of the feed solution was

acidic (pH = 4.0), and the most prevalent oxidation products are low-molecular-weight acid, which enhance the acidity of the solution. Even though the reacting medium is acidic and the operating temperature could be high, the low ion leaching shows a strong interaction between the metal elements and the pillars, which stabilizes the active sites of the catalysts.

Packed-bed reactors require that the catalyst does not deactivate or deactivates very slowly. Therefore, the used catalyst samples after the packed-bed operation deserve further investigation, which includes various detection methods. The details are given in next chapter. In addition, high catalyst effectiveness factor is desirable for its packed bed operation. Catalyst activity (effectiveness factor) would be further enhanced by reducing the catalyst size or modifying the particle pore structure. The details are also given in next chapter.

3.4 Summary

The catalytic liquid-phase oxidation of aqueous phenol solution, conducted in a packed-bed reactor with cocurrent downflow or upflow over Fe-Al pillared clay catalyst, revealed that phenol and TOC can be mineralized at relatively mild operating conditions (170^{o}C and 3.2 MPa). The reactor effluent was almost free of toxic organics, and a biodegradation process may be used as a subsidiary treatment method. Comparisons have been made between the performance of trickle flow (partially wetted catalyst) and upflow packed-bed reactor (completely wetted catalyst). The reaction was found to be liquid-limited at high pressure and low phenol feed concentrations, but it approached gas-limited at low pressure and high feed concentrations of phenol. The upflow reactor performed better at high pressure when liquid reactant limitation controls the rate, due to the completely wetted catalyst in the upflow reactor. The behavior of the downflow and upflow packed-bed reactors was shown to be the result of the interaction of reaction kinetics, mass-transfer phenomena, and reactor hydrodynamics. Reactor temperature, air velocity, and liquid velocity have to be considered as key parameters for tuning the reactor performance. The oxidation of phenol towards the carboxylic acids was found to

be strongly enhanced in the packed-bed reactor. The dissolution of active metal ions from the catalyst and polymer blockage on the catalyst active site were insignificant. The developed CWO process was used to treat a rather high phenol concentration (2000 ppm) over the Al-Fe pillared clay catalysts. The results showed significant phenol abatement and high TOC reduction. Therefore, this process is potentially promising for industrial wastewaters containing phenol.

Chapter 4
Characterization of Pillared Clay Catalysts

4.1 Introduction

Among various porous compounds, pillared clays are novel materials with potential for use as supports due to their tunable pore dimension and their specific catalytic properties, which depend on the type of silicate layers and pillaring agents. The width of the pillar is approximately 7-8 Å and the free distance between pillars is 10-22 Å (Clearfield, 1996). Their distribution in the space between the clay sheets and the surface acid properties of the host lattice can accommodate large molecules susceptible to undergo chemical transformations. The original intent in creating pillared clays was to provide a range of pores such that heavy crude oils containing large refractory molecules could be processed by fluid catalytic cracking. Extensive examination of cracking reactions has shown that gas oil cracking by pillared clay catalyst gives high selective yields of gasoline under moderate conditions (Occelli et al., 1986).

Recently, metal oxide pillars, such as Al_2O_3 and Fe_2O_3 have been successfully introduced between the silicate layers. A preparative route furnishing 1 kg per batch of pillared layer clay catalysts has been developed with a quality similar to that of materials from laboratory preparations (Kaloidas et al., 1995). Collaborated efforts have been made to evaluate such catalyst for the oxidation of phenol, a model pollutant due to its toxicity

and prevalence in industrial processes. This catalyst has remarkable activity and can achieve complete destruction of phenol and phenol intermediates at mild temperatures and pressures (Barrault et al., 2000). Up to now the overall kinetics of CWO of phenol over Al-Fe pillared clay catalyst, prepared and provided by Professor N. Papayannakos at the National Technical University of Athens (NTUA), and the process evaluation in packed-bed reactor have been studied in previous chapters. For both downflow and upflow operation modes, complete phenol (500 ppm) removal and significant total organic carbon (TOC) reduction were achieved at rather mild conditions of temperature (150-170 ^{o}C) and total pressure (1.5-3.2 MPa). Even for a rather high phenol concentration (2000 ppm), such CWO process showed significant phenol conversion (>80%) and high TOC reduction (>70%). In order to further improve the catalyst performance in packed-bed reactors, the catalyst needs to be characterized, and its effectiveness factors at different sizes need to be estimated. These will help in identifying the possibility of further improvement on the catalyst. This study is intended to explore through various characterization techniques the stability of catalyst pore structure under the oxidation conditions of the process used. Intraparticle diffusion is investigated by changing pellet sizes.

4.2 Sample Preparation

Generally the properties of the pillared clays are related to the nature of their constitutive elements (the clay layer and pillar) and also to the bond between these two. This implies that the modifications of the properties of the pillared clay were directed to the synthesis of pillars derived from various metallic hydroxides. Catalyst synthesis comprises two essential steps. The first is a cationic exchange of the natural clay by hydroxyl cations, and the second is the calcination which is to transform the hydroxides into oxide pillars anchored to the clay sheets. Diffusional limitations during the exchange, the structure of the oxide pillars, the distribution of pillars within the particles, and the existence of migrating H^{+} during the calcinations are the factors affecting the properties of the final product.

Al-Fe pillared clay catalyst extrudates were prepared and provided by Professor N. Papayannakos' Process Analysis and Plant Design Group at the National Technical University of Athens (NTUA), Athens, Greece. A stock clay suspension (2 wt%) was prepared and kept under stirring for 48 h before the upper half of the clay suspension was used. The cationic solution containing $AlCl_3$ and $FeCl_3$ (molar ratio of 9:1) was slowly titrated with NaOH solution at 70 ^oC until the OH/cation mole ratio was equal to 1.9. After aged under stirring for 24 h, the cationic complexes were mixed with clay suspension. After 1 h intercalation period and 24 h aging period, the intercalated clay was washed thoroughly with water to remove chloride ions on the clay surfaces, dried at 60-70 ^oC for 24 h, and finally calcined at 500 ^oC for 1 h. The main composition (wt %) was as follows: SiO_2, 52.50; Al_2O_3, 27.56; Fe_2O_3, 7.02 (Barrault et al., 2000).

4.3 Characterization Methods

The schematic diagram for the catalyst characterization methods has been reported as Figure 1-1. The catalyst samples and the colleted liquid phase at the reactor exit were tracked by the methods described below.

The Brunauer-Emmett-Teller (BET) method is the most widely used procedure for the determination of the surface area of solid materials and involves the use of the BET equation. Fresh and used catalysts were characterized with respect to their BET surface area, pore diameter distribution, and total pore volume, which were measured by the nitrogen adsorption isotherms at 77K, using Micrometrics Gemini 2375 sorption instrument. The catalyst samples were degassed at 110 ^oC for 3 h under vacuum prior to the sorption measurements. The pore size distributions were obtained from the desorption isotherms using the Density Functional Theory (DFT). Comparing the BET results of used catalyst to those of fresh catalyst provides important details on catalyst deactivation by carbonaceous deposits. The fractal dimension for each sample was also calculated.

Catalyst texture and morphology were examined by scanning electron microscopy (SEM) on a Hitachi S-4500 microscope operating at acceleration voltages = 10-15 kV, working distance =12-16 mm, and magnification values up to 20000×. Samples were

dusted on a double-sided sticky tape and mounted on microscope slides. Energy dispersion X-ray (EDX) spectra for the fresh and used catalyst samples were recorded using a NORAN Instruments microanalysis system. Topographical details of the catalyst were provided, which enable us to capture the physical and structural changes undergone by the catalyst.

The stability of the Fe/Al pillared clay catalyst to leaching of active metal ingredients into acid solutions was verified by an inductively coupled plasma (ICP) spectroscope with optical emission (Varian with SP-5 Autosampler). After liquid samples were taken at the reactor exit, they were filtered and then diluted by 2% (mass) HNO_3 solution. Atomized by the plasma, the dissolved Al and Fe were detected and their concentrations are calculated based on the calibration functions. Three different wavelengths at 396.15, 237.31, and 309.27 nm were chosen for Al element identification, while wavelengths at 238.20, 239.56, and 259.94 nm were selected for Fe element detection.

4.4 Characterization Results

The experiments, initiated with fresh catalyst packing, lasted continuously for 240 h in packed beds. The results revealed a decline from initial conversion of 100% with fresh catalyst to final conversion of ~80% and ~75% after 240 h for downflow and upflow operation modes, respectively. Higher deactivation level obtained in upflow is attributed to the higher wetting efficiency in upflow mode than in downflow mode. On the base of HPLC analysis, the selectivity of phenol to low molecular weight acids remained constant at different times. Hence, no changes took place in the mechanism of the reaction during deactivation. Poisoning deactivation was unlikely to take place since phenol is free of sulfur and phosphate, which are the heteroelements known to be poisonous to oxidation catalysts (Yurii and Moshe, 1998). The decrease in activity was probably due only to the blocking of the channels and, thus, to a decrease in the number of active sites.

The catalysts collected after 240 h downflow operation exhibit different colors, changing from light beige (original color) to dark brown. Clearly this is indicative of

different reaction degrees and solid-liquid contact types due to the maldistribution of the liquid flow during the downflow operation. The catalysts completely surrounded by liquid film (fully wetted) have more contacts with phenol and intermediates (catechol and benzoquinone) than the partially wetted or fully dry catalysts. These fully wetted catalysts in downflow operation have to withstand the pollutant loading that is shared by all the catalysts in upflow operation, which, in contrast, results in all catalysts having light brown color. The catalysts of dark brown color collected after downflow operation (labeled as Used-Dn in Tables and Figures) were sampled for the characterization purposes, together with the fresh catalyst samples and the catalysts collected after upflow operation (labeled as Used-Up in Tables and Figures).

4.4.1 Pore Size Distribution

The pore size of pillared clay catalyst is determined by the interlayer distance and by the lateral distance or density of the pillars. The former depends on the size of the pillaring agent, while the latter is regulated by the charge density of the layers and the effective charge of the pillars. Surface area of a catalyst is also a key factor influencing catalytic activities. An understanding of the pore size and surface area of a porous media can be achieved by constructing an adsorption isotherm. Figure 4-1 represents the typical nitrogen adsorption isotherm obtained for the fresh Al-Fe pillared clay catalyst. The nearly linear portion of the adsorption curve in the P/P_0 (relative pressure, correlated to the amount of adsorbed nitrogen) ranging from 0.05 to 0.3 reflects the existence of micropores (< 20 Å) and small mesopores (20-30 Å) (Gregg and Sing, 1983). The pore dimension is consistent with that expected from the expanded gallery height (10-22 Å) upon pillaring (Clearfield, 1996). The adsorption isotherm gives a good fit with the BET equation.

The total BET surface area and the micropore area values for the selected catalyst samples are given in Table 4-1. A major part of the surface area is contributed by pores with a diameter characteristic of mesopores. A smaller but significant part is due to micropores. Fresh catalyst has a BET surface area of 145.1 m^2/g, while for the used

catalysts the total surface area decrease significantly by 66% and 60% for catalysts collected after 240 hr downflow and upflow operation, respectively. Corresponding decreases in total pore volume are evident. These data suggest that deposition of carbon on the catalyst leads to pore plugging in both micro- and mesopores blockage.

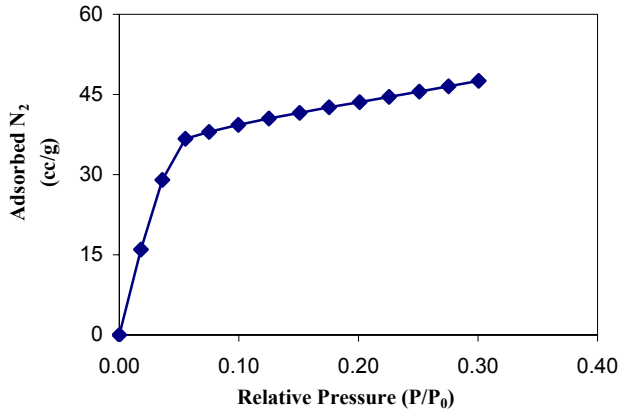

Figure 4-1. Nitrogen adsorption isotherms curve for the fresh Al-Fe pillared clay catalyst.

Table 4-1. Physical properties of various catalyst samples

Sample	BET surface area (m^2/g)		Average pore size (Å)	Pore volume (cm^3/g)	Fractal dimension
	Micro	Total			
Fresh	49.1	145.1	16.2	0.33	2.709
Used-DN	6.9	48.9	20.8	0.11	2.483
Used-UP	8.1	57.8	22.5	0.13	2.631

Classical macroscopic theories such as the BJH (Barrett, Joyner, and Halenda) method, and semiempirical treatments, e.g. HK (Horvath-Kawazoe) method, do not give a realistic description of the filling of micropores and narrow mesopores, thus they tend to underestimate the pore sizes (Allen, 1980). Other methods have been developed that accounted for the sorption and phase behavior of fluids in narrow pores on a molecular level. Treatments such as the Density Functional Theorty (DFT) or methods of molecular simulation (Monte Carlo simulation) provide a much more accurate approach for pore

size analysis by describing the local fluid structure near curved solid walls. They bridge the gap between the molecular level and macroscopic approaches. Adsorption isotherms in model pores are determined based on the intermolecular potentials of the fluid-fluid and solid-fluid interactions. The pore size distribution curves based on DFT method were derived for various types of catalysts and plotted in Figure 4-2. The fresh samples possess a bimodal and a fairly broad pore size distribution around diameter of 17 Å (micropore) and 26 Å (mesopores). The catalyst deactivation considerably reduced the free volume of micropores by 70% and 60% after 240 hr downflow and uoflow operations, respectively. The volume of mesopores were also reduced, but by a less extent (25%) after both operation mode. Hence, the contribution from mesopores to the total volume increases, which in turn shifts the average pore diameter to a higher value, as seen in Table 4-1.

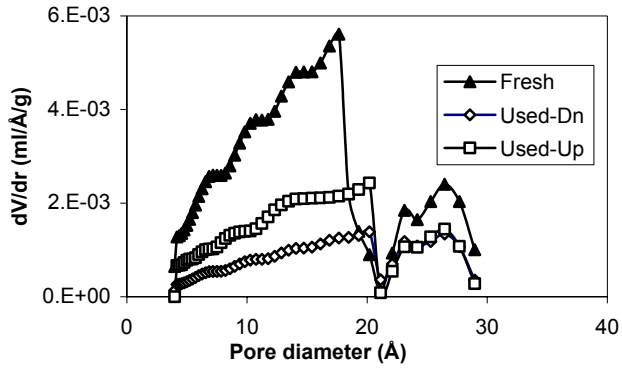

Figure 4-2. Pore size distribution curve for fresh catalyst and used catalysts collected after downflow and upflow packed-bed operation (170 ^{o}C, 3.2 MPa, initial phenol concentration 500 ppm, 200 h).

Surface characterization methods based on fractal geometry describe the topography of real surfaces in terms of a roughness exponent known as fractal dimension, D. Real surfaces are generally rough because of atom packing arrangements and defects, kinks and dislocations. Many real surfaces present surface irregularities that appear to be similar at different scales. These surfaces are referred to as fractal because their

magnitude is proportional to X^D, where X is some characteristic dimension, and D ranges from 2 for smooth surface to 3 for surfaces so rough that they essentially occupy all available volume. Using FHH (Frenkel-Halsey-Hill) method (Pfeifer et al., 1989) based on single gas sorption isotherms, the fractal dimension D accounting for adsorbate surface tension effects is reported in Table 4-1. Relative high value of fractal dimension for fresh catalyst is indicative of its porous and rough surface. A noticeable decline of fractal dimension was detected for the used catalysts, which implied the presence of a smoother and less textured surface. A reduced number of tortuous micropores and more organic coverage on the used catalyst surface are two main factors for the surface roughness decrease.

4.4.2 Electron Microscopy in Conjunction with EDX

To further understand the morphology of catalyst samples and visualize the surface reaction process, the fresh and used catalysts were characterized by electron microscopy in conjunction with energy dispersion X-ray (EDX). Figure 4-3 shows the scanning electron microscopy (SEM) images of fresh catalyst with different magnification, revealing a highly porous and rough surface. The fresh catalyst appeared to have abundance of crystals (highlighted by circles) on the external surface of the supports (Figure 4-3a), as well as inside the pores (Figure 4-3b). Introduction of Fe and Al cations into clay layers results in the appearance of the crystals with sizes ranging from 1 to 10 μm. As expected for amorphous materials, they are irregular in shape. EDX elemental analysis over a number of selected crystals showed that they are composed of silicon (Si), aluminum (Al), oxygen (O) and iron (Fe). Si is a component of the clays which is supposed to stay in the clay layers. However, the existence of large amount of Si in the crystals implies that Si may migrate to the surface in the intercalation process. No carbon was detected in the fresh catalyst sample.

a

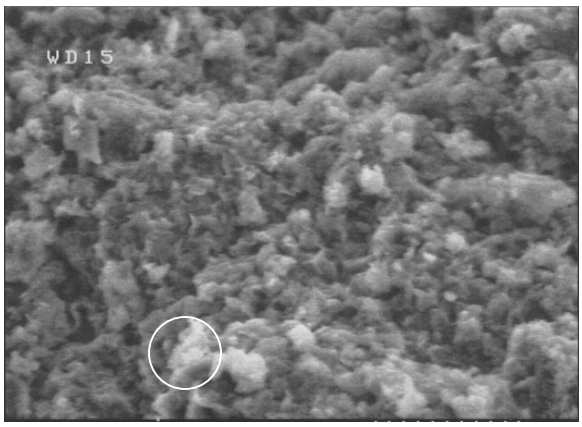

b

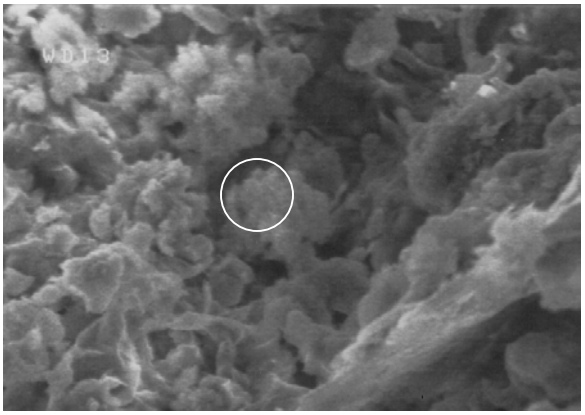

Figure 4-3. SEM images of Fresh Al-Fe pillared clay catalyst with magnification of (a) 3000 (10 μm scale) and (b) 10000 (3 μm scale), crystals marked by circles.

Polymeric compounds of Al, Fe, are among the principal pillaring species quoted in the literature (Coelho and Poncelet, 1990). The insertion of polyoxyhydroxy cations of various metals (Al-Fe) as pillars in the interlayer space confers an acidic nature and free volume on the intracrystalline environment. The resulting pillared clays show large pore size, which allow bulky organic molecules to diffuse through the pores to reach active acidic centers. When the iron content is more important (Fe/Al>0.3), the pillars are largely composed of iron species and important particles of iron oxide distributed inside or outside the porosity (Bergaya and Barrault, 1990). Because only the outer surface of the iron oxide particle is easily available to react with organic molecules, the congregation of iron oxide, if existing, is not beneficial for the dispersion of active site and would lead to a low utilization rate of iron. In this work, the EDX analysis of the

fresh catalysts exhibited a nearly uniform distribution of iron throughout the external surface area. This indicates that the preparation procedure is efficient for obtaining highly dispersed metal-active species.

Figure 4-4(a) shows a typical crystal with size of 1.5 μm in the fresh catalyst, which possesses morphology clearly different from those of used catalysts after 240 hr packed-bed operation, as shown in Figure 4-4(b) and 4-4(c). For the used catalyst, SEM photographs reveals the appearance of many leaf-like materials radiating from the available crystal surface. EDX analyses indicate that species carbon, besides the original elements of Al, Fe, Si, and O, is present in this leaf-like material, as shown in Figure 4-5. This observation suggests Fe oxide in the crystal forms the Fe-O-C bindings and promotes the formation of congregated carbon. Oxidation reactions occur after reactants are adsorbed on active sites located at the crystal surface sites. The weak desorption of the high molecular weight intermediates facilitate the carbon accumulation. The occupation of the active site by carbon contributes to the decreased Fe oxide utilization rate and decreased phenol oxidation rate. However, despite the fact that a lot of crystals were embedded in the carbonaceous deposit, most of them, unchanged in size from the fresh sample, remained visible, as shown in Figure 4-4(b) and 4-4(c). In contrast to the type of uniform cover-up of carbon which makes the crystal active site inaccessible, this leaf-like structure still allows the exposure of Fe oxide to the reactant to pursue the oxidation reaction, based on the fact that catalysts are still active even after long time utilization. The homogeneous distribution of Fe oxide clusters on the surfaces of open mesopores in the pillared clays is also responsible for the lasting catalytic activity.

a

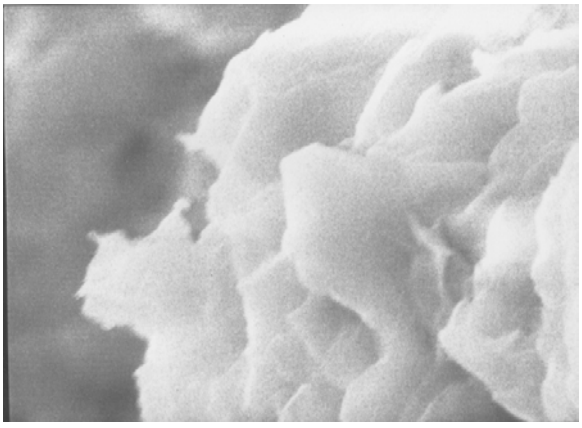

b

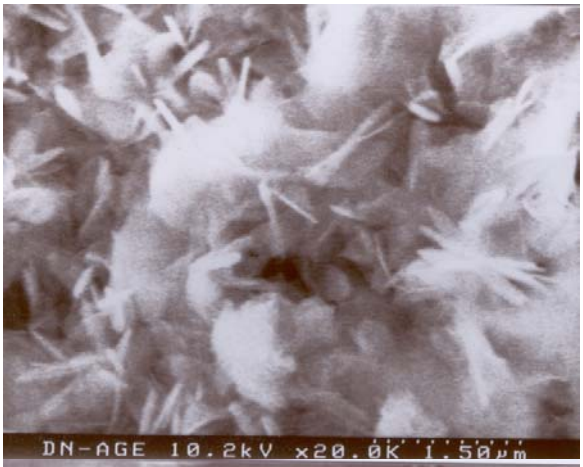

c

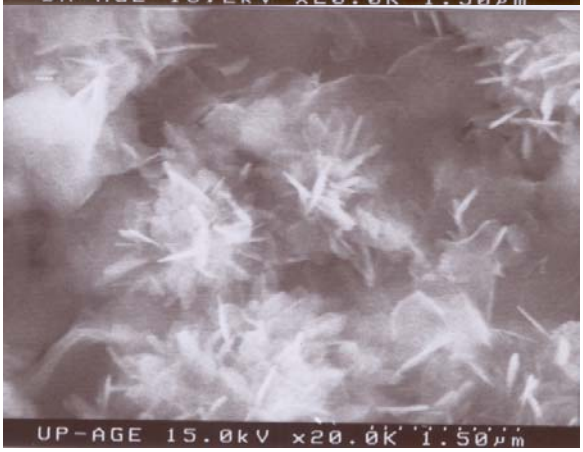

Figure 4-4. SEM image comparison between (a) fresh catalyst, (b) used catalyst collected after downflow packed-bed operation, and (c) used catalyst collected after upflow packed-bed operation (magnification: 20000, 1.5 µm scale).

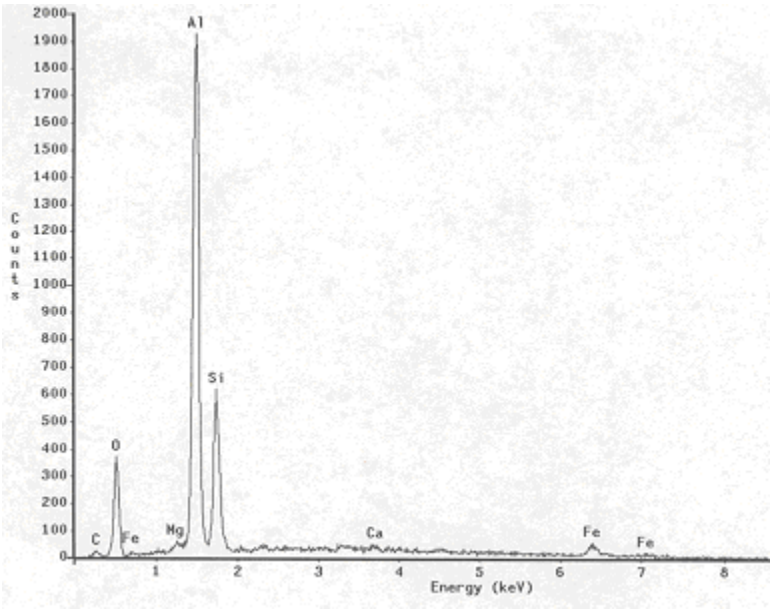

Figure 4-5. EDX result of the leaf-like material in figure 4-4(b) and 4-4(c).

After 240 hr operation, it is not surprising to see a bigger carbon leaves on the catalyst of dark brown color obtained during downflow mode, in comparison with the one obtained from the upflow mode. For the same amount of pollutant loading in the reactor, the former samples, as the portion fully wetted due to liquid maldistribution, have more chances of contacting carbon from the catalyst perspective. This finding is in line with their comparative BET surface areas and pore volumes. The leaf-like carbon clusters may become the seeds for the growth of carbon layer and cross-link with each other, which cause subsequent pore plugging and a decreased BET surface area and pore volume. The carbon clusters may correspond to different chemical natures: mainly aromatic, aliphatic, and partially oxidized (Hamoudi et al., 1998).

4.4.3 Ion Leaching Test

Analysis by plasma emission spectrometry for metal elements contained in the fully oxidized solutions exhibits insignificant Fe and Al leaching from the oxide catalyst. As shown in Figure 4-6, the concentrations of dissolved Al were below 0.3 ppm and 0.15 ppm for downflow and upflow, respectively, confirming the negligible extent of catalyst

leaching in the reaction medium. In the case of Fe, the concentration of dissolved ions was below 0.1 ppm and 0.05 ppm for downflow and upflow operation modes, respectively. The overall Fe leaching after 240 hr operation represents less than 2% of the total iron content present in the fresh catalyst.

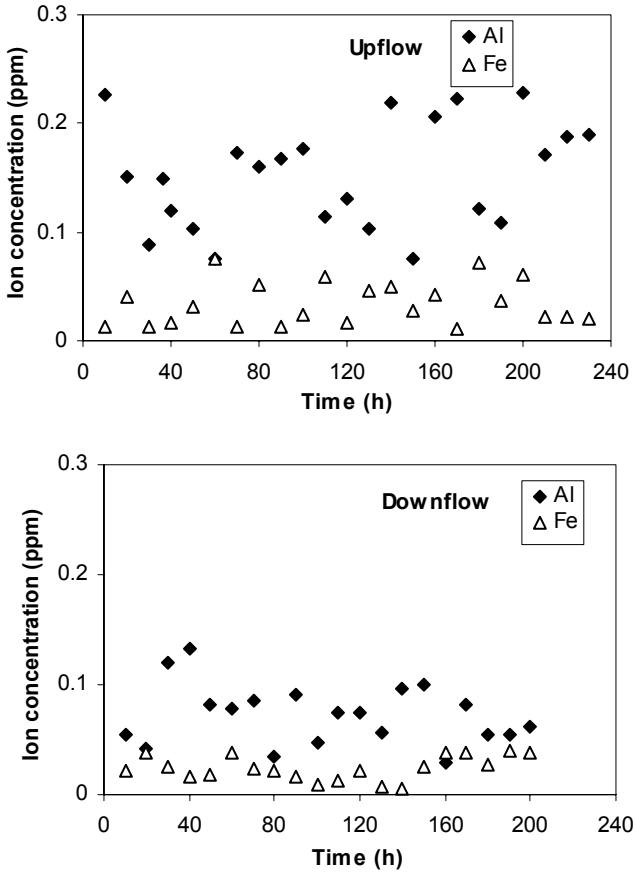

Figure 4-6. Iron and aluminum concentrations in the effluent liquid samples taken during downflow and upflow packed bed operations (170 ^{o}C, 3.2 MPa, 500 ppm initial phenol concentration, 200 h).

The catalyst stability is partly attributed to the stronger binding of the liberated protons to the outer tetrahedral oxygen where Al^{3+} substitutions for Si^{4+} have occurred. A second factor is thought to be the stronger binding or cross-linking of the alumina pillars to the layers (Clearfield, 1996). About 60% of the iron species is bonded to the small oxide

clusters dispersed in the solid, inside or outside the porosity (Gangas and Papayannakos, 1993). In addition, at the elevated temperature used by CWO process, the spacing in the pillar itself or between Al-Si layer and pillar decreases slightly due to contractions of the pillar species upon forming stronger chemical bonds. Regardless of the location, the iron species are highly stabilized by the clay matrix.

4.5 Intraparticle Diffusion

Additional experiments were needed to select the proper size and shape of the catalyst and also to determine the effect of intraparticle mass transfer resistance. To characterize the intraparticle resistance, slurry reactor studies with different catalyst sizes and the extended Weisz-Prater criterion (Froment and Bischoff, 1979) were used. Phenol oxidation was conducted in a slurry system at constant temperature and oxygen partial pressure using a magnetically stirred high-pressure reactor. The experiments were carried out batchwise for the liquid and continuously for the gas by feeding fresh air. The reactor was loaded with 600 cm^3 of feed solution and a given mass of catalyst. The reactor temperature was automatically controlled, while cold water circulation through a coil placed inside the reactor was used for properly quenching the reaction. At preset times, liquid samples were withdrawn, rapidly cooled, filtered and analyzed.

To minimize the external-mass transfer resistances in the following experiments, the rotation speed was kept at 800 rpm. The fresh Al-Fe pillared clay catalyst particles of cylindrical extrudate form (2 × 8 mm) were cut to 2 mm and 1mm long (Batches B1-B3). To get smaller scales, they were also crushed and sieved (Batches B4-B6). Table 4-2 lists the different particle size fractions collected. For extrudates of batches B1-B3, equivalent diameter is $D_p = 6V_p / S_x$. For crushed particles in batches B4-B6, D_p is the average particle diameter. Every batch was washed to remove all fines, then dried overnight prior to use. Catalysts in extrudate form were contained in a fixed basket inside the reactor, while the basket was removed for the batches with crushed catalysts in powder form.

Table 4-2. Catalyst particle size fraction

Batch	Dimension (mm)	Equivalent D_p (mm)	Effectiveness factor η
B1	2(D)×8(L)	2.67	0.32
B2	2(D)×2(L)	2.00	0.51
B3	2(D)×1(L)	1.50	0.60
B4	1.0-0.60 (mesh 16-25)	0.80	0.82
B5	0.60-0.30 (mesh 25-50)	0.45	1.0
B6	0.30-0.15 (mesh 50-100)	0.23	1.0

Experiments over catalysts with various sizes exhibit the internal mass transfer limitations. Using a loading of 5 g of catalyst, these tests were carried out at 170 ^{o}C, 3.2 MPa of total pressure, and 500 ppm initial phenol loading. Figure 4-7 illustrates the impact of the equivalent particle diameter on the initial rate of phenol removal. The effect of the internal mass transfer is significant for D_p above 0.5-0.6 mm. The effectiveness factor can be calculated according to

$$\eta = \frac{r_{obs}}{r_s} \tag{4-1}$$

where r_{obs} is the rate of phenol oxidation with pore diffusion resistance, r_s is the rate of reaction with surface conditions. The calculution of the effectiveness factor will confirm the effect of particle size on reaction rate in the oxidation treatment. Clearly the latter was measured over the catalyst with D_p below 0.5-0.6 mm. The effectiveness factors for different catalyst dimension were shown in Table 4-2. The cylindrical catalyst extrudate (2 × 8 mm) has been investigated in the stirred-tank basket reactor for its apparent kinetics model. However, its effectiveness factor is not satisfying. The effectiveness factors can be increased to fairly high values by cutting the catalyst length to 2 and 1 mm, which can still be suitable for packed-bed operation. Since these low dimension catalyst extrudates facilitate the phenol oxidation rates, they may allow milder conditions in

packed-bed operation conditions to achieve complete phenol mineralization and significant removal of total organic carbon, compared with the current temperature (150-170 ^{o}C) and total pressure (<3.2 MPa).

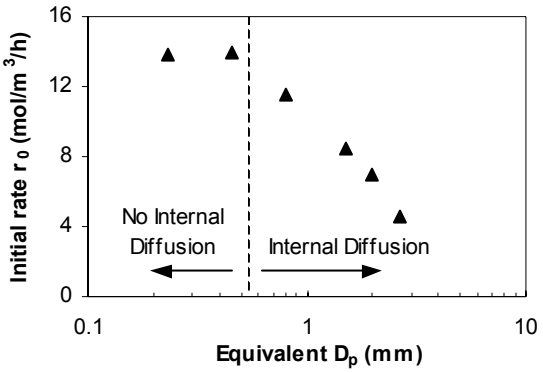

Figure 4-7. Impact of the catalyst particle size on the initial rate of phenol oxidation (T = 170 ^{o}C, P = 3.2 MPa, 5 g catalyst, 500 ppm initial phenol loading).

One criterion was useful for the importance of diffusional limitations based on the experiments with two sizes of catalyst (Froment and Bischoff, 1979). If one assumes that effective diffusivity D_e and reaction rate constant k_v are the same, then the Thiele modules are correlated by eq (4-2).

$$\frac{\phi_1}{\phi_2} = \frac{D_{p1}}{D_{p2}} \tag{4-2}$$

The resulting two observed rates can be correlated according to eq (4-3).

$$\frac{(r_{obs})_1}{(r_{obs})_2} = \frac{\eta_1}{\eta_2} \tag{4-3}$$

If there is no pore diffusion limitation, i.e. $\eta_1 = \eta_2$, the two observed rates are the same. In contrast, appreciable diffusion resistance can occur for small diffusivity, large pellet size D_p or very rapid reaction rate, where the asymptotic relation is $\eta = 1/\phi$. In this case, the two observed rates are inversely proportional to the two pellet sizes.

$$\frac{(r_{obs})_1}{(r_{obs})_2} = \frac{\phi_2}{\phi_1} = \frac{D_{p2}}{D_{p1}} \tag{4-4}$$

The intermediate degrees of pore diffusion limitation will lead to the ratio of observed rates in between the above two extremes. Hence, considering $D_{p2} < D_{p1}$,

$$\frac{D_{p2}}{D_{p1}} < \frac{(r_{obs})_1}{(r_{obs})_2} < 1 \tag{4-5}$$

The ratios between characteristic diameters and between corresponding observed rates are listed in Table 4-3. Based on the above criteria, there is intermediate degree of pore diffusion limitation for large particles. This suggests that the observed rate was strongly affected by the internal mass transfer. To enhance the mass transfer rate of large reactant molecules in the catalyst pore, the synthesis methods can be adjusted so that pore channel gets enlarged or the percentage of mesopore gets higher. The alternative approach to facilitate the contact of reactants with catalyst core is simply cutting the current extrudates to small sizes. The length reduction to 2 or 1 mm provided enhanced effectives factor, and the resulting pressure drop in the packed bed is still affordably low.

Table 4-3. Application of criteria for importance of diffusional limitation

Case		D_{p2} / D_{p1}	$(r_{obs})_1 / (r_{obs})_2$
Sample 1	Sample 2		
B1	B2	0.75	0.78
B1	B3	0.56	0.59
B1	B4	0.30	0.49
B2	B3	0.75	0.76
B2	B4	0.40	0.63
B3	B4	0.53	0.83

In theory, it is preferable to use a catalyst with a small particle size (< 0.5 mm) to minimize the internal mass transfer resistance. Actually the downflow mode of operation using smaller size of catalyst can achieve full wetting of catalyst as well as an almost

plug flow pattern of liquid (even at a lower LHSV) and the data generated in this way represent the true activity of the catalyst. In the up-flow mode of operation, the catalyst will definitely achieve full wetting when a smaller size of catalyst is used. However, the complete removal of liquid axial back mixing in the up-flow mode will depend on the length of the catalyst bed as well as on the level of LHSV. Thus one may expect plug flow pattern of liquid in a bench-scale reactor in the up-flow mode using smaller size of catalyst. Equal performances in these two modes of operation using a smaller size of catalyst have been observed in bench-scale reactors (Wu et al., 1996).

On the other hand for its application in packed-bed reactor, in addition to a large pressure drop across the catalyst bed at the reaction conditions, it is easy for small particles to be washed out by the liquid stream, which implies potential catalyst loss and undesirable secondary pollution to the liquid. Even though this current size of 2 × 8 mm has low effectiveness factor (0.32) at the given conditions, it creates low pressure drop in the packed bed operation. Further development of the catalyst preparation method may stress on the combination of the revision of pore structure together with the modification of catalyst dimension. Hence, one has to balance these factors in order to obtain the optimum catalyst design.

4.6 Summary

Pillared clays represent a diversified range of materials which can be tailored as to their pore size, nature of pillars, choice of layer and cation substitution, type and number of acid sites, and doping to achieve success for a particular reaction. With a bimodal pore size distribution, the novel Al-Fe pillared clay catalyst is able to catalyze relatively large organic molecules (phenol) at soft conditions. Various catalyst characterization methods revealed the catalyst deactivation after long duration via carboneous formation and laydown on the active catalyst site in the CWO process of phenol, while the ion leaching from the catalyst to the acidic solution was insignificant. Restoration of catalyst activity can be obtained by burning out the carbon-containing deposits. From an assessment of the effect of mass transfer resistance on the observed reaction rate, it is found that the

rates under the reaction conditions employed were strongly affected by internal mass transfer. Further investigations are necessary to better control the synthetic process, to better stabilize the composites, to elucidate the structure in more detail, and to improve the catalyst effectiveness. By combining with a proper catalyst extrudate dimension with the modified pore structure, it is possible to achieve high effectiveness factors and low process operation costs.

Chapter 5
Modeling Catalytic Wet Oxidation

The CWO process has been receiving more attention as a promising technology for wastewater treatment. Nevertheless, the successful model is one key element for the establishment of any emergent technology. Thus, we attempt to investigate the CWO process through numerical simulations and aim to give recommendations for a proper operation strategy of the reactors designed for phenol oxidation. Prior to the model application for the scale up of the process, the model is validated against the experimental data obtained in the laboratory packed-bed reactor.

Packed-bed performance depends on a complex interaction of the intra-particle and inter-phase mass transport, reaction kinetics, and hydrodynamics. Most industrially important reactions involve complex reaction kinetics, such as in the catalytic wet oxidation (CWO) of liquid-phase phenol. To interpret the reaction in packed-bed reactors, one needs an assessment of the flow behavior, such as holdup and partial catalyst wetting, as well as the relative importance of the various mass transport resistances (Goto and Smith, 1975).

A lot of attempts were made to develop physically based models for successful prediction of process performance in packed-bed reactors, such as cell model (Brad Sims et al., 1994), a cross-flow model (Tsamatsoulis and Papaynnakos, 1995), and others based on liquid flow mal-distribution (Funk et al., 1990) or stagnant liquid zones in the reactor (Rajashekharam et al., 1998). Among the reactor scale model, the 1D plug-flow model has been used for modeling a large trickle-bed reactor (Froment et al., 1994). The

1D axial dispersion model (ADM) is the simplest model describing differential mixing in packed-bed reactors by superimposing axial dispersion on plug flow (Berger et al., 2002). The combined modeling scheme of flow and reaction have shown that 1D models can provide the axial distribution information on species concentration and selectivity for given reaction kinetics. Such information is important for evaluating the targeted operating units with a wide range of applications conditions.

This chapter is structured as following.

In section 5.1, models reported in literature are evaluated. A reactor scale model and a pellet scale model are modified to remove their disadvantages. Before the modified modeling scheme is applied for the studied CWO process, it is validated against the experimental observations using test reactions reported in the literatures. The details of the model evaluation, scheme modifications, and model verification for packed-bed reactors are presented in Appendix A.

In section 5.2, this model is applied to the studied CWO conditions and its predictions are compared with experimental results in Chapter 3. The apparent kinetics developed in Chapter 2 is used. The model failed to predict the experimental data at conditions where significant phase change occurs (high temperatures, low liquid velocity).

In section 5.3, this model is further modified by accounting for phase change to properly improve the model's capability and predict satisfactorily the obtained experimental results.

5.1 Evaluation of the Axial Dispersion Model (ADM)

The axial dispersion model (ADM) has been used to describe the reactor scale performance. Details of the ADM can be found in Appendix A, where a general modeling scheme is formed by integrating the reactor scale ADM with the pellet scale model.

Khadilkar et al. (1996) has employed a plug-flow reactor scale model proposed by El-Hisnawi (1981) for the reaction of hydrogenation of alpha-methylstyrene (AMS) with

nonlinear intrinsic kinetics. The pellet effectiveness factor was used to connect the intrinsic kinetics with the reactor scale model. However, the pellet effectiveness factor was used as a fitting parameter and calculated at one space-time with the experimental observation, which cannot reflect the actual mass transfer resistance inside the pellet and the pellet external wetting contact with the liquid. In fact, the value of effectiveness factor varies along the axial direction of the reactor. In addition, when catalyst deactivation occurs, the loss of the catalyst active sites leads to a dynamic reaction rate, and the reactant concentrations in the liquid bulk and on the catalyst surface keep changing, which makes difficult the derivation of fitted effectiveness factor.

In our modified modeling scheme, a pellet scale model was combined with a reactor scale axial dispersion model (ADM), so that the values of the effectiveness factor were calculated directly from a pellet scale model at each axial reactor location for a given time. We can thereby get a local effectiveness factor corresponding to the local reactant concentrations, instead of the one obtained from fitting.

Our modeling scheme solves reactor scale and pellet scale model sequentially. The ADM predicts the local concentration along the reactor axis, while the pellet scale model evaluates the local effectiveness factor corresponding to the local reactant concentration. At first the ADM is solved with an initial value of the pellet overall effectiveness factor to predict the profile of local concentrations along the reactor axis, such as the reactant concentrations at the liquid bulk phase and on the catalyst surface. Once the local reactant concentrations at each reactor collocation point are known, the corresponding boundary conditions for the pellet scale model become available. Accordingly, the pellet scale model is solved to evaluate the overall effectiveness factor at every axial collocation point. Then the newly obtained set of pellet overall effectiveness factors are used again as the input to the ADM, where the local reactant concentrations along the reactor axis are updated. The newly obtained local reactant concentrations are employed to compute again the overall effectiveness factor at every axial collocation point. These steps are iterated until convergence is achieved, when the latest values of the pellet overall effectiveness factors along all the reactor axial collocations adequately match the ones

used in the previous iteration. No adjustable parameters have been used in this proposed sequential approach.

In general, for a given intrinsic kinetics, both reactor scale and pellet scale models need to be solved, and the proposed modeling scheme using sequential iterations has been verified as a robust and efficient approach, as seen in Appendix A. Nevertheless, the modeling scheme can be simplified for a given apparent kinetics. Because the pellet scale effectiveness factor has been accounted for in the apparent kinetics expression, there is no need to solve the pellet scale model. Hence, only reactor scale model is solved, and sequential iterations between reactor scale model and pellet scale model is not required.

Since the apparent kinetics expression has been proposed in Chapter 2, it is noteworthy that only reactor scale model is used in sections 5.2 and 5.3.

5.2 ADM Application in CWO

A packed-bed reactor has been advocated as a suitable choice for the treatment of wastewater (Pintar and Levec, 1994). Compared with slurry reactors, it is more advantageous in terms of process selectivity and stability (Stuber et al., 2001). Among a diversity of applications, packed bed has been evaluated for catalytic wet oxidation (CWO) of wastewater containing phenol. Most CWO studies have adopted the downflow operation modes (Eftaxias et al., 2003; Fortuny et al., 1999), while the upflow mode has received more attention recently (Stuber et al., 1996; Santos et al., 2001).

In this section, the ADM model is applied to describe the reaction of aqueous phenol oxidation over Al-Fe Pillared clay catalyst, which is of our interest, and to predict the reactor performance under different operating conditions. The supporting experimental work has been reported in Chapter 3, where an isothermal packed-bed reactor was operated in both downflow and upflow operation, at rather mild conditions of temperature (110-170 ^{o}C) and total pressure (1.5-3.2 MPa).

5.2.1 Effect of Axial Dispersion

The experimental conditions studied in Chapter 3 resulted in significant axial dispersion effects in the liquid phase (Pe_L=21~39 for downflow mode and Pe_L=3~5 for upflow). In fact, axial dispersion has strong impacts on the reactant concentration at the reactor outlet. The differences between the predicted concentrations calculated by the plug flow type and the axial dispersion model depend on the conversion level. Thanos et al. (1996) studied a 1st order hydrotreating reaction over cylindrical extrudates with their dimension close to the one of Al-Fe pillared clay catalysts employed in this work. They found that for conversions up to 85% the differences are not significant, and they can be close to the random experimental error or the error of the concentration measurements. But as the space velocity decreases the conversion increases, and the differences become important. For the extrudates of equivalent diameter (d_{eq}=1.93 mm), the relative deviation of the exit concentration compared to the plug flow case is 5.4% at LHSV =2 h^{-1}, and the relative deviation increases to 170 % at LHSV =0.5 h^{-1}. For the exturates of equivalent diameter (d_{eq}=3.08 mm), the corresponding relative deviations are 11% and 440%, respectively. These relative deviations are very high and may lead to considerable errors in the reactor design and scale-up.

Therefore, the effect of axial dispersion was considered significant, and hence, the axial dispersion model (ADM) was employed to describe the liquid phase in the whole reactor for CWO process, with appropriate inlet and outlet boundary conditions. It is assumed that isothermal conditions exist throughout the reactor and that the liquid reactants/solvents are non-volatile. Gas phase is assumed to be pure at constant partial pressure of the reacting gas. Variation of temperature, velocity, and holdup in the axial direction is assumed to be negligible. The mass balance equations for the species in the gas and liquid bulk phases and at the catalyst surface are considered. The details of the reactor scale axial dispersion model (ADM) has been developed in our previous work and given in Appendix A.

The primary model variables of interest have been the dissolved liquid-phase concentrations of the gaseous reactant (O_2) and the conversion of the liquid-phase

reactant (phenol). The driving force $\left[C_{A,e} - C_{A,L}\right]$ determines the O_2 dissolution from gas to liquid. The mass transfer resistance between liquid and solid phases is reflected in a separate algebraic equation. The intraparticle mass transfer inside the catalyst particles is considered via the overall reaction kinetics. The key differences in modeling downflow and upflow are the values of the mass transfer coefficients ($(ka)_{GL}$, k_{LS}, k_{GS}), the liquid holdup, the axial dispersion coefficient, and the external liquid-solid contacting efficiency. The correlations for mass transfer coefficients, axial dispersion coefficient and hydrodynamic parameters are reported in Appendix A, where the effect of liquid and mass velocity on simulated gas-liquid and liquid-solid transport in both reactors has been accounted for.

Catalyst pellets are divided into three liquid-solid contacting cases: (a) the catalyst surfaces are completely dry, (b) the catalyst surfaces are partially dry, and (c) both catalyst surfaces are completed wetted. The corresponding weights for each category are given as $(1-\eta_{CE})^2$, $2\eta_{CE}(1-\eta_{CE})$, η_{CE}^2, respectively. This way the sum of the weights turns out to be unity. For the latter two wetting types, the external liquid film possesses the same species concentrations. The half wetted and completely wetted catalyst pellets are assumed to be internally completely wetted because of the capillary forces.

During the course of the aqueous phenol oxidation previously carried out in the catalytic trickle bed and upflow packed bed, the reactor was maintained at isothermal conditions. The effect of reaction heat release was insignificant due to the dilute phenol concentration (500-2000 ppm).

5.2.2 Overall Reaction Kinetics

In the experiments for phenol oxidation over packed-bed reactor, only small amounts of intermediate (catechol, hydroquinone, benzoquinone, etc.) were detected at the outlet. Hence, the numerical simulation for the overall lumping rate for phenol mineralization is focused instead of the detailed reaction rates for all intermediates in a comprehensive reaction network. Mineralization of phenol is described as

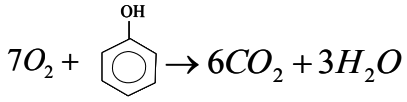

The overall kinetics for phenol oxidation over the pillared clay catalyst has been studied by using a batch reactor from 110 ^{o}C to 210 ^{o}C, at 1.5 to 3.2 MPa and with catalyst loading from 3-10 kg/m^3. In section 2.3.8 in Chapter 2, the developed apparent kinetics expression has been reported as equation (2-4), and the corresponding values for the rate and adsorption equilibrium constants were given for model M4 in Table 2-4. The denominator of such a kinetic expression consists of the adsorption/desorption terms for both reactants. Both the reaction rate constant k_j and the adsorption equilibrium constant K_i contain the prefactor and the activation energy terms. To apply this apparent kinetics in the simulation for packed-bed reactor, the activation energy E for the reaction rate constant k_j, together with prefactor and activation energy ΔE for the adsorption equilibrium constant K_i, are maintained as the reported value given in Table 2-4. However, the Arrhenius prefactors for reaction rate constant k_j, derived from apparent kinetics experiments in the stirred tank reactor with high liquid/solid ratio, may not be applicable for the packed-bed reactor with low liquid/solid ratio. Accordingly, the Arrhenius prefactors for reaction rate constant k_j are adjusted as a fitted parameter using packed-bed experimental data. After the rate constant was fitted to match the conversion at one space-time, it was maintained and used to compare with the experimental data at all other space times.

5.2.3 Numerical Solution

The reactor scale ADM for the liquid phase involves coupled nonlinear ordinary differential equations. Correspondingly, it demands a numerical solution due to the incorporation of the nonlinear reaction rate expressions. One popular approach considered was the use of orthogonal collocation on finite elements (Villadsen and Michelsen, 1978), which is known to work very well for non-steep concentration profiles. The use of multicomponent transport equations added a large set of simultaneous

nonlinear algebraic equations for the interphase concentrations. The source terms involve evaluation of interphase mass fluxes, reaction rates, and temperatures by solution of nonlinear equations at the interface. Hence, on the basis of the orthogonal collocation method, a FORTRAN program using the subroutine COLDAE was developed to solve the coupled nonlinear ODE with algebraic constraints. The solver required a user supplied analytical Jacobian for computational efficiency. For the purpose of spatial discretization, all the concentrations and other scalar variables are defined at the structured grids. The number of collocation points is specified along the reactor length from inlet to outlet for the liquid phase. Grid independence was reached with a large number of collocation points (N>80).

5.2.4 Results and Discussion

It is essential to examine the influence of operating variables, such as bed temperature, liquid and gas velocity, and inlet concentration on the reactor's performance. The summary of operating conditions used in the simulation is listed in Table 3-1 in Chapter 3. The values of the wetting efficiency and mass transfer coefficients between liquid-solid, gas-liquid and gas-solid were calculated using the selected correlation listed in Appendix A. Comparisons between the experimental observations and simulated values for phenol conversion are presented for downflow and upflow.

5.2.4.1 Effect of Temperature

In the trickle-bed reactor, at the given operating conditions the catalyst surface was only partially wetted, and the resulting wetting efficiency was estimated to be in the range of 0.5-0.8. For high LHSV (>0.6 h^{-1}) and lower temperatures (110 and 130 ^{o}C), reasonable agreement between the predicted values and the experimental data is observed, as shown in Figure 5-1(a). However, at low LHSV (0.3 h^{-1}), the axial dispersion model underpredicts the experimental observation, especially for high temperature (150 ^{o}C), where the deviation reaches 30%. For the downflow mode the ADM prediction actually failed at 150 ^{o}C. Compared with experimental data at 150 ^{o}C,

the ADM underpredicts by 30% at low LHSV (0.3 h^{-1}) and overpredicts by 50% at high LHSV (1.2 h^{-1}). The reasonable model predictions at lower temperatures (110 ^{o}C) imply that the selected hydrodynamics correlations and kinetics rate parameters are applicable. One factor that is not accounted for in trickle bed modeling is the phase change, which was originally assumed to be insignificant in ADM. However, this may not be true at temperatures above 150 ^{o}C and at low LHSV (0.3 h^{-1}), where the resulting higher driving force for phase change and long residence time may enhance the evaporation of aqueous solution. Hence, based on the model's changing capability at different temperatures, the phase change is necessary to be incorporated into the original ADM.

For the upflow reactor, as shown in Figure 5-1(b), a similar comparison is observed between the model predictions and the data obtained at three different temperatures. Noticeable deviations of prediction values from experimental ones are observed at 150 ^{o}C, where the ADM underpredicts by 14% at low LHSV (0.3 h^{-1}) and overpredicts by 22% at high LHSV (1.2 h^{-1}). Compared with the prediction results for downflow at all temperatures and LHSV, the ADM for upflow exhibits better predictions of the experimental observations. Contrary to the situation in the trickle-bed reactor, in upflow mode the catalyst is always fully surrounded by liquid, and gas only bubbles through the packed bed. Hence, less amounts of phase change take place due to reduced gas-liquid interfacial area. But the resulting impact of phase change on the mass transfer resistance between multi-phases is still considerable at 150 ^{o}C, where the original simplifying assumption that neglects phase change cannot hold.

A strong evaporation effect was observed by Takematsu and Parsons (1972) for desulfurization of heavy oil, where the low boiling components pass into the vapor phase and are swept out more rapidly than high boiling material which progresses relatively slowly through the bed. In our work, solvent water and low molecular weight acids (acetic acid and oxalic acid) are among the low boiling components, while phenol and intermediate products (benzonquinone, pyrocatechol, etc.) possess high boiling points. The former may be vaporized and move faster, while the latter stay in the liquid phase and have a longer reaction time before removed. This is in line with the experimental

observations, where the exit products are mainly composed of low molecular weight acids, and only small amounts of intermediate products were detected at the reactor outlet.

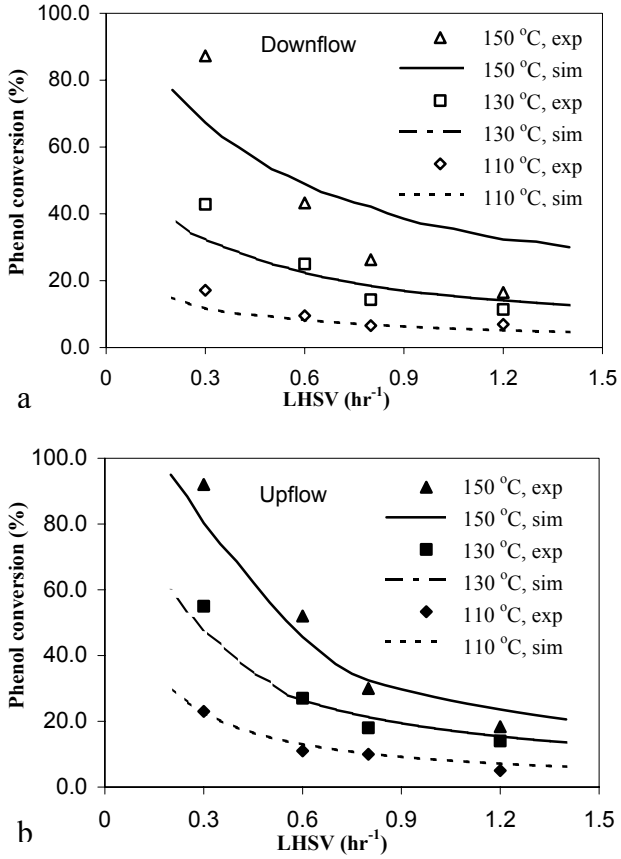

Figure 5-1. Effect of temperature on phenol conversion at different LHSV (a) trickle-bed and (b) upflow packed-bed reactors (Pressure= 3.2 MPa, [phenol]=500 ppm, u_G=0.53 cm/s).

5.2.4.2 Effect of Reactor Pressure

The effect of reactor pressure on predicted phenol conversion was also examined for both downflow and upflow reactors. Oxygen, acting as an oxidizing agent, affects the concentration of catalyst active sites. Among all transport processes, phenol conversion is retarded most by the oxygen mass-transfer from gas to bulk liquid phase. Model predictions imply that an increased phenol removal rate can be achieved by increasing the

reactor temperature and pressure in downflow and upflow operation, as seen in Figures 5-2(a) and 5-2(b), respectively. The model predicted performance for upflow is seen to be strongly dependent on the reactor pressure. In contrast, the pressure dependence of the predicted phenol oxidation rate is marginal in downflow mode. Varying oxygen partial pressure from high to low values may change the reaction from liquid limited to gas limited. Laboratory reactors are often operated in the range of partially to fully wetted catalyst. Hence, the influence of wetting can be either detrimental or beneficial, depending upon which reactant is rate limiting. The predictions of the reactor scale are not satisfactory for both downflow and upflow conditions, when the reaction is either gas limited (1.5 MPa), liquid limited (3.2 MPa), or switching from gas limited to liquid limited at some location in the reactor. The operating pressures range from 1.5-3.2 MPa, while at 150 ^{o}C the saturation pressure for water becomes significant, i.e., 34 % of the total 1.5 MPa pressure. The evaporation effect, hence, should be properly addressed. As the result of evaporation, the gas phase compositions and flow properties are changed. There is a need for updating mass transfer coefficient and interfacial area in order to predict the performance with greater certainty, especially in cases where the rate is affected significantly by external mass transfer.

The ADM, assuming negligible phase change, reasonably predicted the performances of both downflow and upflow reactors at a range of conditions (temperature below 130 ^{o}C and LHSV above 0.6 h^{-1}). However, considerable deviation between the model simulation and experimental observation at higher temperature and lower LHSV implies that the original assumption of negligible phase change may not hold at these conditions. Further development, by incorporating the phase change into the ADM and considering the updates of gas phase composition and velocity, has been achieved to bridge the gap between the current model's capability and the experimental data, as discussed in the next section.

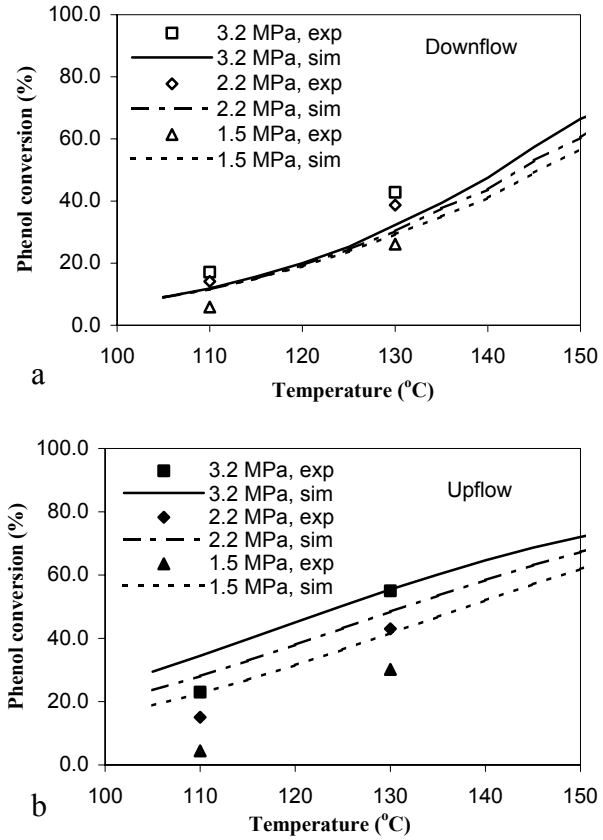

Figure 5-2. Effect of pressure on phenol conversion in (a) trickle-bed and (b) upflow packed-bed reactors (LHSV = 0.3 hr^{-1}, [phenol]=500 ppm, u_G=0.53 cm/s).

5.3 Axial Dispersion Model Accounting for Phase Change

Although literature on trickle-bed reactors is abundant, the majority of studies consider isothermal conditions, non-volatile liquid reactants, and constant phase velocities and holdups. However, the occurrence of vaporization during steady-state reaction in the multiphase is often encountered (Eftaxias et al., 2003). In many situations the liquid evaporation influences the behavior of the packed-bed reactor, especially in trickle-bed downflow operation. The liquid evaporation makes possible a formation of dry zones in catalyst pellets. Reaction then occurs on dry catalyst surfaces, which may

result not only in poor product selectivity but also in catalyst destruction. In fact, several possible states of the catalytic pellet can result from the evaporation of liquid both flowing over the external catalyst surface and filling the pore structure (Harold, 1993). A considerable part of the overall mass transfer resistance resting within the external trickling liquid film disappears, and the internal surface of catalyst gets more effective use based on the much higher gas phase diffusion coefficients in comparison with those in the liquid phase (Watson and Harold, 1993). The more rapid mass transport and less efficient heat removal associated with the gaseous system can lead to significant increases in the undesirable side reaction rates. For wastewaters containing pollutants that tend to polymerize (e.g. phenol), heavy carbonaceous formations on the surface of catalyst particles are enhanced. This phenomenon may cause subsequent catalyst deactivation by strong coke chemisorption on the catalytic sites, which is highly undesirable in plant reactor operation. Therefore, the interactions among phase transition, multiphase transport and the catalytic chemical reactions tremendously complicate any scale-up considerations.

Among the investigations in the field of reactions in trickle bed with volatile components, Collins et al. (1985) studied hydrodesulfurization of benzothiophene at a constant pressure of 68 atm and a temperature range of 546 to 606 K by simulating the global reaction rate in the presence of phase equilibrium effects at each point. They simulated the rate with four solvents with different volatility to study the influence of relative solvent volatility on the reaction rate. Kocis and Ho (1986) modeled their reaction by assuming a series of plug flow reactors, where each was preceded by a vapor-liquid separator and local thermodynamic equilibrium was re-established after the reaction stage. They tested their model for the hydrodesulfurization of dibenzothiophene at 325 ^{o}C and 3.15 MPa. They assumed that liquid flow was not affected by the evaporation of solvent and that catalyst particles were completely covered by liquid. These were valid for their reaction system at dilute liquid reactant concentration. LaVopa and Satterfield (1988) studied the effect of volatility using two test reactions, namely, the hydrodeoxygenation of dibenzofuran and hydrogenation of n-butylbenzene. Their reactor

model assumed a series of stirred tanks with both liquid and vapor flows going in and out of each stage analogous to a distillation tray. They examined the effect of changing the gas/liquid feed ratio on the conversion in the trickle flow regime with liquid only. They also studied the complete vapor regime in presence of solvents with different volatility (hexadecane and squalene) when compared to the reactant. They observed an increase in conversion with a decrease in the gas/liquid ratio due to an increase in liquid reactant partial pressure. Bhatia (1988) theoretically demonstrated the effect of capillary condensation for a vapor mixture containing a volatile and an inert component and examined the possibility of internal recondensation of the volatile reactants and products if the vapor phase is near or at saturation.

The reactor scale axial dispersion model (ADM) has been applied in our previous section 5.2 to account for the non-ideality of two-phase flow, as well as the multiphase mass transfer occurring in the packed-bed process. The selected test reactions in that work were held in ambient temperatures and moderate pressures (1.5 MPa), where the liquid vaporization effect was negligible. The comparison between the model simulation and the experimental observations exhibited that the features available in the original ADM model were sufficient for evaluation of the reaction system without considerable vaporization effect. However, the predictions of the original ADM have shown significant deviation from mimicking reality in lab scale packed-bed applications with mild temperature (110-170 ^{o}C) and moderate pressure (1.5-3.2 MPa) (Guo and Al-Dahhan, 2004 a). Such simulation deviation was attributed to the absence of accounting for phase change (evaporation or condensation) and its effect on holdup and velocities. Further model development is required on the reactor scale, even for steady state performance prediction. Therefore, the focus of this section is to further improve the ADM to account for the phase change, and to enable the model to assess the effects of reaction parameters and of local flow distribution on the performance of CWO process. This section presents the comparison between simulation results and experimental findings for different sets of conditions on the steady-state behavior. The supporting experimental work has been carried out in an isothermal packed-bed reactor operated in

both downflow and upflow operation, where the operating parameters investigated included temperature, reactor pressure, gas flowrate, liquid hourly space velocity (LHSV), and feed concentration (see Chapter 3). The model presented in this study could be used to facilitate the scale-up of these experimental results, to aid the design and optimization of pilot plant or commercial unit, and to properly design any future necessary experiments.

5.3.1 Model Structure

5.3.1.1 Modeling Liquid Phase

Following the mixing-cell approach proposed by Ramachandran and Smith (1979), the ADM, previously evaluated for liquid phase in CWO process in section 5.2, was combined with the discrete cell stack model for gas phase, so that the flow distribution and the phase change in the packed bed are accounted for in a realistic way. The packed-bed is visualized separately for liquid and gas. Liquid phase resumes its original form, i.e. axial dispersion, in the whole reactor, while gas flows through N cells of stirred tanks in series, as shown in Figure 5-3. For $N = 1$, gas phase will perform with complete back mixing. For $N \to \infty$, plug flow will prevail for gas phase, although the grid dependence may be obtained after N gets to a certain limit. Flow patterns for gas phase between these two extremes can be represented by an intermediate value of N.

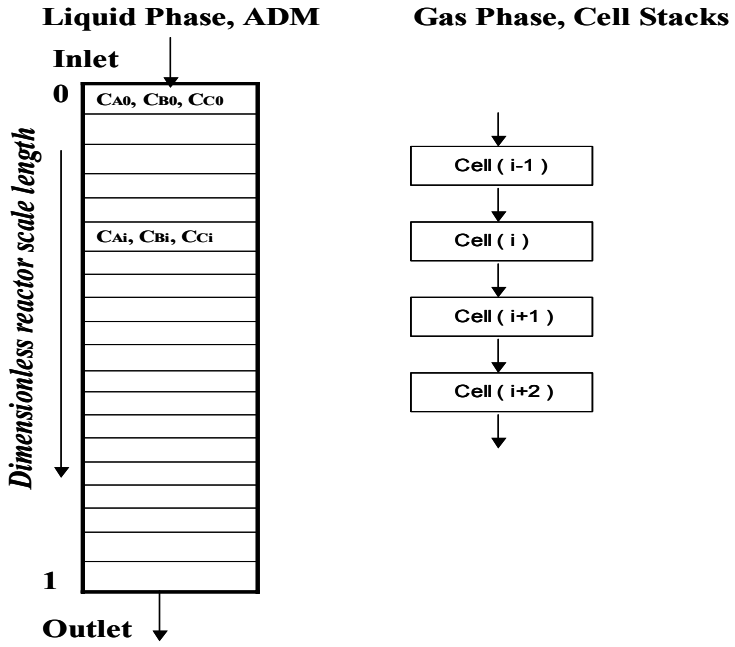

Figure 5-3. Schematic representation of liquid phase ADM and gas phase cell stacks model.

Governing equations for Liquid phase ADM are listed as follows.

$$D_{EL,k}\frac{d^2C_{k,L}}{dz^2}-u_{SL}\frac{dC_{k,L}}{dz}+(K_La_{GL})_k\left[C_{k,e}-C_{k,L}\right]-(k_{LS})_k a_{LS}\left[C_{k,L}-C_{k,LS}\right]=0 \tag{5-1}$$

Mass transfer

$$k_{LS,k}a_{LS}[C_{k,L}-C_{k,LS}]=(1-\varepsilon_B)\eta_{CE}\cdot\sum_r[\nu_{r,k}(-R_r)(C_{k,LS},T)] \tag{5-2}$$

Boundary conditions (5-3)

$$-D_{EL,k}\frac{dC_{k,L}}{dz}=u_{SL}[C_{k,0}-C_{k,L}] \qquad \text{at z=0}$$

$$\frac{dC_{k,L}}{dz}=0 \qquad \text{at z=L} \tag{5-4}$$

where $\dfrac{1}{(K_La_{GL})_k}=\dfrac{1}{k_La_{GL}}+\dfrac{1}{H_kk_Ga_{GL}}$ (5-5)

The mass transfer coefficient in the liquid film, k_L, was calculated by the correlation proposed by Fukushima and Kusaka, (1977, b). The mass transfer coefficient in the gas

film, k_G, was calculated using the correlation reported by Dwivedi and Upadhyah, (1977). The liquid from the pellets upstream brings the liquid reactants, which then diffuse into the pellet. The gas reactants enter the pellet either through the nonwetted part of the catalyst surface or through the wetted part after first dissolving in the liquid film. Driving force $(K_L a_{GL})_k \left[C_{k,e} - C_{k,L}\right]$ determines the phase change between liquid and gas, such as the water vaporization from liquid to gas and O_2 dissolution from gas to liquid. Mass transfer resistance between liquid and solid phase is reflected in a separate algebraic equation (eq. 5-2). The intraparticle mass transfer inside the catalyst particles is considered via the overall reaction kinetics. All correlations used in the above equations can be found in Table A-1 in Appendix A.

5.3.1.2 Modeling Gas Phase

As the backbone for the cells in series, the element cell with one inlet and one outlet for gas phase was built as a module to contain the chemical reaction and mass transfer based on the local species concentration, external wetting efficiency and the flow characteristics. The volatilities of solvent water and product have been incorporated, including the change in gas velocity and its effect on other parameters. By considering the interaction between cells along the axial direction, the cell-stacks create one dimensional (1D) model that is suitable for interpretation of bench scale and pilot scale data.

Since gas phase velocity is two orders of magnitude higher than the liquid phase, and its axial dispersion is usually several orders lower than the liquid phase, the gas phase is assumed to be in plug flow ($N \to \infty$), which is usually expressed as the 1st order ODE. However, by choosing a sequential solution scheme to facilitate the convergence, instead of simultaneously solving such 1st order ODE for gas phase together with 2nd order ODE for liquid phase, the former was modified to be the following explicit equation (5-6),

$$\frac{1}{L}(u_{G,out}C_{k,G} - u_{G,in}\phi_{k,G}) = -(K_L a_{GL})_k\left[C_{k,e} - C_{k,L}\right] - (k_{GS})_k (a_{GS})\left[C_{k,e} - C_{k,GS}\right] \quad (5\text{-}6)$$

Mass transfer

$$k_{GS,k}a_{GS}[C_{k,e} - C_{k,GS}] = (1-\varepsilon_B)(1-\eta_{CE})\cdot\sum_r[\nu_{r,k}(-R_r)(C_{k,GS},T)] \quad (5\text{-}7)$$

Boundary conditions

$$C_{k,G} = \phi_{k,G} \qquad \text{at } z = 0 \quad (5\text{-}8)$$

where $C_{k,G}$, the unknown variable, is concentration of species k at cell outlet. $\phi_{k,G}$ represents the cell inlet concentration for species k, i.e., feed composition from the previous cell. It is necessary to point out that the mass transfer between liquid filling in the solid capillary pore and gas is no longer present in the upflow mode due to the full catalyst wetting contact with liquid bulk.

The physical properties of the fluids, including Henry's constant, are accounted for as functions of temperature and pressure. Henry's constant for O_2 is a well-targeted area in the literature. The effect of the diluted aqueous phenol on the solubility of O_2 was assumed to be negligible. The Henry's constant of solubility He_{O_2} could be expressed by the following correlation in solution temperature (Crammer, 1980).

$$\ln(He_{O_2}/MPa) = -35.4408 + 5.5897\times10^4/T - 2.6721\times10^7/T^2 + 5.8095\times10^9/T^3 - 4.9167\times10^{11}/T^4 \quad (5\text{-}9)$$

where T is the temperature expressed in K. Henry's law constant of solubility (He_k) for other species phenol, H_2O and CO_2, is calculated as

$$He_k = \left.\frac{C_{k,G}}{C_{k,L}}\right|_{at\ G-L\ interface} = \frac{C_{G,bulk}}{C^{equ}_{k,bulk}} = \frac{P_{vap}}{RTC_{total,L}} \quad (5\text{-}10)$$

Vaporization pressure for species k at given temperature is given by Chemical Properties Handbook (Yaws, 1999).

$$\log10(P_{vap}/mmHg) = A + B/T + C\cdot\log10(T) + D\cdot T + E\cdot T^2 \quad (5\text{-}11)$$

Accounting for the high-pressure effect, vaporization pressure is corrected based on equation (5-12), given by Reid et al., (1986).

$$\ln(\frac{P_{2,vap}}{P_{1,vap}}) = \frac{P_{2,L} - P_{1,L}}{RTC_{L,total}} \tag{5-12}$$

where P_{vap} is the vaporization pressure and P_L is the pressure of the gas surrounding the liquid. Usually vaporization pressure $P_{1,vap}$ of species k at temperature T and standard pressure $P_{1,L}$ gets calculated based on equation (5-11). Corresponding to the real high pressure $P_{2,L}$ of the gas surrounding the liquid, $P_{1,vap}$ is corrected to $P_{2,vap}$ according to equation (5-12). Then the corrected vapor pressure $P_{2,vap}$ is substituted back to equation (5-10) to get the Henry's constant.

The molecular diffusivity D_m was evaluated from the correlation of Wilke and Chang (1995). The effective diffusivity D_e was derived from the

$$D_e = \frac{\varepsilon}{\tau} D_m \tag{5-13}$$

where ε and τ represent the porosity and tortuosity factor, respectively. For downflow and upflow operation modes, correlations were given in Appendix A for the external liquid-solid contacting efficiency, liquid holdup, and mass transfer coefficients ($(ka)_{GL}$, k_{LS}, k_{GS}).

5.3.1.3 Parameter Adjustment

A number of studies investigated the heterogeneous model parameters: mass-transfer coefficients (Goto and Smith, 1975), dispersion coefficients (Cassanello et al., 1992), and wetting efficiency (El-Hisnawi, 1981). An implicit assumption in all the heterogeneous models is that each model parameter is of a constant value throughout the reactor. However, in the real reactor, these parameters are affected by the local two-phase flow distribution. Hence, it is necessary to adjust all the corresponding variables from one cell to the other based on the local cell conditions. In the targeted operating conditions, reactor pressure ranges from 1.5 – 3.2 MPa and temperature from 110 to 210 ^{o}C. As

shown in Figure 5-4, water vaporization becomes more significant as the temperature increases. At high temperatures, simulation results are subjected to distortion if the phase change of water is not accounted for properly, as discussed in section 5.2. In contrast, as a nonvolatile species, phenol's phase change is negligible. Species concentrations in both liquid and gas were affected by the vaporization of solvent water, dissolution of O_2, and escape of product CO_2 to gas phase. In addition, pressure drop took place when the gas and liquid flow through the packing materials. Figure 5-5 reflects that the physical properties, flow properties, and thermo properties involved in this model are calculated as functions of the local pressure, temperature, and species concentration.

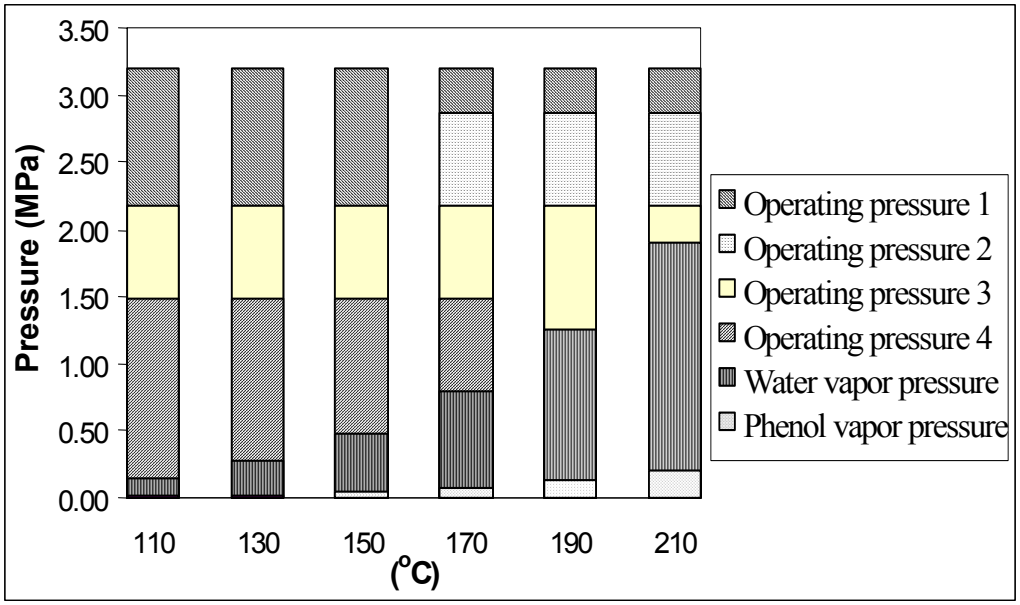

Figure 5-4. Comparison between operating pressure and vapor pressure at different temperatures.

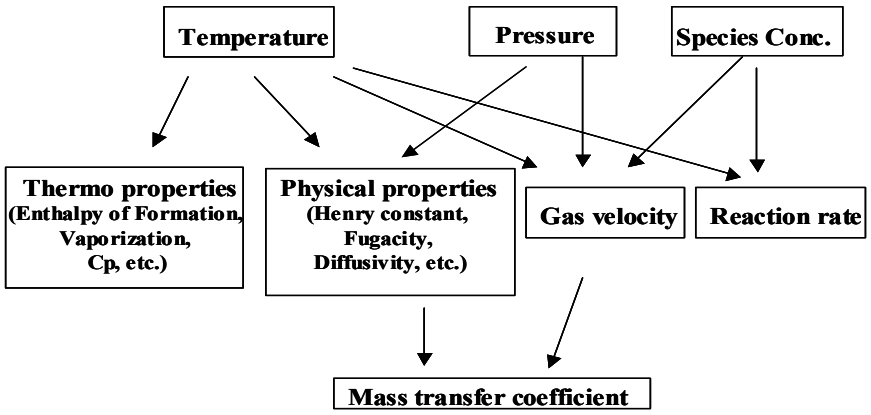

Figure 5-5. The properties and parameters studied in the model.

The change of total molar gas flux (F_G) from the inlet to the outlet of an element cell can be derived by summing up the L.H.S. of eq. (5-6) for all the species. Therefore,

$$\frac{1}{L}(F_{G,out} - F_{G,in}) = \sum_k \left\{ -(K_L a_{GL})_k \left[C_{k,e} - C_{k,L}\right] - (k_{GS})_k (a_{GS}) \left[C_{k,e} - C_{k,GS}\right] \right\} \quad (5\text{-}14)$$

As the total molar gas flux undergoes changes because of the mass transfer from the flowing liquid film and the static liquid inside the catalyst pore to the gas, the gas velocity has to be updated. The variation in gas velocity has been accounted for as follows

$$u_{G,out} = u_{G,in}\left(\frac{P_{in}}{P_{out}}\right) + (F_{G,out} - F_{G,in}) \cdot \frac{RT}{P_{out}} \quad (5\text{-}15)$$

where the two-phase pressure drop in one cell was calculated explicitly from the correlation reported by Ramachandran and Chaudhari, (1983).

5.3.1 Numerical Solution

ADM is solved for liquid phase along the whole reactor with the given boundary conditions. Then cell-stack model is solved for the gas phase by dividing the reactor into a series of cells (N_G=100). The reactor scale ADM for liquid phase involves coupled nonlinear 2nd order ordinary differential equations, which demand numerical solutions. Hence, on the basis of the orthogonal collocation method, which is known as a robust

method for solving boundary value problems (Villadsen and Michelsen, 1978), a FORTRAN program using the solver subroutine COLDAE was developed to solve the coupled nonlinear ODE with algebraic constraints (eqs. 5-1 to 5-4). The solver required a user supplied analytical Jacobian for computational efficiency. However, for the cases with involved nonlinear kinetics expression, it was difficult to exactly evaluate the analytical Jacobian due to the implicit nature of the algebraic equations. The numerical Jacobian evaluated by a finite difference approximation generalized the application of the program to any type of kinetics expression and yielded the correct values of the derivatives with respect to the concentrations series. This improved the convergence accuracy at the cost of large computational effort required due to repetitive function calls for evaluation of each column of the Jacobian matrix.

The number of collocation points is specified along the reactor length from inlet to outlet for liquid phase. Grid independence was reached with a large number of collocation points (N>80). The section between two adjacent collocation points forms one cell for gas phase. The local information at each collocation point, including component concentrations in liquid phase, provides the boundary conditions for gas phase in each cell. The computation of the cell-stack model for gas phase is in a sequential mode. A set of boundary conditions for flow velocities and species concentration is given at the first layer of cells (input cells). A whole set of solutions for species concentrations in gas phase at each cell interface can be accomplished layer-by-layer starting from the entrance of the bed, accounting for the necessary parameter updates. The change of gas superficial velocities and pressure leads to a newly obtained group of mass transfer coefficients and wetting efficiency in each cell. Hence, these values are then employed again to compute the ADM for liquid phase at every axial collocation point in order to update the axial species concentration profile in liquid phase. The boundary conditions for gas phase in each cell, therefore, are updated. Based on the newly obtained values, the cell-stack model for gas phase is solved again layer-by-layer from the reactor entrance to exit. These iterative steps are repeated until convergence is achieved, when the latest values of the species concentrations along all the reactor axial

collocation points adequately match the ones obtained in the previous iteration. The convergence and stability of the numerical calculation in each cell can be tracked and analyzed.

5.3.2 Results and Discussion

The simulation for trickle bed and upflow packed bed for phenol oxidation is conducted over a range of operating conditions. The effect of phase change with different liquid residence time is examined. As shown in Figure 5-6, phenol conversion is calculated as a function of liquid hourly space velocity (LHSV), by liquid phase ADM considering or neglecting phase change. The simulation shows that the phase changes, including water evaporation and CO_2 escape from liquid to gas, have a substantial influence on TBR performance at temperature above 150 ^oC for different liquid flow rates.

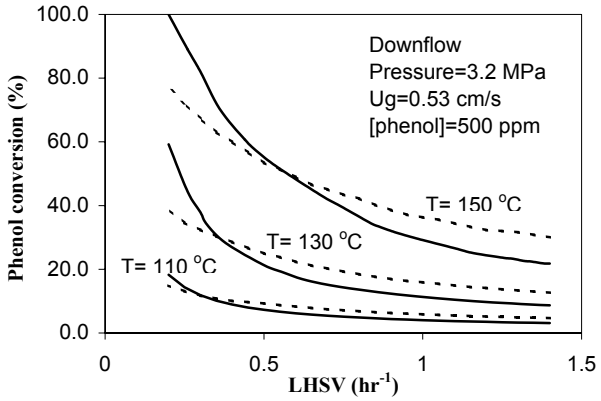

Figure 5-6. Effect of evaporation on phenol conversion in trickle-bed reactor. Solid line: simulation by liquid phase ADM considering phase changes. Dash line: simulation by liquid phase ADM neglecting phase changes.

With the LHSV decreasing at 150 ^oC, phenol conversion increases from 20% to 100% for the case accounting for phase change, while it increases from 30% to 77% without considering phase change. For low liquid LHSV, difference in phenol conversion caused by phase change effects are more significant. The wetting efficiency ranges from 0.4 to

0.8, as LHSV increases. The link between reaction degree and wetting can be elucidated by several factors. For longer liquid residence time, water evaporation and phenol mineralization to CO_2 become more favorable. The fraction of liquid within the pores of the pellet has more chance to transfer to the gas phase, which creates a large capillary driving force for liquid flow into the pellet. Thus, more reactant from the liquid phase gets inside the catalyst pellet and reaches the catalyst active site. On the other hand, the catalyst pellet, assumed to be internally filled up with liquid, is exposed partially to the gas phase, which facilitates the gas reactant to diffuse into catalyst pores. In this case, the contact between O_2 and liquid phase phenol over the catalyst active sites is therefore enhanced, which results in higher phenol conversion. Correspondingly, the degree of liquid coverage on the pellet surface is increased, which assist the access of liquid reactant from flowing liquid bulk phase to the film over catalyst. Since the reaction is limited by liquid phase reactant, such limitation is alleviated by better liquid spreading, especially for low liquid velocity. Therefore, it is evident that phase changes are crucial to be accounted for in the design and scale up calculations for this process at the conditions studied. However, employing same operating condition in upflow packed bed, the incorporation of phase change insignificantly affects the simulation results for phenol conversion. It is not surprising since in reality the catalyst is always fully surrounded by liquid and gas only bubbles through the packed bed. Hence, water evaporation has very little impact on the mass transfer resistance between multi-phases, as well as the reactant conversion.

The comparison between the experimental observations and simulated values for phenol conversion is presented for downflow and upflow in Figure 5-7(a) and 5-7(b), respectively. In the trickle-bed reactor, at the given operating conditions the catalyst surface was only partially wetted and the resulting wetting efficiency was estimated to be in the range of 0.5-0.8. The impact of liquid volatility is especially apparent for low liquid velocities. Compared with the previous model predictions neglecting the phase change (section 5.2), the build-in of a cell-stack for gas phase, accounting for the update of its velocity and the resulting impact on mass transfer, considerably alters phenol

removal profiles for downflow reactor and pushes the simulation result to better meet the experimental observation. A good agreement between the model predictions and the data obtained at three different temperatures is observed. Thus, the proposed model satisfactorily represents the experimental data for a wide range of operating conditions.

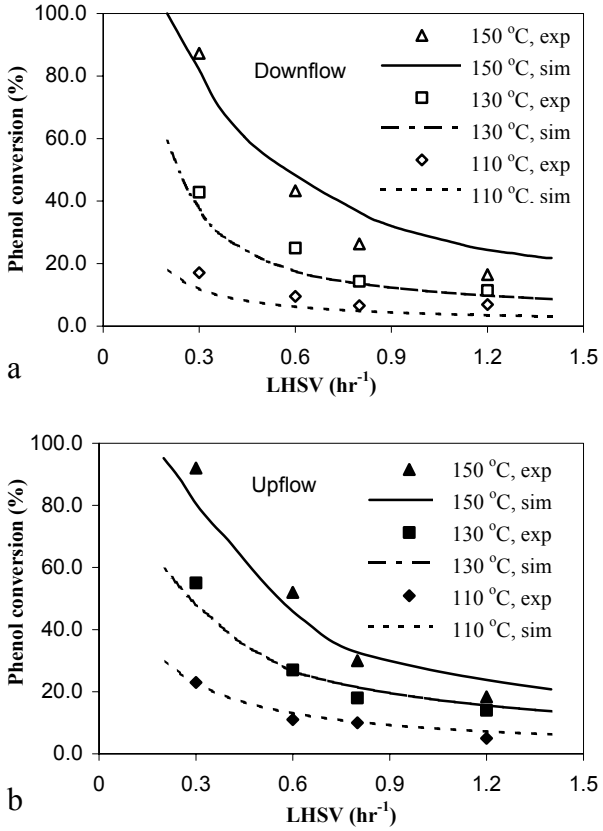

Figure 5-7. Phenol conversion as a function of LHSV at different temperature in (a) trickle-bed and (b) upflow packed-bed reactors (Pressure=3.2 MPa, [phenol]=500 ppm, u_G=0.53 cm/s).

Oxygen plays a dual role in the reaction system by acting as an oxidizing agent and affecting the concentration of catalyst active sites. The higher the partial pressure of oxygen in the gas phase, the higher the rate. Varying oxygen partial pressure from high to low values may transfer the reaction from liquid limited to gas limited. At lower operating pressure, the role of water evaporation becomes escalated. By maintaining the total operating pressure, the lack of O_2 partial pressure gets aggravated. Hence, the

reaction is prone to be gas-limited at low operating pressure. Among all transport processes phenol conversion is retarded most by the oxygen mass-transfer from gas to bulk liquid phase. This factor predominates even though the overall rate is not particularly fast. As seen in Figure 5-8(a) and 5-8(b), the model predicted performance of downflow and upflow is seen to be strongly dependent on the reactor pressure.

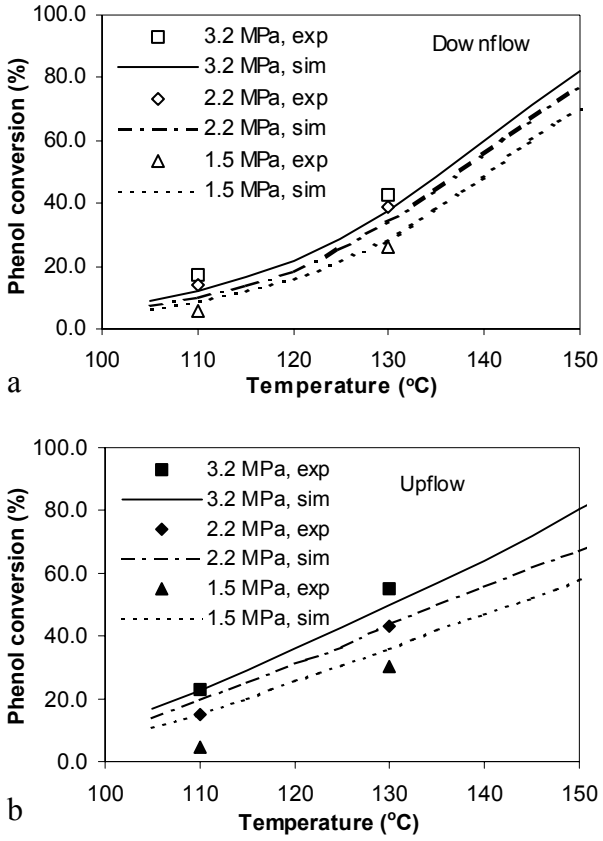

Figure 5-8. Effect of pressure on phenol conversion in trickle-bed and upflow packed-bed reactors (LHSV = 0.3 hr^{-1}, [phenol]=500 ppm, u_G=0.53 cm/s).

The effect of gas velocity at a constant LHSV of 0.6 hr^{-1}on the global rate of oxidation is shown in Figure 5-9. The results indicate that, beyond a certain value (3 mm/s) the effect of gas velocity is negligible for upflow reactor, while it is noticeable for downflow reactor. As the gas is only sparingly soluble, the variation in gas velocity would have

considerable influence on the gas-liquid mass transfer coefficient and liquid film spreading over the pellet in downflow reactor. Since the upflow reactor always gives rise to fully wetted catalyst, no explicit dependence of phenol conversion on gas velocity is observed.

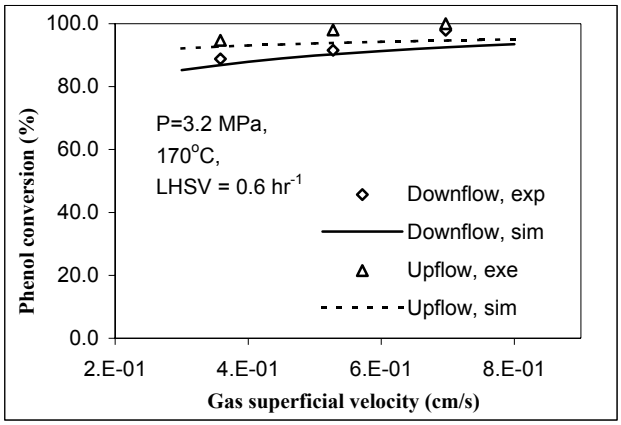

Figure 5-9. Effect of gas velocity on phenol conversion at downflow and upflow reactor.

Phenol feed concentration is another critical reaction parameter. Phenol conversion is plotted in Figure 5-10(a) and 5-10(b) as a function of phenol inlet concentration at different temperature for both downflow and upflow operation modes. In the selected concentration range, it is shown that phenol conversions decrease with increasing phenol concentration. High phenol concentration provides high reaction rate, and yet the strong oxygen limitation becomes present. The conversion drop-off from full to partial wetting is marginal. As reactant depletion concerns oxygen, incomplete wetting is to be preferred versus complete wetting because gas enters in the catalyst mainly through the gas-solid interface.

Both model predictions and experimental data implies that increased phenol removal rate can be achieved by increasing the reactor temperature and pressure, as well as by using lower liquid velocity or long liquid residence time. Since the stronger conditions may result in higher operating cost and enable catalyst to deactivate, the balance has to be chosen between the desirable phenol mineralization rate and its corresponding cost. The

contacting effectiveness in trickle beds is generally poor at low liquid flow rates under which conditions an improved rate of reaction would be anticipated by using an upflow rather than downflow reactor. Most of the simulation conditions lead to the liquid-limited reaction. So phenol conversions obtained in the trickle-bed reactor should be lower when compared to predicted values based on full wetting contact in upflow reactor. Trickle-bed operation, however, leads to less pressure drop which reduces pumping costs and helps keep the bed in place. With an upflow reactor some designs may lead to fluidization of the catalyst unless the catalyst were held in place by suitable mechanical methods.

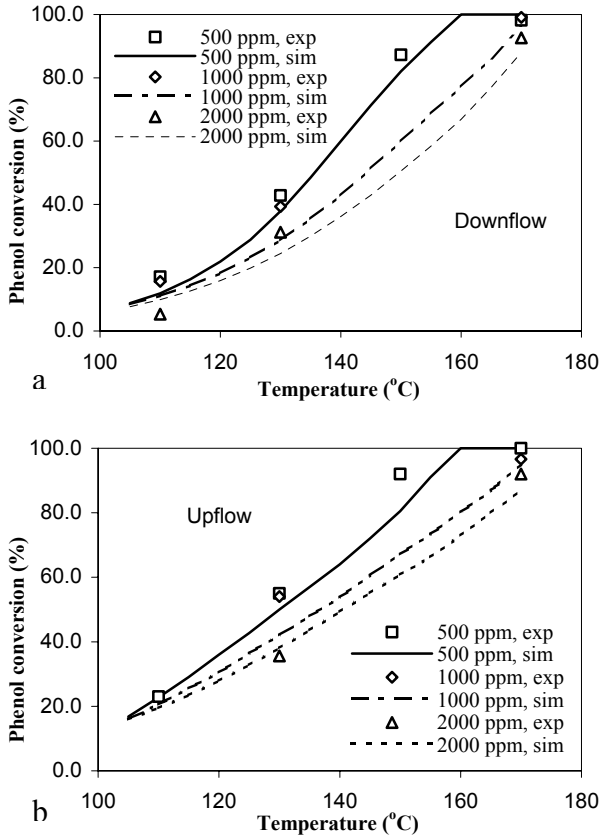

Figure 5-10. Phenol conversion at different phenol inlet concentrations for (a) dowflow in trickle-bed and (b) upflow packed-bed reactors. (Pressure = 3.2 MPa, LHSV = 0.3 hr^{-1}, u_G=0.53 cm/s).

5.4 Summary

It is necessary to incorporate the complexities of phase transition coupled with a catalytic reaction into a model to mimic the phenomena occurring in the real operation. The proposed approach, using a cell-stack model to provide the flow field updates, is designed to bridge the gap between the reactive flow and the complex interphase mass transfer. A sequential approach is proposed to couple the discrete cell series for gas phase with the axial dispersion model for liquid phase. CWO of phenol over pillared clay catalyst with known kinetics was presented for the investigated case. Both the downflow and upflow operation modes under varied conditions were considered for simulation. The comparison between the model simulation and experimental observations has shown that the approach employed to couple the flow and reaction is capable of providing the distribution information on species concentration. The impact of the phase change is significant for the flow distribution in trickle-bed reactor, while in upflow packed-bed reactor it is marginal because of the complete surrounding of liquid to the solid catalyst. The magnitude of the rate enhancement phenomenon pointes out the need to account for phase transition in the packed bed. Not doing so could result in improper design and operation of the reactor. The sequential modeling scheme for complex flow and reaction is suggested here as a practical engineering approach, particularly for isothermal systems in which the flow distribution is significantly affected by volatile species. The developed 1D model with the module of element cell builds up a solid foundation for its expansion to 2D, which allows the prediction of the performance of the reactor subject to either uniform distribution or gross maldistribution of gas and liquid phases.

Chapter 6
Thesis Accomplishments and Future Work

6.1 Summary of Thesis Accomplishments

The ensemble of the accomplishments of this work allows responding to the main theme postulated: the experimental and theoretical study of the CWO of phenol using Al-Fe pillared clay catalyst and multiphase reaction system. Each portion of the accomplishments is summarized as follows.

6.1.1 Evaluation of Catalytic Wet Air Oxidation

Wet air oxidation proved to be an effective technique to meet the discharge standards for phenol concentration. The employed conditions were much milder than those in typical industrial operations. The wet air oxidation kinetics of an aqueous solution of phenol was studied over extrudates of Al-Fe pillared clay catalyst. A Langmuir-Hinshelwood kinetic model was developed on the basis of equilibrium adsorption of phenol and dissociated oxygen on two distinct types of active sites. This model was able to predict well the experimental results over the entire range of the variables studied.

Comparison was shown between the behavior of a packed-bed reactor with two modes of operation, downflow and upflow. Because of the completely wetted catalyst, the upflow reactor generally performs better for high pressures and low feed concentrations when the liquid reactant limitation controls the rate. For both operation modes, complete phenol removal and significant total organic carbon (TOC) reduction can be achieved at rather mild conditions of temperature (150-170 ^{o}C) and total pressure (1.5-3.2 MPa), above which the operating pressure has to be uneconomically high to exceed the vapor

pressure of the liquid phase. The results show that the phenol and TOC conversion are considerably affected by the temperature, while the air pressure only has minor influence. Total elimination of TOC is difficult since acetic acid, as the main intermediate, is resistant to catalytic wet oxidation. The catalytic wet oxidation of aqueous phenol shows an optimal performance at a pH value of about 4.0.

6.1.2 Evaluation of Pillared Clay Catalyst

All tests were conducted over extrudates of Fe-Al pillared clay catalyst with dimension (2 × 8 mm) as provided. The catalyst is stable and maintains its activity during the long-term experimental process. Various characterization methods were employed for fresh and aged pillared clay catalysts previously used for 240 hr in packed-bed operation. Surface analysis showed that the incorporated Al and Fe species were homogeneously dispersed between the silicate layers. During the packed-bed operation, leaf-like carbon deposits were found to build up on the catalyst active sites, and trace amounts of Fe and Al were detected in the liquid effluent, precluding a leaching type of deactivation. The catalyst exhibited a fairly stable phenol conversion rate over a long period (240 hr) at elevated temperature and pressure (170 ^{o}C, 3.2 MPa). Under the same conditions, slurry reactor analysis showed that the overall reaction rate was appreciably limited by the internal mass transfer. Further catalyst screening test is required to enhance the particle effectiveness factor. The tests involve various formulations having differences in composition, support materials as well as in preparation methods.

6.1.3 Reactor Scale Modeling for Process Evaluation

The obtained kinetic model was implemented in a reactor scale axial dispersion model (ADM), which is evaluated, modified, and verified for its application in CWO process in packed-bed reactors. This model is used to account for multiphase mass transfer, liquid phase non-ideality, liquid-solid wetting contact, and nonlinear reaction kinetics. Effect of liquid evaporation is significant under the selected operating conditions. Shown to be suitable and efficient, the computational approach accounts for the observed catalyst

activities combined with local transport and catalyst wetting effects. Quantitative comparison of simulated model predictions and lab scale experimental data are presented. The model satisfactorily simulates the concentration profiles in the reactor at steady-state operation. Hence, the model allows the designers to determine the effect of catalyst activity, operating and feed conditions on reactor performance. In addition, the validated model allowed studying numerically the scale up of the laboratory packed-bed reactor to a pilot scale reactor.

An interpretation of the experimental observation is incomplete without an adequate reactor model that will enable to predict the influence of the key operation parameters on the reactor performance. Thus, such a model is a potential tool to correctly guide the design and scale up of multiphase reactors minimizing experimental efforts, that are time consuming, costly and often difficult to carry out.

6.2 Recommendations for Future Research

Several recommendations can be made for extending the work conducted in different parts of this study as listed below.

6.2.1 Catalyst Design and Evaluation

Pillared clay catalyst with dimension (2 × 8 mm) is evaluated as it is supplied. However, its low effectiveness factor implies the necessity for its future improvement. The intraparticle diffusion tests have shown that smaller sizes (2 × 2 mm, 2 × 1 mm) enhance the effectiveness factor. The small particle size also leads to high pressure drop in packed-bed reactor. Hence more experiments with the smaller size catalyst should be conducted in stirred tank reactors to properly select the catalyst dimension based on the reasonable intraparticle diffusion effect. The intrinsic kinetics experiments needs to be performed with catalyst powder, and appropriate intrinsic kinetic models should be developed as a reference to calculate the surface reaction rates at any given conditions.

On the other hand, the intraparticle diffusion resistance of large aromatic molecules gets decreased with enlarged distance between pillared layers or larger pore size. In addition, parallel analysis of catalyst structure and composition should allow characterizing the pore size and surface to provide the means for the optimization of catalytic performance either by surface modification, or by proper manufacturing design. Hence, catalyst preparation method needs to be revisited and modified.

6.2.2 Scale-Up of CWO Process

Further experimentation on comparison of the two modes of operation in packed-bed reactors is recommended for phenol oxidation to confirm the model simulations and generalize the conclusions obtained from this study for any given set of reactions. This will also help establish a robust scale-up strategy for packed-bed reactors. This work can be augmented by studying the same reaction in a bed diluted with fines to see if the decoupling between hydrodynamics and kinetics is observed for complex reactions shown in this study. In addition, catalysts with smaller size, new composition, or improved structure need to be tested in packed-bed for the comprehensive evaluation of their performance.

In the context of modeling, one may focus on more studies of the determination of mass transfer and hydrodynamic parameters for relevant industrial reaction systems. The availability of these parameters could greatly improve the reliability of model-aided design and scale up of multiphase processes.

6.2.3 Non-isothermal Modeling Scheme

The rigorous approach based on multiphase transport and its influence on the overall reaction was shown to be comprehensive enough in modeling reactor scale phenomena. This model is recommended for predicting performance of packed beds with complex reactions and volatile components. Current modeling scheme is constructed for the isothermal condition. However, phase change and non-isothermal conditions, which would alter the flow structure and temperature inside the bed, are likely to occur in many

industrial applications, including the CWO of high organic concentration. By considering the energy balance along the packed bed, it can be extended to simulate the non-isothermal operation typically applied in the industry, such as the exothermic reaction of alpha-methylstyrene hydrogenation in an adiabatic reactor.

6.2.4 2D Modeling Scheme

Further model development can expand this work for multi-dimensional case where the influence of flow maldistribution can be incorporated, both on the reactor and pellet scale, where multicomponent and phase changes are involved. The developed 1D model will be extended to the mixing-cell network model to simulate the performance of packed-bed reactors in 2D domains, by incorporating a proper radial mixing rule into a 2D mixing-cell network model. Such an approach will allow predicting the axial and radial distributions of species concentration and temperature inside the packed-bed, which is valuable information for characterizing the reactor operation.

Appendix
Modeling Catalytic Reactions in Packed-Bed Reactors

A1 Model Development

Most of the published works on packed-bed models aim to describe the hydrodynamics of reactors in cold flow, such as hydrocarbons-nitrogen or water-air, (Iliuta et al., 1996), which are not reactive at all. However, the present work focuses on packed-bed models incorporating reactions. For the model formulation, the following reaction type is considered:

A (g) + ν_B B (l) → Products

where the gaseous species, A, reacts with the liquid species, B. The primary model variables of interest are the liquid phase concentrations of the dissolved gaseous reactant and the resulting conversion of the liquid phase reactants. Mass transfer resistances consist of two cases: the interphase resistance between the gas, liquid, and solid phase, as well as the intraparticle resistance inside the catalyst particles. The interphase mass transfer is reflected in the reactor scale model, whereas the intraparticle mass transfer is tackled via the pellet scale model.

The model development is based on several general assumptions: the gas and liquid flow rates are constant throughout the reactor; axial dispersion in the gas phase is negligible; conditions are uniform in the radial direction and maintain steady state; the concentration level of pollutant in the feed stream is so low that isothermal conditions prevail; local thermal equilibrium and mass transfer equilibrium exist between the gas

and liquid phases; and no correction of effective diffusivity is made to account for progressive deactivation by carbonaceous deposits.

A1.1 Reactor Scale Model

Considering gas and liquid in plug flow subject to the above assumptions, the plug-flow reactor scale model allows for different reaction rates on the dry and wetted pellets by considering gas-liquid and liquid-solid mass transport along with the pertinent kinetics. El-Hisnawi (1981) employed the heterogeneous plug flow model for low-pressure operation in a trickle bed reactor to solve the gas-limited reaction problem due to externally dry catalyst areas. An overall wetting efficiency (η_{CE}) was introduced in the plug-flow model to account for the partial wetting of the catalyst particles. The key factors incorporated in the model were partial wetting and transport of gaseous reactant to dry external areas of the catalyst, resulting in high rates observed in the experimental data for gas-limited reaction. The surface concentration of the limiting reactant was obtained by solution of the reaction transport equation at the catalyst surface, and then it was substituted into the plug flow equation to obtain the profile for the non-limiting reactant along the reactor length. Analytical solutions were derived for first order kinetics for the resulting coupled linear ordinary differential equations at low pressure.

Khadilkar et al. (1996) has employed El-Hisnawi's plug-flow model for the reaction of hydrogenation of AMS at high pressure (1.5 MPa), where a numerical solution was demanded due to nonlinear kinetics exhibited by the reaction. The pellet effectiveness factor in El-Hisnawi's model was fitted at one space-time with the experimental observation. Then the effectiveness factor was used as a fitting parameter for the other space-time, which, however, in no way reflected the actual mass transfer resistance inside the pellet and the pellet external wetting contact with the liquid.

Axial dispersion can be severe in trickle flow or bubbly flow reactors with increasing conversion, reaction order, or higher eddy diffusivities, such as when conversion reaches about 90 % for a laboratory scale trickle-bed reactor of 0.3 m in length (Mears, 1971). Several criteria have been proposed in the literature for appraising the significance of the

axial dispersion effect. An early one was developed by Mears (1971) for liquid-limiting reactions based on the minimum bed-length required to neglect the axial dispersion effect. Later, based on the development of an approximate solution of the axial dispersion model, Cassanello et al. (1992) established a general criterion valid for either liquid or gas-limited reactions. By applying the criterion to the conditions used for our test reaction of AMS hydrogenation and phenol oxidation, we found that the axial dispersion effects cannot be neglected for both cases. In addition, as exhibited in Figure A-1, significant differences were found in the conversion predictions, depending on whether the liquid phase behavior is described according to the plug flow or the axial dispersion models at relatively high space-time. For both the downflow and upflow cases, the deviation of ADM from plug flow is more than 15% at low liquid superficial velocity with a space-time around 250 seconds. Therefore, axial dispersion can be considered significant under the employed conditions, and the ADM is applied in the following modeling scheme.

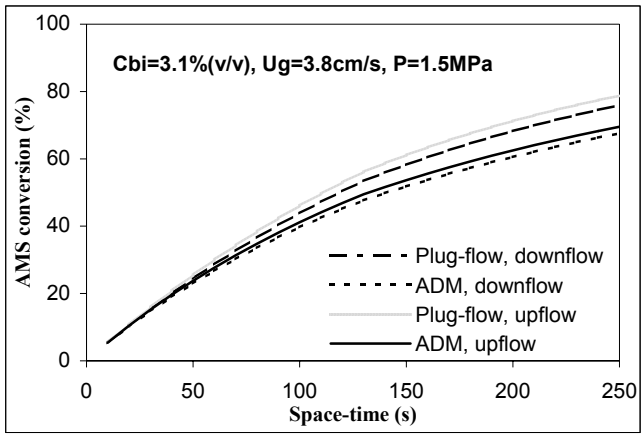

Figure A-1. The influence of axial dispersion on the conversion of alpha-methylstyrene.

Axial dispersion is accounted for in the reactor model via the dispersion coefficient D_{EL} for the reactants A and B, as well as the product C in the liquid phase. The dispersion coefficient is obtained by assuming that all the mixing processes follow Fick's Laws. The axial dispersion model at steady state can be described as follows for all three components, A, B, and C, in the liquid phase.

Generalized governing equation for ADM

$$D_{EL,A}\frac{d^2C_{A,L}}{dz^2}-u_{SL}\frac{dC_{A,L}}{dz}+(ka)_{GL}\left[C_{A,e}-C_{A,L}\right]-k_{LS,A}a_{LS}\left[C_{A,L}-C_{A,LS}\right]=0 \qquad \text{(A-1)}$$

$$D_{EL,B}\frac{d^2C_{B,L}}{dz^2}-u_{SL}\frac{dC_{B,L}}{dz}-\nu_B k_{GS,A}a_{GS}\left[C_{A,e}-C_{A,GS}\right]-k_{LS,B}a_{LS}\left[C_{B,L}-C_{B,LS}\right]=0 \qquad \text{(A-2)}$$

$$D_{EL,C}\frac{d^2C_{C,L}}{dz^2}-u_{SL}\frac{dC_{C,L}}{dz}-k_{LS,C}a_{LS}\left[C_{C,L}-C_{C,LS}\right]=0 \qquad \text{(A-3)}$$

Mass transfer

$$k_{LS,m}a_{LS}[C_{m,L}-C_{m,LS}]=\eta_o(1-\varepsilon_B)\eta_{CE}\cdot r_m(C_{m,LS}) \qquad m = A, B, C; \qquad \text{(A-4)}$$

$$k_{GS,A}a_{GS}[C_{A,e}-C_{A,GS}]=\eta_o(1-\varepsilon_B)(1-\eta_{CE})\cdot r_A(C_{A,GS}) \qquad \text{(A-5)}$$

Boundary conditions (Danckwerts type)

$$-D_{EL,m}\frac{dC_{m,L}}{dz}=u_L\left[C_{m,0}-C_{m,L}\right] \qquad m=A, B, C; \qquad \text{at z = 0} \qquad \text{(A-6)}$$

$$\frac{dC_{m,L}}{dz}=0 \qquad m=A, B, C; \qquad \text{at z = L} \qquad \text{(A-7)}$$

When the dispersion is dominated by molecular diffusion, the boundary conditions are of Danckwerts type. The analysis of the construction arrangement of two-phase flow reactors suggests that the Danckwerts boundary conditions represent the best approximation of the reality for the majority of the real reactors (Iliuta et al., 1996). The above equations can be written in dimensionless form by introducing the following variables.

Let $\xi=\frac{z}{L}$; $\alpha_{GL}=\frac{(ka)_{GL}L}{u_{SL}}$; $\alpha_{GS}=\frac{k_{GS,A}a_{GS}L\nu_B}{u_{SL}}$;

$\alpha_{LS,m}=\frac{k_{LS,m}a_{LS}L}{u_{SL}}$; $C_{A,e}=\frac{P_{A,G}}{H_A}$; $c_{m,L}=\frac{C_{m,L}}{C_{A,e}}$; for m=A,B,C

$\beta_1=\frac{L\eta_{CE}\eta_o(1-\varepsilon_B)}{u_{SL}C_{A,e}}$; $\beta_2=\frac{L(1-\eta_{CE})\eta_o(1-\varepsilon_B)\nu_B}{u_{SL}C_{A,e}}$; $Pe=\frac{u_{SL}L}{D_{EL}}$

Substitution of the above dimensionless groups into the equations leads to the following ordinary differential equations:

Dimensionless ADM

$$\frac{1}{Pe}\frac{d^2 c_{A,L}}{d\xi^2} - \frac{dc_{A,L}}{d\xi} + \alpha_{GL}\left(1 - c_{A,L}\right) - \alpha_{LS,A}\left(c_{A,L} - c_{A,LS}\right) = 0 \qquad \text{(A-8)}$$

$$\frac{1}{Pe}\frac{d^2 c_{B,L}}{d\xi^2} - \frac{dc_{B,L}}{d\xi} - \alpha_{GS}\left(1 - c_{A,GS}\right) - \alpha_{LS,B}\left(c_{B,L} - c_{B,LS}\right) = 0 \qquad \text{(A-9)}$$

$$\frac{1}{Pe}\frac{d^2 c_{C,L}}{d\xi^2} - \frac{dc_{C,L}}{d\xi} - \alpha_{LS,C}\left(c_{C,L} - c_{C,LS}\right) = 0 \qquad \text{(A-10)}$$

Mass balance

$$\alpha_{LS,m}\left[c_{m,L} - c_{m,LS}\right] = \beta_1 r_m \left(c_{m,LS}\right) \text{ ; for m=A,B,C} \qquad \text{(A-11)}$$

$$\alpha_{GS}\left[1 - c_{A,GS}\right] = \beta_2 r_A \left(c_{A,GS}\right) \qquad \text{(A-12)}$$

Boundary conditions

$$\frac{1}{Pe}\frac{dc_{m,L}}{d\xi} = \left[c_{m,L} - c_{m,0}\right] \qquad m = A, B, C; \qquad \text{at } \zeta = 0$$

$$\frac{dc_{m,L}}{d\xi} = 0; \qquad m = A, B, C; \qquad \text{at } \zeta = 1.0$$

If we were to neglect the axial dispersion in the liquid, the calculations would be markedly simplified. The two-point boundary value problem would be eliminated, and the axial dispersion model would turn out to be the original plug-flow model proposed by El-Hisnawi (1981). Similar to the El-Hisnawi model, the above reactor scale ADM requires the pellet effectiveness factor, η_0, to be supplied as a known parameter. For a linear apparent kinetics expression that includes the intraparticle resistance, the Thiele modulus allows us to derive the pellet scale effectiveness factor. However, complex kinetics expressions are often found in the literature, especially when catalysts suffer from deactivation, which leads to varied reaction rates due to the loss of the catalyst active sites. In such cases, the apparent reaction kinetics expression cannot suitably predict the evolution of the reactor performance.

Pintar et al. (1997) set the value of the effectiveness factor to 1.0, assuming that the reaction rate at given reaction conditions is not influenced by internal transport resistance. Generally, however, the intraparticle diffusion resistance is significant (large Thiele modulus) and the reaction rate is large compared to the internal diffusion rate. The transport effect can be explained by the inability of the liquid reactant to diffuse rapidly enough to the zones adjacent to the dry catalyst surface where the gas reactant is abundant. Thus, the internal transport greatly affects the observed reaction rate, and the effectiveness factor has to be determined by considering the pellet scale phenomena. One of the pellet scale models was proposed by Beaudry et al., (1987) to illustrate the intraparticle diffusion-reaction process. Such a model is discussed in the next section and is employed in the present work.

A1.2 Pellet Scale Model

Beaudry et al. (1987) described catalyst pellets in the form of infinite slabs with both sides exposed to either gas or liquid, or as a half-wetted pellet exposed to gas on one side and liquid on the other. The approach for the evaluation of the overall effectiveness factor for partially wetted catalyst particles was in line with the concept proposed by Ramachandran and Smith (1979), who considered the intraparticle diffusion as the result of contributions arising from the liquid-covered surface of the particles (based on the external wetting efficiency) and from the gas-covered surface. Accordingly, this model divided the effectiveness factor of catalyst pellets into three liquid-solid contacting categories: (a) both catalyst surfaces are completely dry, i.e., gas-covered (η_{od}); (b) one of the catalyst surfaces is actively wetted and the other one is dry (η_{odw}); (c) both catalyst surfaces are completed wetted, i.e., liquid covered (η_{ow}), as exhibited in Figure A-2.

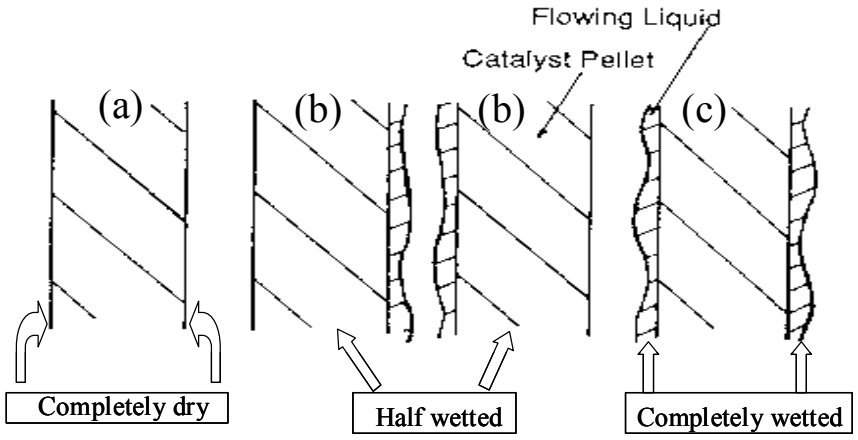

Figure A-2. Representation of possible catalyst pellet wetting contact.

Intuitively, this approach represents the reality better than assuming that all particles have the same fraction of external wetting. The reactor-scale overall effectiveness factor, η_0, can be defined as the weighted average of η_{od}, η_{odw}, and η_{ow}, based on the general consideration of the presence of all three categories, with the corresponding weights given as $(1-\eta_{CE})^2$, $2\eta_{CE}(1-\eta_{CE})$, and $\eta_{CE}{}^2$, respectively. This way the sum of the weights turns out to be unity. The contacting efficiency, η_{CE}, is the fraction of the external catalyst surface area that is actively wetted. Therefore, the overall effectiveness factor is given as

$$\eta_o = (1-\eta_{CE})^2 \eta_{od} + 2\eta_{CE}(1-\eta_{CE})\eta_{odw} + \eta_{CE}^2 \eta_{ow} \qquad \text{(A-13)}$$

where η_{od}, η_{odw}, and η_{ow} are calculated as integral functions of reactant concentration along the pellet scale length based on an inactively wetted surface or an actively wetted surface. In other words, pellet reactant concentration profiles, as shown in Figure A-3, have to be available before the overall effectiveness factor can be obtained.

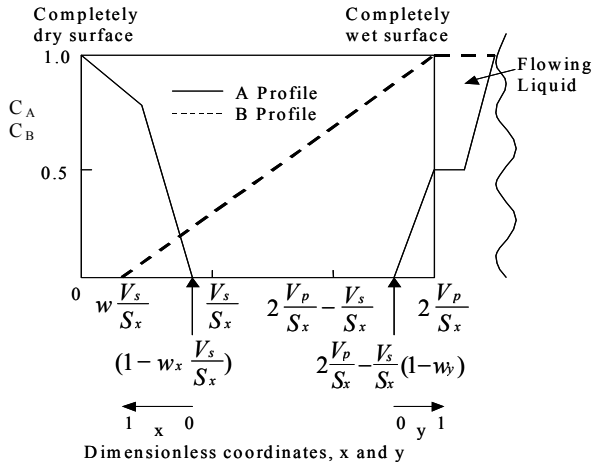

Figure A-3. Possible concentration profiles along the pellet scale at liquid reactant limiting conditions.

At low pressure, the gaseous reactant supplied from both sides of the pellet is depleted completely within a short distance depending on the extent of the gas reactant limitation. The term $(1-w_x)V_s/S_x$ shows the distance from the fully dry surface, and the term $(1-w_y)V_s/S_x$ shows the distance from the fully wetted surface. The distance measured from the fully dry surface to the plane where the liquid reactant depletes completely is noted as term wV_s/S_x. The above-mentioned terms are also shown in Figure A-3. The concentration distribution of reactants within the pellet was obtained via a group of dimensionless differential equations, as listed below. The details concerning derivation of the governing equations and the description of each term for a pellet scale model were reported by Beaudry et al., (1987).

Governing equations

$$\frac{d^2 c_A}{dx^2} - (1 - w_x - w)^2 \left(\frac{V_s}{S_x}\right)^2 \frac{(-r_A)}{D_{eA}} = 0 \qquad 0< x< 1 \qquad \text{(A-14)}$$

$$\frac{d^2 c_B}{dx^2} - (1 - w_x - w)^2 \left(\frac{V_s}{S_x}\right)^2 \frac{(-r_B)}{D_{eB}} = 0 \qquad 0< x< 1 \qquad \text{(A-15)}$$

$$\frac{d^2 c_A}{dy^2} - (1 - w_y)^2 \left(\frac{V_s}{S_x}\right)^2 \frac{(-r_A)}{D_{eA}} = 0 \qquad 0< y< 1 \qquad \text{(A-16)}$$

$$\frac{d^2 c_B}{dy^2} - (1 - w_y)^2 \left(\frac{V_s}{S_x}\right)^2 \frac{(-r_B)}{D_{eB}} = 0 \qquad 0< y< 1 \qquad \text{(A-17)}$$

Boundary conditions

$$\left.\frac{dc_A}{dy}\right|_{y=1} = (2 - w) Bi_{ls,A} (c_{A,L} - c_A|_{y=1}) \qquad \left.\frac{dc_B}{dy}\right|_{y=1} = (2 - w) Bi_{ls,B} (c_{B,L} - c_B|_{y=1})$$

$$\left.\frac{dc_A}{dx}\right|_{x=1} = \frac{1 - w_x - w}{w + 1/Bi_{gs,A}} (c_{A,L} - c_A|_{x=1}) \qquad c_A|_{x=0} = c_A|_{y=0} - 2\left(\frac{v_p}{v_s} - 1\right)\left.\frac{dc_A}{dy}\right|_{y=0}$$

$$c_B|_{x=1} = 0 \qquad \left.\frac{dc_B}{dx}\right|_{y=0} = 0$$

$$\left.\frac{dc_A}{dx}\right|_{x=0} = -\frac{1 - w_x - w}{1 - w_y}\left.\frac{dc_A}{dy}\right|_{y=0} \qquad \left.\frac{dc_B}{dx}\right|_{x=0} = -\frac{1 - w_x - w}{1 - w_y}\left.\frac{dc_B}{dy}\right|_{y=0}$$

$$c_B|_{x=0} = c_B|_{y=0} - \frac{2(v_p/v_s - 1) + w_x + w_y}{1 - w_y}\left.\frac{dc_B}{dy}\right|_{y=0}$$

where $Bi = \frac{kV_s}{D_{EL} S_x}$, $c_{m,L} = \frac{C_{m,L}}{C_{A,e}}$ for m = A, B

The boundary conditions listed above are based on the reactant concentrations in the reactor liquid phase, which have to be calculated from the reactor scale model. By assuming the concentration of gas reactant dissolved in the liquid phase changes very little due to the slight solubility of gas, Beaudry et al. (1987) replaced the dimensionless liquid concentration c_{AL} by unity and used the reaction with linear reaction kinetics at low pressure (gas-limited conditions). Analytical solutions for reactor outlet conversion have been derived for the outlet conversion of the nonvolatile reactant by substituting the overall effectiveness factor into a reactor scale plug flow model, which didn't account for the interphase mass transfer.

The catalyst effectiveness factor addressed so far is only for simple linear kinetics under isothermal conditions. Several issues still remain unresolved at this stage. Most of the important reactions represent the complex consecutive/parallel reaction pathway described by Langmuir-Hinshelwood kinetics (Pintar and Levec, 1994). In addition, the assumption that the concentration of gas reactant dissolved in the liquid phase changes very little can hardly be supported from a practical point of view (Pintar et al., 1997).

The knowledge of reactant concentration in the liquid bulk phase is still necessary to define the boundary conditions for the pellet scale model.

Khadilkar et al. (1996) explored the Beaudry model for the nonlinear reaction rate of hydrogenation of AMS at high pressure (1.5 MPa), which demands the numerical solution of the reaction-diffusion equations (eq. A-14 to A-17). In their approach, pellet scale equations were solved for a range of selected bulk liquid reaction concentrations given as the boundary conditions. Then the pellet effectiveness factor was fitted as a polynomial function of bulk concentrations. This polynomial was then used at each space-time to solve the reactor scale plug flow equations originally proposed by Beaudry et al., (1987).

However, polynomial fitting is still an approximation process, which may be not possible when one wants to derive a polynomial from the concentrations of multi-component reactants. In addition, when catalyst deactivation occurs, the loss of the catalyst active sites leads to a dynamic reaction rate. Thus, the reactant concentrations in the liquid bulk and on the catalyst surface keep changing, which makes the fitted polynomial derivation not feasible. The fitting error may lead to significant deviation for the pellet overall effectiveness factor, η_o, and hence, noticeable error in the reactor scale simulation results. In this work, the sensitivity of the ADM to the parameter η_o has been tested by predicting the AMS conversion based on different values of effectiveness factor for the whole reactor, as shown in Figure A-4. It is confirmed that changing the parameter η_o leads to considerable deviation from the reactor scale model simulation.

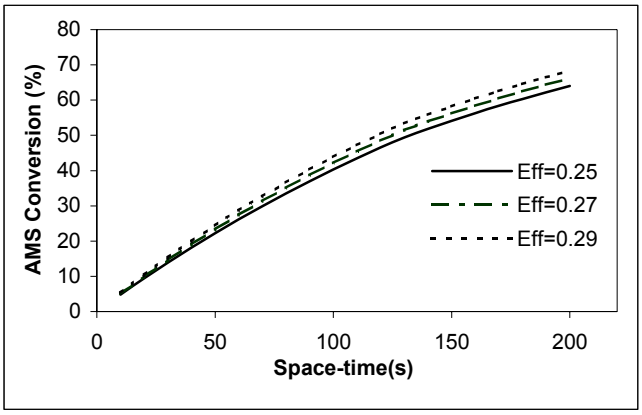

Figure A-4. Sensitivity of ADM to the effectiveness factor for hydrogenation of AMS (P=1.5 MPa, downflow, $C_{AMS,0}$ =3.8% (v/v), u_G=3.8 cm/s).

The overall effectiveness factor is varied at each axial location, and the range of its variation is significant. Thus, in this work, the developed computational scheme allows us to calculate the values of the effectiveness factor directly from the pellet scale model for a given time at each axial reactor location. We can thereby get a local effectiveness factor corresponding to the local reactant concentrations, instead of the one obtained from polynomial fitting.

A2 Computation Scheme

A2.1 Sequential Approach

In this work, the performance of a packed bed over a range of operating conditions has been investigated by using the ADM in combination with the pellet scale model. Both the reactor scale ADM and the pellet scale model involve coupled nonlinear ordinary differential equations. Correspondingly, both of them demand a numerical solution due to the incorporation of the nonlinear reaction rate expression. Hence, on the basis of the orthogonal collocation method, a FORTRAN program using the subroutine COLDAE was developed to solve the coupled nonlinear ODE with algebraic constraints. Orthogonal collocations are known as a robust method for solving boundary value problems (Villadsen and Michelsen, 1978). Twenty-one collocation points are specified

for both reactors and catalyst pellets, in order to set up a matrix configuration with one dimension for the reactor scale from inlet to outlet and the other dimension for the pellet scale from the side covered by gas (fully dry) to the side covered by liquid (fully wet), as shown in Figure A-5. Thus, the local information at each cell, including component concentrations and effectiveness factors, can be computed numerically.

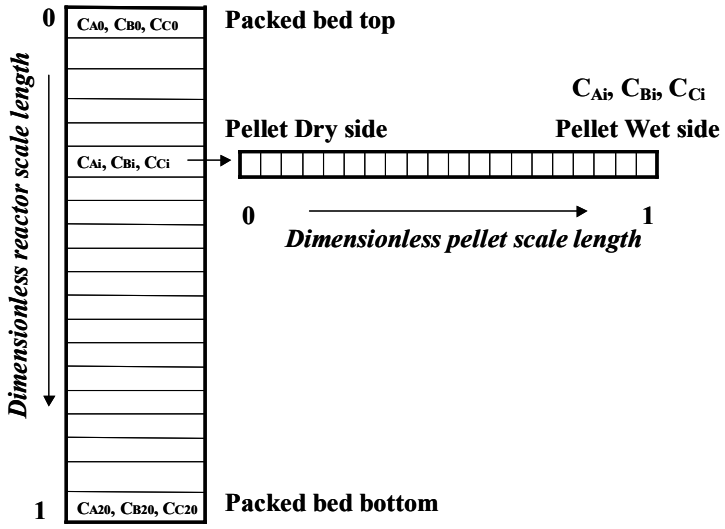

Figure A-5. Configuration of matrix cell based on the discretization of reactor and pellet scale.

When catalyst deactivation exists, the solution is more complicated due to the dynamic behavior of the catalyst. The reaction investigated in this work is the catalytic oxidation of phenol over a deactivating catalyst. Both the intrinsic reaction rates and the loss rate of the catalyst active site fraction are given as functions of the catalyst active site fraction and of the reactant and product concentrations in the liquid bulk. Details of the kinetics will be discussed in a later section. The computational scheme presented above is designed for the reactor and pellet at steady state conditions. To consider the dynamic problem, in which the catalysts deactivate as the time progresses, the time scale needs to be incorporated. Correspondingly, upwind discretization of the time dimension is carried out in constant steps to divide the reaction duration into a series of time zones. The solution scheme starts with time equal to zero, with the initial condition given as unity for

the catalyst active site fraction, so that the initial intrinsic reaction rates are simplified to the function of reactant concentrations in the liquid bulk. The proposed sequential scheme of the combination of reactor scale and pellet scale models is now applicable to obtain the local concentration distribution for the initial time point. Based on the obtained local concentrations, a small value of the time step is chosen so that the catalyst deactivation rate at each matrix cell during that time step can be calculated. Hence, after the time proceeds to the next preset point, the catalyst active site fraction at each cell is available, and the intrinsic reaction rates, once again, become the functions of the unknown variables of the local concentrations. Therefore, at this preset time point, the proposed sequential scheme is employed again for calculating the local concentrations. This way the local information at the specified cell and the specified time, including the species concentration and catalyst active site fraction, can be captured and the dynamic performance of packed bed and catalyst pellet can be depicted.

A2.2 Mass Transfer Coefficients

Reaction kinetics and transport dynamics are closely interlinked, and their effects on the reactant conversions are inseparable. Therefore, to properly know the behavior of the packed-bed reactors, hydrodynamic parameters are important and need to be considered. These include the degree of catalyst wetting, the mixing and flow pattern of the fluids, the axial dispersion coefficient, and the liquid holdup. The selection of hydrodynamic conditions depends not only on the processing requirement, but also on the contacting pattern. As shown in Figure A-6, the nature of multiphase contacting in various flow modes (cocurrent upflow or concurrent downflow) is distinct. When the bed is operated in the trickle flow regime under partial wetting conditions for the pellets, gas is the continuous phase and liquid is the dispersed phase. However, the packed-bubble column operates in the bubbly flow regime with fully wetted pellets. In this regime, the solid particles are wetted by the continuous liquid phase, whereas the gas phase is dispersed as bubbles flowing through the packing channels. The key differences in modeling downflow and upflow modes are the values of the mass transfer parameters and the

catalyst wetting efficiency. Since upflow operation is characterized by high liquid holdups, it was assumed external wetting is complete. Tables A-1 lists various correlations in the literature used to calculate the model parameters, which include the external liquid-solid contacting efficiency, liquid holdup, mass transfer coefficients ($(ka)_{GL}$, k_{LS}, k_{GS}), and the axial dispersion coefficient.

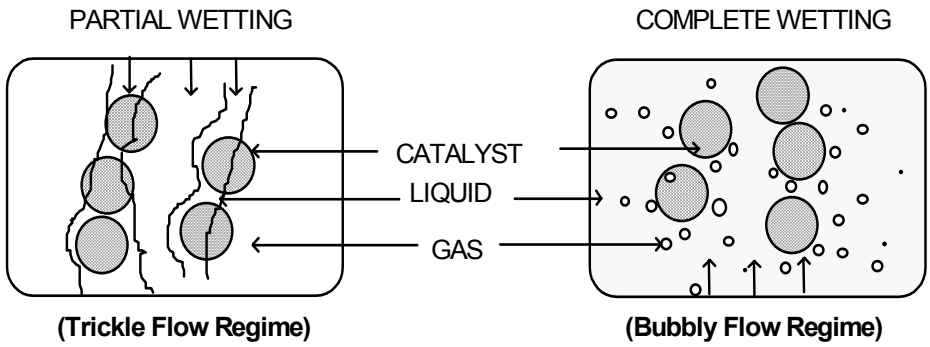

Figure A-6. Contacting pattern in the trickle flow regime and bubble flow regime.

Table A-1. Summary of various correlations used in the models

Model parameter	Reference for Trickle Bed	Reference for Bubble Flow Column
Gas-liquid mass transfer coefficient, $(ka)_{GL}$	Fukushima and Kusaka (1977, a)	Reiss (1967)
Liquid-solid mass transfer coefficient, k_{LS}	Tan and Smith (1980)	Specchia (1978)
Gas-solid mass transfer coefficient, k_{GS}	Dwivedi and Upadhyah (1977)	0.0
Wetting efficiency, η_{CE}	El-Hisnawi (1981)	1.0
Axial dispersion coefficient	Cassanello et al. (1992)	Cassanello et al. (1992)
Liquid holdup,ε_L	Fukushima and Kusaka (1977, b)	Bensetiti et al. (1997)

A3 Results and Discussion

Many experimental investigations in the literature have dealt with hydrogenation or oxidation in moderately concentrated organic solutions or solutions with a large excess of liquid reactants. To validate the proposed model scheme, the hydrogenation of AMS to cumene in hexane solvent was taken as a model reaction. We sought to compare the simulation results with the experimental observations taken from Khadilkar et al., (1996). Then the reaction of aqueous phenol oxidation, which is of our interest, was applied to the proposed model to predict the performance of the reactor and catalyst pellet under different operating conditions. The employed design parameters of the three-phase reactors, the characteristics of the porous catalyst particles, and the operating conditions are indicated in Table A-2. The trickle flow regime experimentally covered in this work for these two reactions is shown in Figure A-7.

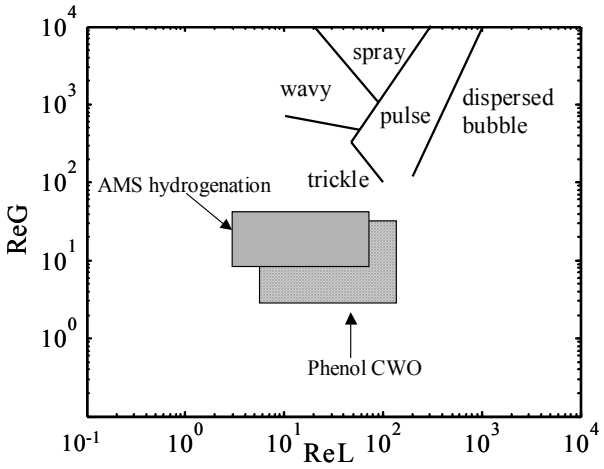

Figure A-7. Region of trickle flow regime covered experimentally in this work for AMS hydrogenation and phenol oxidation, (flow map proposed by Fukushima and Kusaka (1977, b)).

Table A-2. Design and operating conditions

Property	Hydrogenation of AMS	CWO of Phenol
Temperature, ^{o}C	25	80
Pressure, MPa	0.3-1.5	0.5
Reactor diameter, cm	2.2	5.1
Bed height, cm	27.5	200
Bed porosity	0.40	0.36
Catalyst particle size, cm	ϕ0.13*0.56	ϕ0.3
Density of catalyst particle, kg/m^3	1222	1760
Superficial liquid velocity, cm/s	0.09-0.5	0.1-0.22
Superficial gas velocity, cm/s	3.8-14.4	1.0-10.5
Feed concentration, mol/l	0.23-0.60, (3.1-7.8% (v/v))	0.001-0.03

A3.1 Model Scheme Validation

In the liquid phase, both hydrogen and AMS have low concentrations, which make the effect of the reaction heat release insignificant. The intrinsic kinetics expression of hydrogenation of AMS has been studied by Khadilkar et al., (1996), who fitted separate Langmuir-Hinshelwood rate expressions (eq. A-18) for different pressures.

$$r_B\left[\frac{mol}{m^3 \cdot s}\right] = \frac{k_{vs} C_{\alpha ms} C_{H2}}{(1 + K_1 C_{\alpha ms} + K_2 C_{cume})^{\beta}} \qquad \text{(A-18)}$$

According to the taxonomy (Khadilkar et al., 1996), the ratio of the diffusion fluxes of the two reactants ($\gamma=(D_{eB}C_{Bi}/\nu_B(D_{eA}C_A$*) is indicative of the relative availability of the species at the reaction site. The reaction can be considered gas reactant limited for $\gamma>>1$ or liquid reactant limited for $\gamma<1$. At high pressure (1.5 MPa) and a low feed concentration of AMS ($C_{B,0}$=3.1 %, v/v), the reaction is liquid-limited ($\gamma<1$), such as in Figures A-8a and A-8b, where the effect of the flow direction on reactor performance is shown. As pressure is decreased from 1.5 MPa to 0.3 MPa, and feed concentration of AMS is increased to $C_{B,0}$=6.8% (v/v), the reaction is transformed to a gas-limited regime

(γ>1), such as in Figures A-9a and A-9b, where the effect of feed concentration on upflow performance is shown.

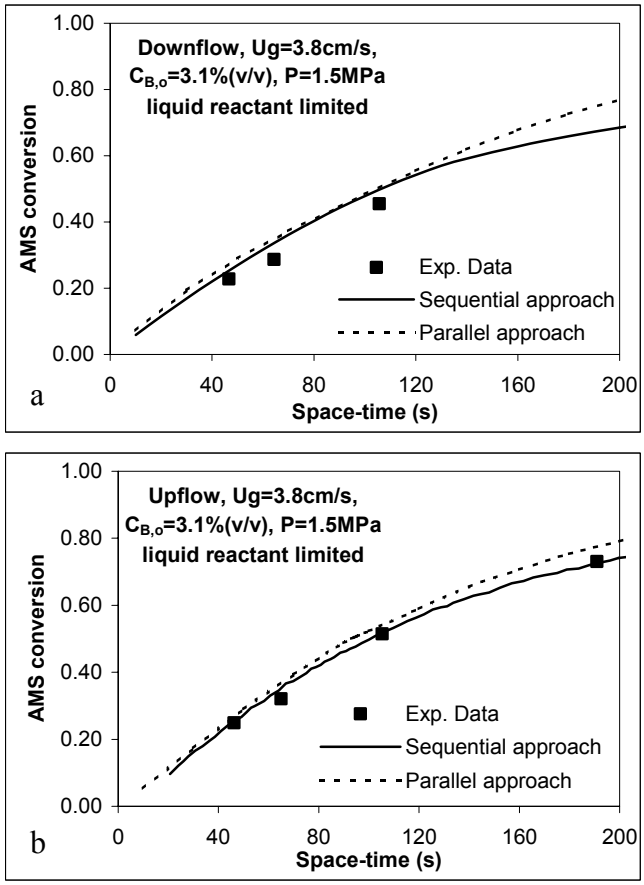

Figure A-8. (a) Downflow and (b) upflow performance at high pressure: experimental data and model predictions. The curves correspond with the predictions via parallel approach proposed by Larachi et al., (2001) and the one via sequential approach proposed in this work.

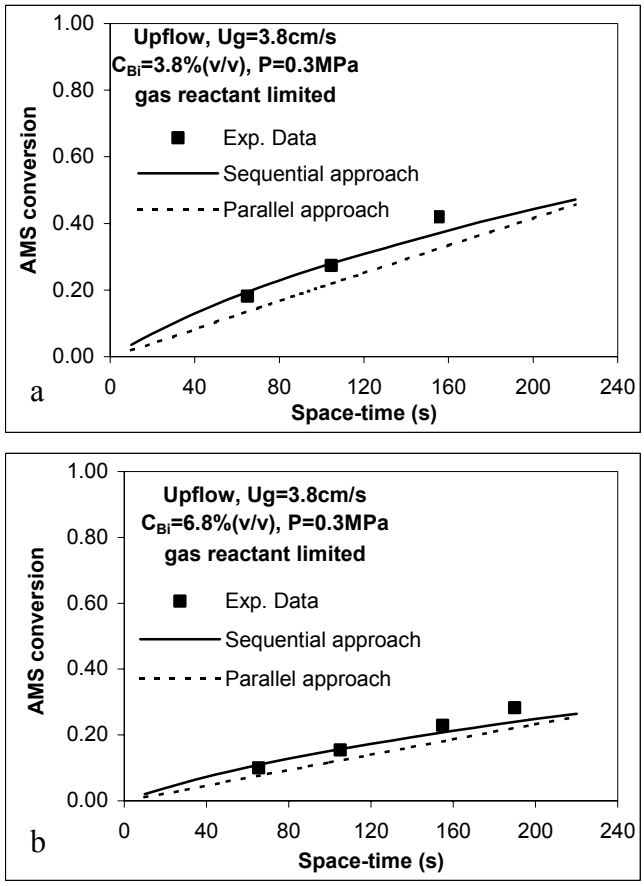

Figure A-9. Effect of feed concentration on upflow performance: experimental data and model predictions.

The curves in Figures A-8 and A-9 correspond with the predictions of the sequential approach proposed in this work and the parallel approach proposed by Iliuta and Larachi (2001). The two approaches contain different sets of transport and hydrodynamic correlations. In all the exhibited cases, the results predicted by both approaches agree reasonably with the experimental observations. In the parallel approach, the external liquid holdup is divided into static and dynamic portions. For high flow rates, such division is reasonable. However, the dynamic liquid holdup decreases with decreasing liquid flow rate, i.e., with increasing the liquid space-time (Iliuta et al., 1996). When the liquid space-time reaches 200 s, the liquid flow rate is so low that the discrepancy between the dynamic and static liquid holdup is no longer distinct, which means that the

split-up of the external holdup is not necessary. Nevertheless, the parallel approach always assumes there is a difference between these two portions. Hence, for the liquid-limited reaction in Figure A-8a and A-8b, the deviation between these two approaches becomes larger as the space-time increases. Such deviation is not shown for the gas-limited reaction in Figure A-9a and A-9b, where both the liquid holdup and the gas pressure can affect the AMS conversion.

Since the suitability of the sequential approach to describe the reactions in packed bed has been validated, it is applied to the other test case, which is the CWO of phenol over a deactivating catalyst.

A3.2 Wet Air Oxidation of Aqueous Phenol

Catalyst deactivation was overlooked in most of those investigations dealing with CWO, which have focused on the evaluation of catalyst performance in terms of the removal rate of pollutant with simplified or complex rate equations (Levec and Smith, 1976; Maugans and Akgerman, 2003). In fact, catalyst deactivation occurs in general cases due to the polymer deposition on the catalyst surface, or due to the leaching of the catalyst active sites. Hence, the time variable also needs to be taken into account to describe dynamic catalytic behavior. Although catalyst deactivation due to active ingredient leaching out in the hot acidic reaction media is documented (Pintar and Levec, 1992), the activity loss due to the carbon deposits on catalyst surface has been mostly discounted. Hamoudi and Larachi (1999), who studied phenol oxidation in a slurry reactor over a newly developed but rapidly deactivated MnO_2/CeO_2 catalyst, have reported that oxidative coupling reactions contribute significantly to rapid catalyst deactivation via coke deposition on the surface of catalyst pellets. Relatively few reports have been published on modeling a packed-bed reactor for a multi-step complex reaction system with such a deactivating catalyst.

A3.2.1 Intrinsic Kinetic Model

In this evaluation of wet air oxidation of aqueous phenol in packed beds, the reaction proceeds between phenol and an excess of soluble oxygen in the presence of a deactivating MnO_2/CeO_2 mixed oxide catalyst. The complete multiple deactivation-reaction network describing phenol CWO has been reported by Hamoudi and Larachi, (1999), in which all the intervening species are grouped into four lumps. Chemical phenol (lump B) is oxidized by O_2 and converts into a chemisorbed aqueous breakdown intermediate lump(C) that further degrades into an oxidation end-product lump D (total inorganic Carbon). All three lumped species can instantaneously adsorb or desorb. A Langmuir-Hinshelwood kinetic model based on this deactivation-reaction network was proposed to predict the reaction rate of the various carbon lumps as well as the rate of decline of catalyst activity. The kinetic model and its calculated parameters successfully described the time course of the four carbon lumping species involved in the slurry reaction (Hamoudi and Larachi, 1999).

$$r_B\left[\frac{mol}{kgcat \cdot \min}\right] = \frac{k_2 K_1 \varphi C_{BL}}{1 + K_1 C_{BL} + K_3 C_{CL} + K_3' C_{DL}}$$

$$r_C\left[\frac{mol}{kgcat \cdot \min}\right] = \frac{(k_2 K_1 C_{BL} - k_2' K_3 C_{CL})\varphi}{1 + K_1 C_{BL} + K_3 C_{CL} + K_3' C_{DL}}$$

$$-\frac{d\varphi}{dt} = \frac{(k_4 K_1 C_{BL} + k_4' K_3 C_{CL})\varphi}{1 + K_1 C_{BL} + K_3 C_{CL} + K_3' C_{DL}}$$

where φ is the catalyst active site fraction with the initial condition given as φ = 1 at time t = 0. Computation of γ results in γ<1 for the CWO operating conditions employed in Table 2. Hence the wet air oxidation in this study is a liquid-reactant limited reaction. The assumption of an isothermal condition is justified because the low phenol concentration in the liquid phase solution results in insignificant heat generation. Due to the relatively small phenol concentration, the physical properties of water are used for the liquid phase. Under the mild operating conditions, the fugacity and activity for oxygen and water are assigned unity values. The diffusivities of phenol and oxygen and values of viscosities and densities for water at the operating conditions were estimated from the literature correlations (Reid et al., 1986).

A3.2.2 Comparison of Trickle Bed and Packed Bubble Flow Reactor Performance

In Figures A-10 and A-11, both the sequential approach and the parallel approach have been employed to predict the phenol oxidation reaction. The difference in exit phenol conversion calculated by the two approaches is within 6%, as shown in Figure A-10. The sequential and parallel approaches can also be compared for their ability to predict catalyst deactivation. As evident in Figure A-11, at identical simulation conditions, calculated profiles of the activity function of catalyst in the operation time range 0 – 35 h exhibited a maximum relative error of 6% between the two approaches. The maximum relative error of 20% was reached after a rather long operation time (110 h). Both of the maximum relative errors were obtained at the reactor outlet. Such prediction difference between the two approaches for the catalyst deactivation can be attributed to the correspondingly different concentration profiles. For downflow operation with identical inlet conditions, as exhibited for AMS hydrogenation in Figures A-8a and A-8b, a more noticeable difference between the concentration profiles predicted by the two approaches results from the longer residence time of reactants in the packed-bed. Similarly, for the case of CWO in Figure A-11, the differences between the concentration predictions by the two approaches also become larger with the longer residence time. Such concentration differences in turn lead to the different predictions of catalyst active site fraction, which displays the maximum difference at the reactor outlet. Nevertheless, comparing two time durations such as 35 h and 110 h, the trends captured by the two approaches are always similar. Taking into account the long process duration, the distinct model type and correlations used to describe the flow field, and the different methods used for the parameters' estimation, this comparison between the two approaches is still satisfying. In Figures A-10 and A-11, the curves obtained by the parallel approach simulation are similar to those reported by Larachi et al., (2001).

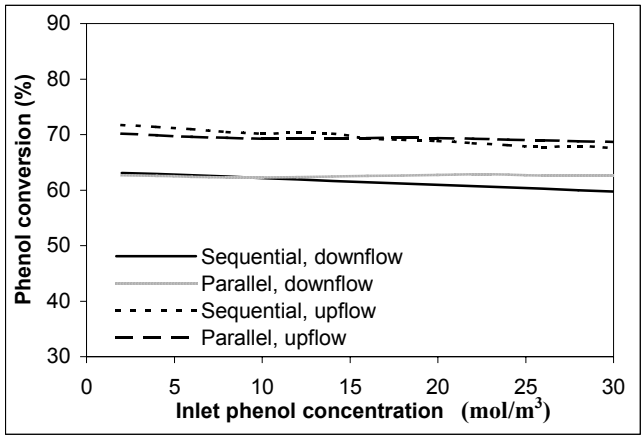

Figure A-10. Effect of inlet phenol concentration on phenol conversion in fixed bed reactors, time=5 h, u_{SL}=0.15 cm/s, u_G=2.8 cm/s, P=0.5 MPa, T=80 ^oC.

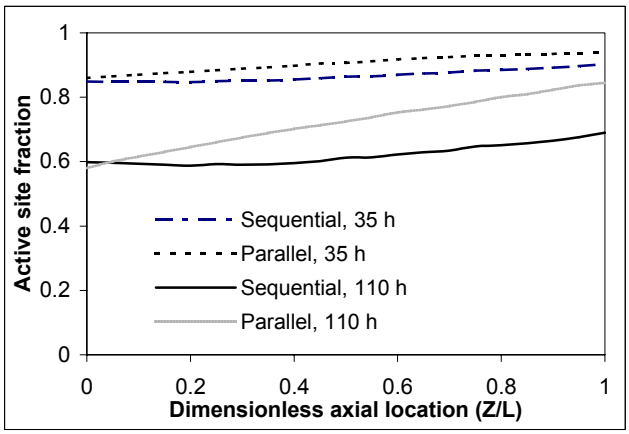

Figure A-11. Comparison of axial distribution of active site, downflow, time=35 and 110 h, $C_{B,0}$=6 mol/m^3, pellet fully wet side.

In Figure A-10, the comparison of downflow and upflow packed-bed performances is achieved by studying phenol conversion at identical operating conditions after the catalyst has been used for 5 hours. Figure A-10 also shows that the exit phenol conversion in upflow mode was 10% higher than in the downflow mode, regardless of the feed phenol concentration. In a liquid-limited reaction, the conversion will be governed by the degree of catalyst wetting. Since upflow has higher external wetting

efficiency (100%) than downflow, it will facilitate the transport of the liquid reactant to the catalyst and enhance the reaction rate. This finding is in line with the case of AMS hydrogenation, where both experimental observation (Khadilkar et al., 1996) and model simulations (this work) show that an upflow reactor should be preferred for liquid-limited reactions.

To make the comparison in Figures A-12 to A-14 between downflow and upflow more meaningful, the dimensionless reactor length axis point 0 corresponds to the packed-bed inlet, and 1 corresponds to the packed-bed outlet. Since the sequential approach performs equivalently as the parallel approach in the validation of AMS hydrogenation, the former is used for the following evaluations. Although upflow mode will produce higher phenol conversion than downflow mode, this achievement is at the expense of more severe catalyst deactivation, as shown in Figure A-12. When the inlet phenol concentration is 6 mol/m^3, the catalyst activity loss is more in upflow than in downflow after 5 h operation, although the discrepancy is very small. When the inlet phenol concentration increases up to 22 mol/m^3, the upflow mode will do more appreciable harm to catalyst activity than downflow mode after 5 h operation. This is clear since the high phenol concentration will result in high oxidation intermediate lump concentration, and both concentrations will enhance the deactivation rate. In contrast, the effect of phenol feed concentration on conversion is not significant, as shown in Figure A-10. When the inlet concentration increases by 14 times, the change in conversion is within 6% in both upflow and downflow.

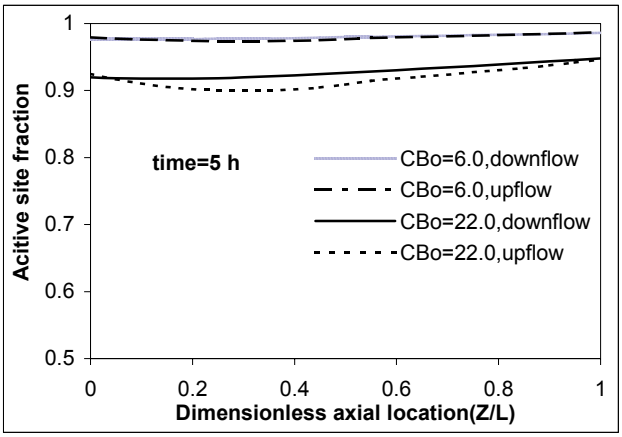

Figure A-12. Effect of inlet phenol concentration on the catalyst surface deactivation in the upflow and downflow packed beds, u_{SL}=0.15 cm/s, u_G=2.8 cm/s, pellet fully wet side.

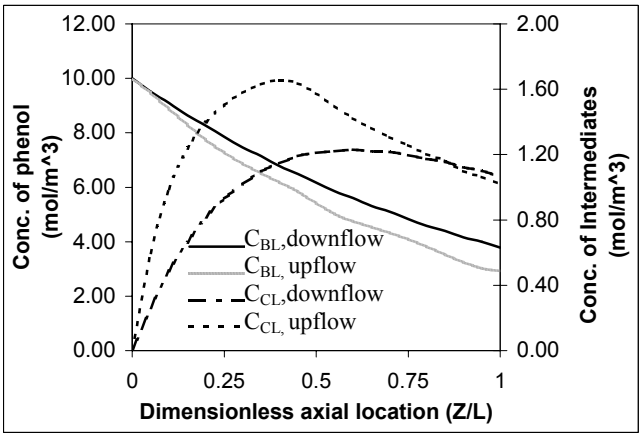

Figure A-13. Predicted concentration profiles for phenol (C_{BL}) and intermediate lump (C_{CL}) in liquid phase as a function of catalyst bed length, u_{SL}=0.15 cm/s, u_G=2.8 cm/s, $C_{B,0}$=10.0 mol/m^3, P=0.5 MPa, pellet fully wet side.

Since both phenol and the oxidation intermediate lump determine the rate of catalyst deactivation, we have to consider their effects simultaneously. Figure A-13 exhibits typical species concentration profiles along the packed-bed reactor at the given operating conditions after 5 h operation. Along the axis, phenol is consumed, so its concentration keeps decreasing. However, the oxidation intermediate C builds up in the first part of the reactor. With the consumption of phenol and increasing amount of C, the reaction rate of

C will become negative, which can be shown from its reaction rate expression, where the concentration of C inhibits its production rate. Thus, concentration of intermediate C reaches a maximum value before the reactor outlet. At a given axial location in upflow mode, such as the middle of the reactor, the phenol concentration profile is lower than the one in downflow mode by 8%, while the concentration of product C at the same location in upflow is 22% higher than in downflow mode. Thus, when upflow mode is used, although phenol contributes less to the deactivation function, product C's contribution goes up and overtakes phenol's effect on the deactivation function. The rate of activity loss in upflow is still more than in downflow mode, which leads to the lower activity fraction profile.

The prediction of catalyst activity over time is instructive because one can learn the catalyst life expectancy, after which "coked" catalyst should be subject to burn-off and regeneration for long-term exploitation. Simulated axial profiles of activity site fraction in the time rage of 0 - 200 h indicate the expected feature of time-declining activity, as shown in Figure A-14 for the trickle-bed operation. The simulation for the upflow reactor follows the same trend, although the upflow results in higher catalyst deactivation than the downflow. It can be expected that the majority of catalyst would completely lose its function after 300 hours of operation. Although the wet oxidation of phenol over this kind of catalyst removed phenol remarkably fast at mild pressure and temperature, the catalyst underwent severe deactivation, which made its wide application undesirable. Hence, a different catalyst is required for feasible CWO of aqueous phenol, such as the Al-Fe pillared clay catalyst.

Both phenol conversion and catalyst deactivation should be taken into consideration when one needs to choose between upflow and downflow operation. Upflow could result in both higher phenol conversion and a higher catalyst activity loss rate, especially for wastewater that contains a high concentration of phenol. The balance between these two factors will decide the operation mode, and the catalyst's life and regeneration cycle need to be taken into account as important factors. This point is decisive in the design and selection of the three-phase reactor type for hosting the CWO.

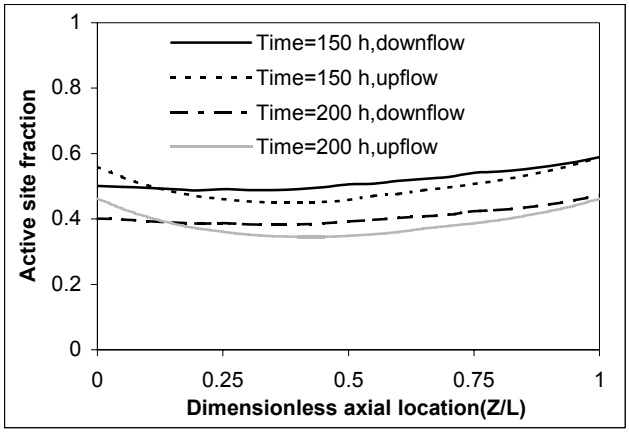

Figure A-14. Catalyst surface deactivation with time in the upflow and downflow packed beds, u_{SL}=0.15 cm/s, u_G=2.8 cm/s, $C_{B,0}$=6.0 mol/m^3, pellet fully wet side.

As described in the computation scheme for the dynamic behavior, the local information at each matrix cell, such as catalyst active site fractions, is shown in Figures A-15a for the trickle bed and A-15b for the packed-bed bubble column. Such information can illuminate the details of the physical phenomena inside the reactor and pellet at different operation conditions. Note that in Figures A-15a and A-15b the dimensionless reactor length axis point 0 corresponds to the packed-bed top, and 1 corresponds to the packed-bed bottom.

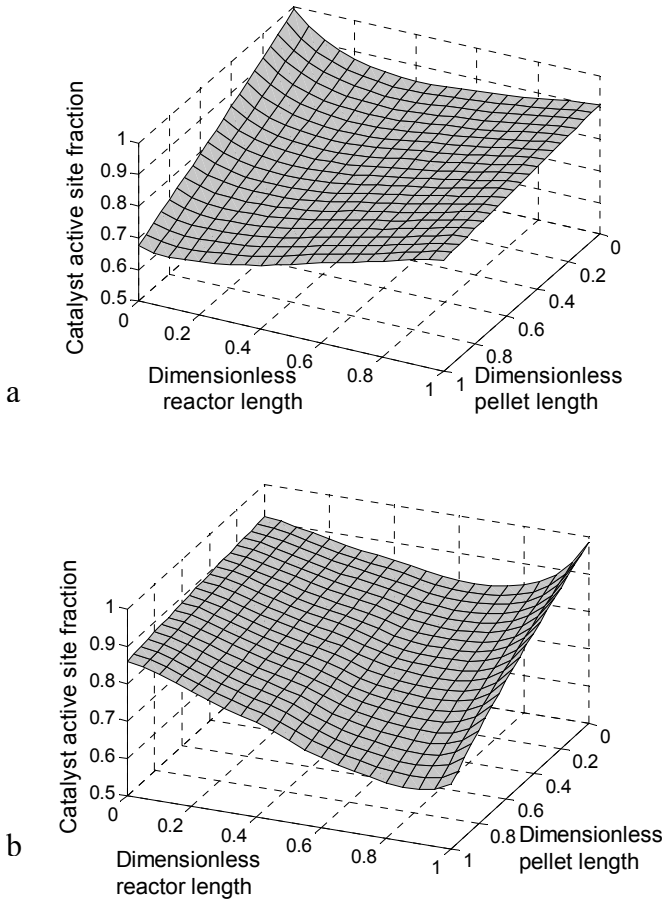

Figure A-15. Distribution of catalyst active site fraction in (a) TBR and (b) PBC, according to the proposed matrix configuration, time = 110 h, $C_{B,0}$=6.0 mol/m^3, P=0.5 MPa, T=80 ^oC.

A3.2.3 Influence of Liquid and Gas Superficial Velocity

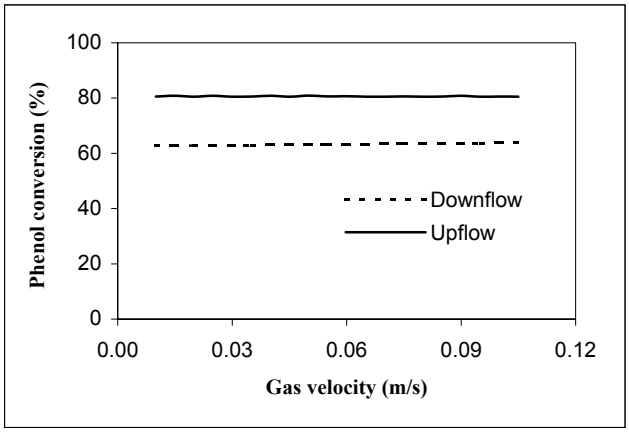

Figure A-16. Comparison of effect of gas velocity on the exit phenol conversion, upflow and downflow, u_{SL}=0.15 cm/s, $C_{B,0}$=6.0 mol/m^3, time=5 h.

The effect of gas velocity on phenol conversion is shown in Figure A-16 for both downflow and upflow operation. Because the gas is only barely soluble, increasing the velocity has little effect on phenol conversion, even though increasing velocity will lead to an increase in the external gas-liquid mass transfer coefficients (Stuber et al., 1996). Such a negligible influence of gas velocity has earlier been observed by Goto and Smith (1975) for the oxidation of formic acid.

The comparison of effect of liquid superficial velocity on the exit phenol conversion is shown in Figure A-17 for both downflow and upflow modes. The effect of liquid superficial velocity on the axial phenol conversion profile is obvious. A lower feed flow rate is preferred because the longer residence time will allow for higher phenol conversion. A similar trend of simulation results can be obtained in the cocurrent upflow packed-bed reactor where gas flows through the liquid in bubble flow. Although a high liquid superficial velocity enhances the mass transfer coefficient, it actually lowers the liquid reactant residence time, which corresponds to the decreased exit conversion. Such a behavior confirms that liquid reactant limiting behavior is observed for the CWO reaction, as the flow regime has already implied. Thus, the external mass transfer

coefficients are dependent mostly on the liquid velocity in the downflow and upflow mode, which is in line with the model simulation and experimental verification for the hydrogenation of 2,4-dinitrotoluene (DNT) in a trickle bed (Rajashekharam et al., 1998).

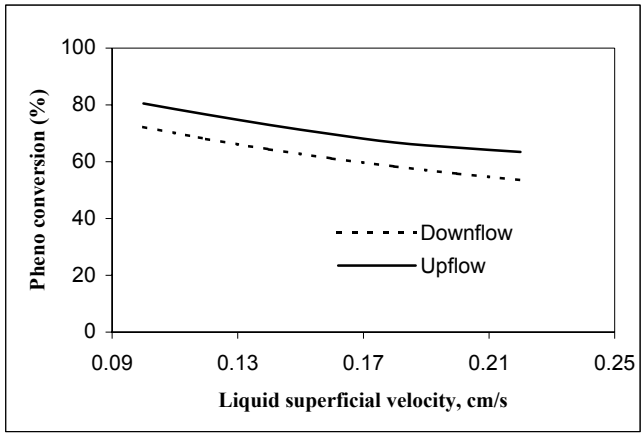

Figure A-17. Effect of liquid superficial velocity on the exit phenol conversion, upflow and downflow, u_G=2.8 cm/s, $C_{B,0}$=6.0 mol/m^3, time=5 h.

A3.2.4 Sensitivity of Model to Mass Transfer Coefficients

In this modeling work, a group of correlations were employed to predict the hydrodynamic parameters and interphase mass transfer resistance. However, the values of mass transfer coefficients predicted from different correlations sometimes may be dramatically different (Lemcoff, et al., 1988). Thus, it is necessary to evaluate the reliability and sensitivity of model predictions to various parameters. The sensitivity of trickle-bed reactor models with respect to external mass transfer resistances was studied theoretically by Toppinen et al., (1996) and Rajashekharam et al., (1998). In their work, an increase or decrease in the mass transfer coefficient of up to 10 times the original estimated values results in remarkably different simulation results. Thus, the mass transfer coefficients listed in Table A-1 have also been scaled up or down to investigate the sensitivity of the proposed reactor models to the mass transfer coefficients.

The effect of liquid-solid's mass transfer on the exit conversion is shown in Figure A-18a, which indicates that its influence of on phenol conversion is significant. An increase in the value of k_{LS} by 10 times improved the phenol conversion by 9%. Also, when the

k_{LS} value was decreased by 10 times, the phenol conversion decreased by approximately 22%. Clearly, the liquid-solid mass transfer resistance is an important factor. Similarly, the effect of gas-liquid mass transfer on the exit conversion is shown in Figure A-18b. The results show that an increase or decrease in the $(ka)_{GL}$ value by 10 times does not substantially change phenol conversion. The insignificant difference in phenol conversion was maintained over the entire range of liquid velocity. The sensitivity of the model with respect to the gas-solid mass transfer coefficient is shown in Figure A-18c, which was obtained by increasing and decreasing the value of k_{GS} by 10 times. All three curves almost fall into the same line, which evidences the model is insensitive to the gas-solid mass transfer coefficient over the investigated range of liquid flowrates.

Hence, the liquid-reaction limited characteristic of CWO is proved once more, and the relative importance of mass transfer resistance on the exit phenol conversion for the CWO process is liquid-solid k_{LS} > gas-liquid $(ka)_{GL} \approx$ gas-solid $k_{GS,}$ in descending order.

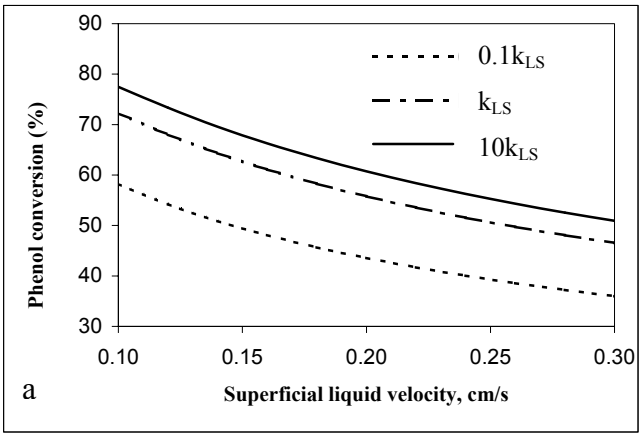

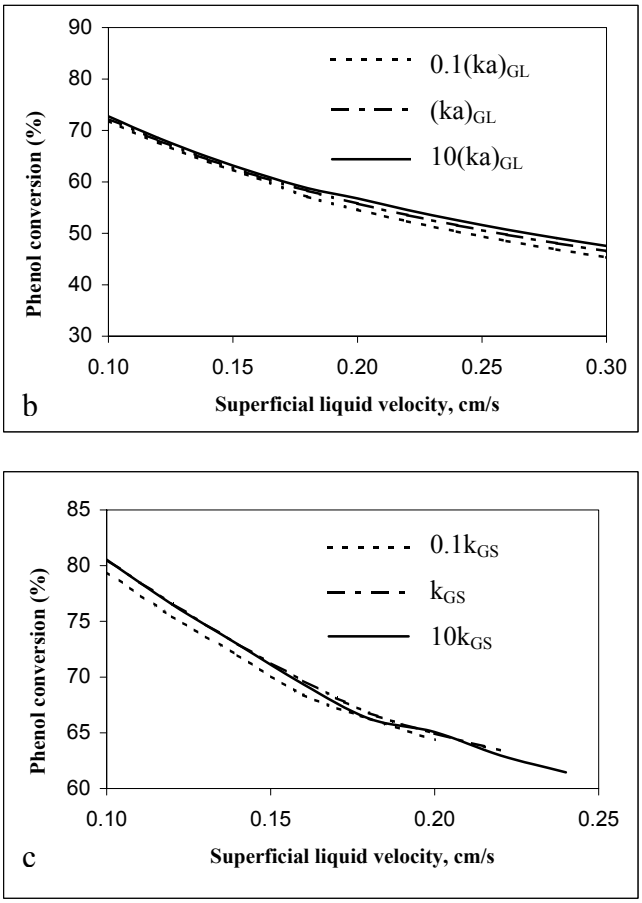

Figure A-18. Sensitivity of the models with regards to (a) liquid-solid, (b) gas-liquid, and (c) gas-solid mass transfer coefficients in trickle bed reactor, $C_{B,0}$=6.0 mol/m^3, time=5 h, P=0.5 MPa, T=80 ^{o}C.

A4 Summary

In this work, a sequential approach has been developed for applying the ADM in combination with the pellet scale model. The ADM predicted the local concentration along the reactor axis, whereas the pellet scale model evaluated the local effectiveness factor corresponding to the local reactant concentration. Such a sequential approach incorporates the nonlinear reaction kinetics expressions into the pellet scale model and the ADM, without any fitting parameter. Experimental observations for AMS hydrogenation have been used to validate the developed modeling scheme. The

comparable simulation results from the parallel and sequential approaches exhibit that both approaches are as good in terms of the simulation capability, and hence, they can be used for simulation for such reaction and others in packed-bed reactors. To account for unsteady state reactor behavior, the sequential scheme was utilized to predict the catalytic wet oxidation of phenol in a packed bed with newly developed but rapidly deactivated catalyst pellets of MnO_2/CeO_2. The simulation described the time evolution of catalyst deactivation at pellet scale along the reactor axis. The simulation suggests that liquid-reactant limited reactions such as wet oxidation can obtain higher conversion in a packed bubble column than in a trickle bed. However, a higher axial catalyst deactivation rate also results from the upflow mode than from the downflow mode. In both upflow and downflow, an increase of gas velocity does not affect the phenol conversion significantly, and the external mass transfer coefficients are dependent mostly on the liquid velocity. The MnO_2/CeO_2 catalyst is not applicable for the packed bed operation, and its commercial application is unfeasible. A new catalyst is required for the CWO process. The proposed sequential approach could be used for the evaluation and design of the new catalyst, once the reaction kinetic expressions are available.

References

Al-Dahhan M. H. and Dudukovic M. P., (1995) Catalyst Wetting Efficiency in Trickle-bed Reactors at High Pressure. *Chem. Eng. Sci.*, 50, 2377.

Al-Dahhan M. H., Larachi F., Dudukovic M. P. and Laurent A., (1997) High-pressure Trickle-bed Reactors: A Review. *Ind. Eng. Chem. Res.*, 36, 3292-3314.

Alejandre A., Medina E., Rodriguez X., Salagre P., Cesteros Y. and Sueiras J. E., (2001) Cu/Ni/Al Layered Double Hydroxides as Precursors of Catalysts for the Wet Air Oxidation of Phenol Aqueous Solutions. *Appl. Catal. B.: Environmental*, 195-207.

Allen T., (1980) *Particle Size Measurement*, 4th ed., Chapman and Hall: London.

Aurora S., Pedro Y., Beatriz D. and Felix G. O., (2001) Catalytic Wet Oxidation of Phenol: Kinetics of the Mineralization Rate. *Ind. Eng. Chem. Res.*, 40, 2773.

Autenrieth R. L., Bonner J. S., Akgerman A., Okaygun M. and Mccreary E. M., (1991) Biodegradation of Phenolic Wastes. *J. Hazard. Mater*., 28.

Baillod C. R., Lamparter R. A. and Barna B. A., (1985) Wet Oxidation for Industrial Waste Treatment. *Chem. Eng. Prog*., 52-56.

Baker E. G., Sealock L. J., Butner R. S., Elliott D. C. and Neuenschwander G. G., (1989) Catalytic Destruction of Hazardous Organics in Aqueous Wastes: Continuous Reactor System Experiments. Hazard. *Waste Hazard. Mater*., 6, 87.

Barrault J., Abdellaoui M., Bouchoule C., Majeste A., Tatibouet J. M., Louloudi A., Papayannakos N. and Gangas N. H., (2000) Catalytic Wet Peroxide Oxidation over Mixed (Al-Fe) Pillared Clays. *Appl. Catal. B.: Environmental*, 27, 225.

Beaudry E. G., Dudukovic M. P. and Mills P. L., (1987) Trickle-bed Reactors: Liquid Diffusional Effects in a Gas-Limited Reaction. *AIChE J*., 33, 1435.

Bej S. K., Dalai A. K. and Maity S. K., (2001) Effect of Diluent Size on the Performance of a Micro-scale Fixed Bed Multiphase Reactor in Up Flow and Down Flow modes of Operation. *Catal. Today*, 64, 333-345.

Bensetiti Z., Larachi F., Grandjean B. P. A. and Wild G. (1997) Liquid Saturation in Cocurrent Upflow Fixed-Bed Reactors: a State-of-the-art Correlation. *Chem. Eng. Sci., 52*, 4239.

Bergaya F. and Barrault J., (1990) *Mixed Al-Fe Pillared Laponites: Preparation, Characterization and Their Catalytic Properties in Syngas Conversion, in Pillared Layered Structures: Current Trends and Applications* (Mitchell I.V. Ed.), Elsevier Science Publishers. London and New York.

Berger R. J., Perez-Ramirez J., Kapteijn F. and Moulijn J. A., (2002) Catalyst Performance Testing: Bed Dilution Revisited. *Chem. Eng. Sci., 57*, 4921.

Berty J. M., (1991) (to Berty Reaction Engineers, Ltd.) *Catalyst for Destruction of Toxic Organic Chemicals*. U.S. Patent 5,021,383, June 4.

Beziat J., Besson M., Gallezot P. and Durecu S., (1999) Catalytic Wet Air Oxidation on a Ru/TiO_2 Catalyst in a Trickle-Bed Reactor. *Ind. Eng. Chem. Res*., 38, 1310-1315.

Bhatia S. K., (1988) Steady State Multiplicity and Partial Internal Wetting of Catalyst Particles Exposed to Saturated Vapor. *AIChE J*., 34, 969-979.

Bishop D. F., Stern G., Fleischman M. and Marshall L. S., (1968) Hydrogen Peroxide Catalytic Oxidation of Refractory Organics in Municipal Wastewater. *Ind. Eng. Chem. Process Des. Dev*., 7, 110.

Bond G. C., (1974) *Heterogeneous Catalysis: Principles and Applications*. Oxford University Press: Oxford, U.K.

Bos A. N. R., Lefferts L., Marin G. B. and Steijns M. H. G. M., (1997) Kinetic research on Heterogeneously Catalyzed Processes: A Questionnaire on the State-of-the–art in Industry. *Appl. Catal. A: General*, *160*, 185.

Brad Sims W., Gaskey S. W. and Luss D., (1994) Effect of Flow Regime and Liquid Velocity on Conversion in a Trickle Bed Reactor. *Ind. Eng. Chem. Res.*, 22, 2530.

Brock T. D. and Madigan M. T., (1988) *Biology of Microorganisms*, Prentice-Hall: Englewood Cliffs, N.J.

Canney P. J. and Schaeffer P. T., (1983) Wet Oxiation of Toxics: A New Application of Existing Technology. *Toxic Hazard Waste, Proc. 15th Mid Atl. Ind. Waste Conf.*, LaGrega M. D., Hendrian L. K. Eds., 277-284p Chem. Abstr. 100, 197152.

Cassanello M. C., Martinez O. M., and Cukierman A. L., (1992) Effect of the Liquid Axial Dispersion on the Behavior of Fixed Bed Three Phase Reactors. *Chem. Eng. Sci., 47*, 3331.

Clearfield A., (1996) *Preparation of Pillared Clays and Their Catalytic Properties, in Advanced Catalysts and Nanostructured Materials* (Moser W. R. Ed.), Academic Press, San Diego.

Coelho A. V. and Poncelet G., (1990) *Preparation, Characterization and Some Catalytic Properties of Different Smectites Pillared with Hydroxy-Aluminum and Hydroxy-Gallium Solutions, in Pillared Layered Structures: Current Trends and Applications* (Mitchell I.V. Ed.), Elsevier Science Publishers. London and New York.

Collins G. M., Hess R. K. and Ackgerman A., (1985) Effect of Volatile Liquid Phase on Trickle-bed Reactor Performance. *Chem. Eng. Commun.*, 35, 281-291.

Colombo A. J., Baldi G. and Sicardi S., (1976) Solid-liquid Contacting Effectiveness in Trickle-bed Reactors. *Chem. Eng. Sci.*, 31, 1101.

Crammer S. D., (1980) The Solubility of Oxygen in Brines from 0 to 300 ^{o}C. *Ind. Eng. Chem. Res.*, 19, 300.

De Angelo D. J. and Wilhelmi A. R., (1983) Wet Air Oxidation of Spent Caustic Liquors. *Chem. Eng. Prog.*, 79, 68-73.

Deans H. A. and Lapidus L., (1960) A Computational Model for Predicting and Correlating the Behavior of Fixed-bed Reactors: 1. Derivation of Model for Nonreactive Systems, *A.I.Ch.E. J.*, 6, 656.

Devlin H. R. and Harris I. J., (1984) Mechanism of the Oxidation of Aqueous Phenol with Dissolved Oxygen. *Ind. Eng. Chem. Fundam.*, 23, 387.

Dietrich M. J., Randall T. L. and Canney P. J., (1985) Wet Air Oxidation of Hazardous Organics in Wastewater. *Environ. Prog.*, 4, 171-177.

Ding Z. Y., Aki S. N. V. K. and Abraham M. A., (1995) Catalytic Supercritical Water Oxidation: Phenol Conversion and Product Selectivity. *Environ. Sci. Technol.*, 29, 2748.

Ding Z. Y., Frish M. A., Li L. and Gloyna F., (1996) Catalytic Oxidation in Supercritical Water. *Ind. Eng. Chem. Res.,* 35, 3257.

Dojlido R. and Best G. A., (1993) *Chemistry of Waters and Water Pollution*, Ellis Horwoood: New York.

Dudukovic M. P., Larachi F. and Mills P. L., (1999) Multiphase reactors-revisited. *Chem. Eng. Sci.*, 54, 1975-1995.

Duggleby R. G., (1984) Regression Analysis of Nonlinear Arrhenius Plots: An Empirical Model and a Computer Program. *Comput. Biol. Med*., 14, 447.

Dwivedi P. N. and Upadhyah S. N., (1977) Particle-Fluid Mass Transfer in Fixed and Fluidized Beds. *Ind. Eng. Chem. Proc. Des. Dev.*, *16*, 157.

Eftaxias A., Larachi F. and Stuber F., (2003) Modeling of Trickle Bed Reactor for the Catalytic Wet Air Oxidation of Phenol. *Canadian J. Chem. Eng*., 81, 784-794.

El-Hisnawi A. A., (1981) *Tracer and Reaction Studies in Trickle-bed reactors.* D. Sc. Dissertation, Washington University, St. Louis, Missouri,

Fortuny A., Bengoa C., Font J., Castells F. and Fabregat A., (1999) Water Pollution Abatement by Catalytic Wet Air Oxidation in a Trickle Bed Reactor. *Catal*. *Today*, 53, 107-114.

Fortuny A., Ferrer C., Bengoa C., Font J. and Fabregat A., (1995) Catalytic Removal of Phenol from Aqueous Phase Using Oxygen or Air as Oxidant. *Catal*. *Today*, 24, 79.

Fortuny A., Font J. and Fabregat A., (1998) Wet Air Oxidation of Phenol Using Active Carbon as Catalyst. *Appl. Catal. B.: Environmental*, 19, 165.

Frish M. A., Li L. and Gloyna E. F., (1994) *Proceedings of the 49th Annual Purdue University Industrial Wastewaters Conference*, Purdue, IN.

Froment G. F. and Bischoff K. B., (1979) *Chemical Reactor Analysis and Design*, John Wiley & Sons.

Froment G. F., Depauw G. A. and Vanrysselberghe V., (1994) Kinetic Modeling and Reactor Simulation in Hydrodesulfurization of Oil Fractions. *Ind. Eng. Chem. Res., 33*, 2975.

Fukushima S. and Kusaka K., (1977, a) Liquid-phase Volumetric and Mass-transfer Coefficient, and Boundary of Hydrodynamic Flow Region in Packed Column with Cocurrent Downward Flow. *J. Chem. Eng. of Japan*, *10*, 468.

Fukushima S. and Kusaka K., (1977, b) Interfacial Area and Boundary of Hydrodynamic Flow Region in Packed Column with Cocurrent Downward Flow. *J. Chem. Eng. of Japan***,** *10*, 461.

Fukushima S. and Kusaka K., (1979) Gas-liquid Mass Transfer and Hydrodynamic Flow Region in Packed Columns with Cocurrent Upward Flow. *J. Chem. Eng. of Japan*, 12, 296.

Funk G. A., Harold M. P. and Ng K. M., (1990) Novel Model for Reaction in Trickle Beds with Flow Maldistribution. *Ind. Eng. Chem. Res*., 29, 738.

Gangas N. H. and Papayannakos, N. G., (1993) *Final Report of Feasibility Award*, FA-1010-91, Contract Number: BRE2-063, Sections III. 4 to III. 6.

Gao F., Lu B. and Shen D., (1988) Reactor Design Principle and Pilot Test for the Treatment of Cotton Slurry Black Liquor by Wet Air Oxidation. *Huaxue Fanying Gongcheng Yu Gongyi*, 4, 81-8.

Goto S. and Smith J. M., (1975) Trickle Bed Reactor Performance Part II: Reaction Studies. *AIChE J.*, 21, 706.

Goto S. and Mabuchi K., (1984) Oxidation of Ethanol in Gas-liquid Upflow and Downflow Reactors. *Canadian J. Chem. Eng*., 62, 865-869.

Green D. A., Leese K. E., Mack K. L. and McMichael W. J., (1983) Pollution Control in Coal Gasification. NTIS Report DOE/MC/ 16441-1423, RTI-2224/01-01F, *Chem. Abstr*., 99, 217805.

Gregg S. J. and Sing K. S. W., (1983) *Adsorption, Surface Area and Porosity*, 2nd ed., Academic: London.

Guo J. and Al-Dahhan M., (2003, a) Catalytic Wet Oxidation of Phenol by Hydrogen Peroxide over Pillared Clay catalyst. *Ind. Eng. Chem. Res.*, 42, 2450-2460.

Guo J. and Al-Dahhan M., (2003, b) Kinetics of Wet Air Oxidation of Phenol over a Novel Catalyst. *Ind. Eng. Chem. Res*., 42, 5473-5481.

Guo J. and Al-Dahhan M., (2004, a) A Sequential Approach to Modeling Catalytic Reactions in Packed Bed Reactors. *Chem. Eng. Sci.*, 59, 2023-2037.

Guo J. and Al-Dahhan M., (2004, b) Liquid Holdup and Pressure Drop in the Gas-liquid Cocurrent Downflow Packed-bed Reactor under Elevated Pressures. *Chem. Eng. Sci.*, 59, 5387-5393.

Guo J. and Al-Dahhan M., (2005) Catalytic Wet Air Oxidation of Phenol in Concurrent Downflow and Upflow Packed-Bed Reactors over Pillared Clay Catalyst. *Chem. Eng. Sci.*, 60, 735-746.

Hamoudi S., Belkacemi K. and Larachi F., (1999) Catalytic Oxidation of Aqueous Phenolic Solutions Catalyst Deactivation and Kinetics. *Chem. Eng. Sci*., *54*, 3569.

Hamoudi S., Belkacemi K., Sayari A. and Larachi F., (2001), Catalytic Oxidation of 4-chloroguaiacol Reaction Kinetics and Catalyst Studies. *Chem. Eng. Sci*., 56, 1275.

Hamoudi S., Larachi F., Graciela C. and Myrian C., (1998) Wet Oxidation of Phenol Catalyzed by Unpromoted and Platinum-Promoted Manganese/Cerium Oxide. *Ind. Eng. Chem. Res.*, 37, 3561.

Hao O. J., Phull K. K., Davis A. P. and Maloney S. W., (1992) Preliminary Results of Wet Air Oxidation of TNT Red Water. *Hazard Ind. Wastes 24th*, 110-19.

Harf J., Hug A., Vogel F. and Von Rohr P. R., (1999) Scale-Up of Catalytic Wet oxidation under moderate conditions. *Environ. Prog*., 18(1), 14-20.

Harold M. P., (1993) *Impact of Wetting in Multiphase Catalytic Reaction System. Computer Aided Design of Catalyst*, Marcel Dekker, New York, 391.

Herskowitz M., (1985) Modeling of a Trickle Bed Reactor: the Hydrogenation of Xylose to Xylitol. *Chem. Eng. Sci*., 40, 1309.

Higashi K., Kawahara A., Murakami I., Wakuda S., Yamane M. and Takasuka S., (1992) Decomposition of Phenol by Wet Oxidation with Solid Catalyst. *Yosui to Haisui*, 33, 1007, Chem. Abstr., 116, 66367.

Higashi K., Kawahara A., Murakami I., Wakuda I., Yamane M. and Takeda S., (1994) Decomposition of Nitrobenzene by Wet Oxidation with Noble Metal Catalysts. *Shigen Kankyo Taisaku*, 30, 452, Chem. Abstr., 121, 133403.

Himmelblau D. M., (1960) Solubilities of inert gases in water. 0^{o}C to near the critical point of water. *J. Chem. Eng. Data*, 5, 10-16.

Hochman J. M. and Effron E., (1969) Two-phase Cocurrent Downflow in Packed Beds. *Ind. Eng. Chem. Fundam*., *8*, 63.

Iliuta I. and Larachi F., (2001) Wet Air Oxidation Solid Catalysis Analysis of Fixed and Sparged Three-phase Reactors. *Chem. Eng. Proc.*, *40*, 175.

Iliuta I., Thyrion F. C. and Muntean O., (1996) Residence Time Distribution of the Liquid in Gas-liquid Cocurrent Upflow Fixed-bed Reactors. *Chem. Eng. Sci*., *51*, 4579.

Imamura S., (1999) Reviews: Catalytic and Noncatalytic Wet Oxidation. *Ind. Eng. Chem. Res*., 38, 1743.

Imamura S. and Ando M., (1989) Oxidation of Tristearin on Manganese/Cerium Oxide. *Ind. Eng. Chem. Res*., 28, 1453.

Imamura S., Dol A. and Ishida S., (1985) Wet Oxidation of Ammonia Catalyzed by Cerium-Based Composite Oxides. *Ind. Eng. Chem. Prod. Res. Dev.*, 24, 75.

Imamura S., Fukuda I. and Ishida S., (1988) Wet Oxidation Catalyzed by Ruthenium Supported on Cerium (IV) Oxides. *Ind. Eng. Chem. Res.*, 27, 718.

Ito M. M., Akita K. and Inoue H. (1989) Wet Oxidation of Oxygen- and Nitrogen-Containing Organic Compounds Catalyzed by Cobalt (III) Oxide. *Ind. Eng. Chem. Res*., 28, 894.

Jaffe S. B., (1976) Hot Spot Simulation in Commercial Hydrogenation Processes, *Ind. Eng. Chem*. *Res*., 15, 410.

Jiang Y., Khadilkar M. R., Al-Dahhan M. H. and Dudukovic M. P. (2000) Single Phase Flow Modeling in Packed Beds. *Chem. Eng. Sci*., 55, 1829.

Jie W., Liu J. and Xu H., (1992) Catalytic Air Oxidation of Phenol in Aqueous Solution. *Shuichuli Jishu* 17, 179, Chem. Abstr., 116, 66361.

Kaloidas V., Koufopanos C. A., Gangas N. H. and Papayannakos N. G., (1995) Scale-up Studies for the Preparation of Pillared Layered Clays at 1 kg per Batch Level. *Microporous Materials*, 5, 97.

Katzer J. R, Ficke H. H. and Sadana A., (1976) An Evaluation of Aqueous Phase Catalytic Oxidation. *J. WPCF*, 48, 920.

Keckler K. P., Brandenburg B. L., Momont J. A. and Lehman R. W., (1993) Treatment of Wastewater from Acrylonitrile Manufacturing Plant. *Chem. Abstr.*, 118, 197432.

Khadilkar M. R., Wu Y. X., Al-Dahhan M. H., Dudukovic M. P., and Colakyan M., (1996) Comparison of Trickle-bed and Upflow Reactor Performance at High Pressure: Model Predictions and Experimental Observation. *Chem. Eng. Sci.*, *51*, 2139.

Kochetkova R. P., Shiverskaya I. P., Kochetkov A. Y., Panfilova I. V., Kovalenko N. A., Eppel S. A., Minchenko V. A. and Babikov A. F. (1993) Technological Parameters of Liquid-Phase Oxidation of Wastewater Phenols. *Koks Khim*. 9, 44, Chem. Abstr., 119, 55256.

Krajnc M. and Levec J., (1994) Catalytic Oxidation of Toxic Organics in Supercritical Water. *Appl. Catal. B.: Environmental*, 3, 101.

Kufner R. and Hofmann H., (1990) Implementation of Radial Porosity and Velocity Distribution in a Reactor Model for Heterogeneous Catalytic Gas Phase Reactions (TORUS-Model). *Chem. Eng. Sci*., 45, 2141-2146.

Larachi F., Iliuta I. and Belkacemi K., (2001) Catalytic Wet Air Oxidation with a Deactivating Catalyst Analysis of Fixed and Sparged Three-phase Reactors. *Catal. Today, 64*, 309.

Larachi F., Laurent A., Wild G. and Midoux N., (1991) Some Experimental Liquid Saturation Results in Fixed-bed Reactors Operated under Elevated Pressure in Cocurrent Upflow and Downflow of the Gas and the Liquid. *Ind. Eng. Chem. Res.*, *30*, 2404-2410.

Larachi F., Laurent A., Wild G. and Midoux N., (1992) Pressure Effects on Gas-liquid Interfacial Areas in Cocurrent Trickle-flow Reactors. *Chem. Eng. Sci.*, 51, 2139.

LaVopa V. and Satterfield C. N., (1988) Some Effects of Vapor-liquid Equilibriaa on Performance of a Trickle-bed Reactor. *Chem. Eng. Sci.*, 43, 2175.

Lemcoff N. O., Cukierman A. L. and Martinez O. M., (1988) Effectiveness Factor of Partially Wetted Catalyst Particles: Evaluation and Application to the Modeling of Trickle Bed Reactors. *Catalysis reviews: science and engineering*, *30*, 393.

Levec J. and Smith J. M., (1976) Oxidation of Acetic Acid Solutions in a Trickle-bed Reactor. *AIChE J*., *22*, 159.

Levenspiel O., (1996) *The Chemical Reactor Omnibook*, OSU Book Stores, Inc., Corvallis, Oregon.

Li L., Chen P. and Gloyna, E., (1991) Generalized Kinetic Model for Wet Oxidation of Organic Compounds. *AIChE J*., 37, 1687.

Lin J. C. and Chang C. J., (1992) Reduction of COD of Industrial Wastes Using Subcritical Water Oxidation. *J. Environ. Sci. Health, Part A*, 27(7), 1655-73.

Lin S. H., Ho S. J. and Wu C. L., (1996) Kinetics and Performance Characteristics of Wet Air Oxidation of Organics Compounds in Aqueous Media. *Catal. Today*, 29, 317-322.

Lin S. H., Ho S. J. and Wu C. L., (1996) Kinetic and Performance Characteristic of Wet Air Oxidation of High-Concentration Wastewater. *Ind. Eng. Chem. Res.*, 35, 307.

Luck F., (1996) A Review of Industrial Catalytic Wet Air Oxidation Processes. *Catal. Today*, 27, 195.

Mann M. D., Wilson W. G. and Hendrikson J. G., (1985) Gasifier Wastewater Treatment: Phase I Cooling Tower Assessment. *Environ. Prog*., 4 (1), 33.

Matsuno M. and Yamamoto S., (1989) Wet Oxidation of Organic Wastewaters. Jpn. Kokai Tokkayo Koho JP 01310794, Dec. *Chem. Abstr*., 112, 164466.

Matthews R. W., (1992) Photocatalytic Oxidation of Organic Contaminants in Water: an Aid to Environmental Preservation. *Pure and Applied Chemistry*, 64, 1285.

Maugans C. B. and Akgerman A., (1997) Catalytic Wet oxidation of Phenol over a Pt/TiO2 Catalyst. *Water Res.*, 31(12), 3116-3124.

Maugans C. B. and Akgerman A., (2003) Catalytic Wet Oxidation of Phenol in a Trickle Bed Reactor over a Pt/TiO_2 Catalyst. *Water Research*, *37*, 319.

Mears D. E., (1971) Tests for Transport Limitations in Experimental Catalytic Reactors. *Ind. Eng. Chem. Proc. Des. Dev.*, *10*, 541.

Mishra V. S., Mahajani V. V. and Joshi B., (1995) Wet Air Oxidation. *Ind. Eng. Chem. Res.*, 34, 2.

Moore J. W. and Ramamoorthy S., (1984) *Organic Chemicals in Natural Waters*, Springer-Verlag: New York.

Moser W. R., (1996) *Advanced Catalysts and Nanostructured Materials*, Academic Press: San Diego.

Occelli M. L. and Finseth D. H., (1986) Nanostructured Materials. *J. Catal*., 99, 316.

Pauli O. and Franke G., (1971) Behavior and Degradation of Technical Preservatives in the Biological Purification of Sewage. *Biodeterior. Mater. Proc. 2nd Int. Biodeterior. Symp*., Walters A. H. Ed., Appl. Sci. Publ. Ltd.: Barking, England.

Pfeifer P., Obert M. and Cole M. W., (1989) *Fractal BET and FHH Theories of Adsorption: A Comparative study.* Proc. R. Soc. London A, 423, 169.

Pintar A. and Levec J., (1992) Catalytic Oxidation of Organics in Aqueous Solutions: Kinetics of Phenol Oxidation. *J. Catal.*, *135*, 345.

Pintar A. and Levec J., (1992) Catalytic Liquid-Phase Oxidation of Refractory Organics in Wastewater. *Chem. Eng.* Sci., 47, 2395.

Pintar A. and Levec J., (1994) Catalytic Liquid-phase Oxidation of Phenol Aqueous Solutions: A Kinetic Investigation. *Ind. Eng. Chem. Res.*, *33*, 3070.

Pintar A., Bercic G. and Levec J., (1997) Catalytic Liquid-phase Oxidation of Aqueous Phenol Solutions in a Trickle-Bed. *Chem. Eng. Sci.*, *52*, 4143.

Pradt L. A., (1972) Development in Wet Oxidation. *Chem. Eng. Prog.*, 68, 72.

Press H. W., Teukolsly S. A., Vetterling W. T. and Flannery B. P. (1992) *Numerical Recipes, the Art of Scientific Computing*, Cambridge University Press: Cambridge, U.K.

Pruden B. B. and Le H., (1976) Wet Air Oxidation of Soluble Components in Wastewater. *Canadian J. Chem. Eng*., 54, 319.

Rajashekharam M. V., Jaganathan R. and Chaudhari R. V., (1998) A Trickle-bed Reactor Model for Hydrogenation of 2,4-Dinitrotoluene: Experimental Verification. *Chem. Eng. Sci.*, *53*, 787.

Ramachandran P. A. and Chaudhari R. V., (1983). *Three-phase Catalytic Reactors*. Gordon and Breach Science Publishers, New York.

Ramachandran P. A. and Smith J. M., (1979) Effectiveness Factors in Trickle Bed Reactors. *A.I.Ch.E. J*., *25*, 538.

Ramachandran P. A. and Smith J. M., (1979) Mixing-Cell Model for Design of Trickle-Bed Reactors. *Chem. Eng. Sci.*, 17, 91.

Reid R. C., Prausnitz J. M. and Poliing B. E., (1986) *The Properties of Gases and Liquids*. 4th Edn. McGraw-Hill, New York, U. S. A.

Reiss L. P., (1967) Concurrent Gas-liquid Contacting in Packed Columns. *Ind. Eng. Chem. Prod. Res. Dev*., 6, 486.

Sadana A. and Katzer J. R., (1974) Involvement of Free Radicals in the Aqueous-Phase Catalytic Oxidation of Phenol over Copper Oxide. *J. Catal*., 35, 140.

Sadana A. and Katzer J. R., (1974) Catalytic Oxidation of Phenol in Aqueous Solution over Copper Oxide. *Ind. Eng. Chem. Fundam.*, 13, 127.

Santos A., Yustos P., Durban B. and Garcia-Ochoa F., (2001) Catalytic Wet Oxidation of Phenol: Kinetics of Phenol Uptake. *Environ. Sci. Technol*., 35, 2828-2835.

Satterfield C. N., (1980) *Heterogeneous Catalysis in Practice*. McGraw-Hill: New York,

Schneider P. and Smith J. M., (1968) Adsorption Rate Constants from Chromatogroaphy. *A.I.Ch.E. J*., 14, 762.

Schnitzlein K. and Hofmann H., (1987) An Alternative Model for Catalytic Fixed Bed Reactors. *Chem. Eng. Sci*., 42, 2569.

Shende R. V. and Levec J., (1999) Wet Oxidation Kinetics of Refractory Low Molecular Mass Carboxylic Acids. *Ind. Eng. Chem. Res*., 38, 3830.

Silva A. M. T., Branco I. C., Ferreira R. Q. and Levec J., (2003) Catalytic Studies in Wet Oxidation of Effluents from Formaldehyde Industry. *Chem. Eng. Sci.*, 58, 963.

Specchia V., Baldi G. and Glanetto A., (1978) Solid-liquid Mass Transfer in Concurrent Two-phase Flow through Packed Beds. *Ind. Eng. Chem. Prod. Res. Dev.*, 17, 362.

Spivey J. J., (1987) Complete Catalytic Oxidation of Volatile Organics. *Ind. Eng. Chem. Res*., 26, 2165.

Stuber F., Polaert I., Delmas H., Font J., Fortuny A. and Fabregat A., (2001) Catalytic Wet Air Oxidation of Phenol Using Active Carbon: Performance of Discontinuous and Continuous Reactors. *J. Chem. Tech. and Biotech*, 76, 743-751.

Stuber F., Wilhelm A. M. and Delmas H., (1996) Modeling of Three Phase Catalytic Upflow Reactor: A Significant Chemical Determination of Liquid-solid and Gas-liquid Mass Transfer Coefficients. *Chem. Eng. Sci., 51*, 2161.

Takematsu T. and Parsons B. I., (1972) *A Comparison of Bold Feed and Top-Feed Reaction Systems for Hydrodesulfurization*. Dept. of Energy, Mines and Resources, Fuels Res. Centre Tech. Bull. TB161.

Tan C. S. and Smith J. M., (1980) Catalyst Particle Effectiveness with Unsymmetrical Boundary Conditions. *Chem. Eng. Sci*., *35*, 1601.

Thanos A. M., Galtier P. A. and Papayannakos N., (1996) Liquid Flow Non-Idealities and Hold-up in a Pilot Scale Packed Bed Reactor with Cocurrent Gas-liquid Upflow. *Chem. Eng. Sci*., 51, 2709-2714.

Toppinen S., Aittamaa J. and Salmi T., (1996) Interfacial Mass Transfer in Trickle-Bed Reactor Modeling. *Chem. Eng. Sci., 51*, 4335.

Tsamatsoulis D. and Papayannakos N., (1995) Simulation of Non-ideal Flow in a Trickle Bed Reactor by a Cross-flow Model. *Chem. Eng. Sci*., 50, 3685.

Tukac V. and Hanika J., (1998) Catalytic Wet Oxidation of Substituted Phenols in the Trickle Bed Reactor. *J. Chem. Tech. and Biotech.*, 71, 262-266.

Turpin J. L. and Huntington R. L., (1967) Prediction of Pressure Drop for Two-phase, Two-Component Cocurrrent Flow in Packed beds. *A.I.Ch.E. Journal*, 13, 1196.

Villadsen J. and Michelsen M. L., (1978) *Solution of Differential Equation Models by Polynomial Approximation*. Prentice-Hall, NJ, U. S. A.

Walas S. M., (1985) *Phase Equilibria in Chemical Engineering*, Butterworth-heinemann: Newton, MA.

Wammes W. J. A., Mechielsen S. J. and Westerterp K. R., (1990) The Influence of Reactor Pressure on the Hydrodynamics in a Cocurrent Gas-liquid Trickle-bed Reactor. *Chem. Eng. Sci.*, 45, 3149.

Watson P. C. and Harold M. P., (1993) Dynamic Effects of Vaporization with Exothermic Reaction in a Porous Catalytic Pellet. *AIChE J.*, 39, 989-1006.

Wilhelmi A. R. and Ely R. R., (1976) A Two Step Process for Toxic Wastewaters. *Chem. Eng.* February.

Wilke C. R. and Chang P., (1955) Correlation for Diffusion Coefficients in Dilute Solutions. *AIChE J.*, 1, 264.

Wu Y., Khadilkar M. R., Al-Dahhan M. and Dudukovic M. P., (1996) Comparison of Upflow and Downflow Two Phase Flow Reactors With and Without Fines. *Ind. Eng. Chem. Res*., 35, 397.

Yaws C. L., (1999) *Chemical Properties Handbook*, McGraw-Hill.

Yurii I. M. M. and Moshe S., (1998) Catalytic Abatement of Water Pollutants. *Ind. Eng. Chem. Res*., *37*, 309.

Zhang Q. and Chuang K. T., (1999) Treatment of Combined Bleach Plant Effluents via Wet oxidation over a Pd-Pt-Ce/Alumina Catalyst. *Environ. Sci. Technol.*, 33, 3641-3644.

Zhang, X. and Savage P. E., (1998) Fast Catalytic Oxidation of Phenol in Supercritical Water. *Catal. Today*, 40, 333-342.

VITA

Name **Jing Guo**

Degrees

B.Sc. Chemical Engineering, June 1997
Beijing University of Chemical Technology, China.

M.Sc. Chemical Engineering, June 2000
Beijing University of Chemical Technology, China

D.Sc. Chemical Engineering, (expected) May 2005
Washington University, St. Louis, MO, USA.

Industrial Experience

Summer Intern (05/2004 – 08/2004)
Corning Incorporated, Corning, NY, USA.

Process Engineer (05/1999 – 11/1999)
Beijing Organic Chemical Plant, China

Professional Societies American Institute of Chemical Engineers

Journal Publications

1. Guo J., Al-Dahhan M., Catalytic Wet Oxidation of Phenol by Hydrogen Peroxide over Pillared Clay Catalyst. *Ind. Eng. Chem. Res.*, 2003, 42, 2450-2460.
2. Guo J., Al-Dahhan M., Kinetics of Wet Air Oxidation of Phenol over a Novel Catalyst. *Ind. Eng. Chem. Res.*, 2003, 42, 5473-5481.
3. Guo J., Al-Dahhan M., A Sequential Approach to Modeling Catalytic Reactions in Packed Bed Reactors. *Chem. Eng. Sci.*, 2004, 59, 2023-2037.
4. Guo J., Al-Dahhan M., Liquid Holdup and Pressure Drop in the Gas-liquid Cocurrent Downflow Packed-bed Reactor under Elevated Pressures. *Chem. Eng. Sci.*, 2004, 59, 5387-5393.
5. Guo, J., Al-Dahhan, M., Catalytic Wet Air Oxidation of Phenol in Concurrent Downflow and Upflow Packed-Bed Reactors over Pillared Clay Catalyst. *Chem. Eng. Sci.*, 2005, 60, 735-746.
6. Jiang Y., Guo, J., Al-Dahhan, M., Multiphase Flow Packed Bed Reactor Modeling: Combining CFD and Cell Network Model. *Ind. Eng. Chem. Res.* 2005, in press.

7. Guo J., David K., Al-Dahhan M., IT-based Development of an Internet-mediated, Real-time Undergraduate Experiment for Chemical Engineering Unit Operation Laboratory. *Chem. Eng. Edu.* 2005, submitted.

Conference Presentations

1. Guo J.; Al-Dahhan M., Liquid Holdup and Pressure Drop in the Trickle-bed Reactor under Elevated Pressures, *18th international Symposium on Chemical Reaction Engineering (ISCRE-18)*, 237, Chicago, June 6-9, (2004).
2. Guo J.; Al-Dahhan M., Modeling Verification and Application for Catalytic Wet Oxidation in Packed Bed Reactors, *AIChE Annual Meeting*, 513d, San Francisco, Nov. 16-21, (2003).
3. Guo J.; Al-Dahhan M., Pellet Scale Modeling of Catalytic Reaction, *Chemical Reaction Engineering IX*, Quebec City, Quebec, Canada, June 29- July 4, (2003).
4. Guo J.; Al-Dahhan M., Modeling of Catalytic Reaction in Trickle Bed and Up-flow Packed Bed Reactors, *AIChE Annual Meeting*, 373aj, Indianapolis, Nov. 3 - 8, (2002).
5. Guo J.; Al-Dahhan M., Phenol Oxidation by Hydrogen Peroxide over Pillared Clay Catalyst, *AIChE Annual Meeting*, 373d, Indianapolis, Nov. 3 - 8, (2002).
6. Guo J.; Al-Dahhan M., Catalytic Wet Oxidation of Phenol by Hydrogen Peroxide or Air over Pillared Clay Catalyst, *The Mid-America Environmental Engineering Conference (MAEEC)*, St. Louis, Sept. 22, (2001).

May, 2005